ABSTRACT

SUO, DINGJIE. High Intensity Focused Ultrasound (HIFU) Based Thrombolysis Using Multiple Frequency Excitations. (Under the direction of Dr. Yun Jing).

High intensity focused ultrasound (HIFU) based thrombolysis has emerged as a promising drug-free approach for ischemic stroke treatment. The large amount of acoustic power required by this approach, however, poses a critical challenge to the future clinical translation because of the potential thermal damages. In this dissertation, multi-frequency acoustic waves at MHz range (near 1.5 MHz) were first introduced as HIFU excitations to reduce the required treatment power as well as the treatment time. It was found that dual-frequency thrombolysis efficiency was statistically better than that of single-frequency, under the same acoustic power and excitation condition. Microbubbles (MBs) combined with dual-frequency focused ultrasound (DFFU) for thrombolysis *in vitro* was then proposed to further reduce the power required. MBs are widely used in therapeutic ultrasound thrombolysis due to the nonlinear characteristics of their harmonic responses, coalescence and cavitation effects, which could further enhance efficiency. It was shown in this study that MBs, with sufficient concentration, could significantly lower the power threshold for thrombolysis for both DFFU and single-frequency focused ultrasound (SFFU). MBs mediated DFFU thrombolysis were then studied with a flow system that mimicked the blood flow in the artery of the brain. It was found that the cavitation threshold of a DFFU excitation yielded a lower level than that of a SFFU excitation. All the experimental results indicated that multi-frequency ultrasound could improve the thrombolysis efficiency. However, this was not well established numerically. Hence, a numerical investigation on the inertial cavitation threshold of MBs under multi-frequency ultrasound irradiation was then investigated to confirm the benefit of using

multi-frequency ultrasound for various applications. The main contribution and findings of this dissertation are as follows:

1) For the HIFU along study, when varying the acoustic power while fixing the duty cycle at 5%, it was found that almost 30% of the power can be saved by dual frequency ultrasound to achieve the same thrombolysis efficiency. In the experiment where the duty cycle was increased from 0.5% to 10%, it was shown that dual-frequency ultrasound can achieve the same thrombolysis efficiency with only half of the duty cycle of single-frequency. Dual-frequency ultrasound could also accelerate the thrombolysis by a factor of 2-4 as demonstrated in this study. The measured cavitation doses of dual-frequency and triple-frequency excitations were at about the same level, both significantly higher than that of single-frequency.

2) For the MBs mediated thrombolysis study, SFFU needed about 96%-156% higher energy to achieve the same thrombolysis efficiency as that of DFFU. The thrombolysis efficiency was also found to increase with the duty cycle. The measured cavitation signals reveal that the enhanced inertial cavitation may contribute to the improved thrombolysis under DFFU and MBs. By adding the flow system, the inertial cavitation was higher than the static model. One reason could be the dissolution of MBs into the flow that lowered the concentration of MBs by a significant amount. In both cases, the inertial cavitation thresh holds of DFFU were lower than SFFU.

3) For the numerical study, we investigated the inertial cavitation threshold of MBs under multi-frequency ultrasound irradiation. The relationships between the cavitation threshold and MB size at various frequencies and in different media were investigated. The results for single, dual and triple frequency sonication showed that inertial cavitation thresholds

can be reduced by introducing additional frequencies, which was consistent with previous experimental work. In addition, no significant difference was observed between dual frequency sonication with various frequency differences. This study also provided a possible route for optimizing ultrasound excitations for initiating inertial cavitation.

High Intensity Focused Ultrasound (HIFU) Based Thrombolysis Using Multiple Frequency Excitations

by
Dingjie Suo

A dissertation submitted to the Graduate Faculty of
North Carolina State University
in partial fulfillment of the
requirements for the degree of
Doctor of Philosophy

Mechanical Engineering

Raleigh, North Carolina

2017

APPROVED BY:

_____	_____
Dr. Yun Jing Committee Chair	Dr. Xiaoning Jiang
_____	_____
Dr. Paul A. Dayton	Dr. Marie Muller

BIOGRAPHY

Dingjie Suo was born in 1989, Xuzhou, China. He graduated from Nanjing Foreign Language School in 2008 and then received his B.S. degree in Mechanical Engineering from Beijing Institute of Technology in 2012. He received his M.S. degree in Mechanical Engineering from University of Southern California in 2013. After that, he joined Dr. Yun Jing's Acoustics and Ultrasonics lab at North Carolina State University in 2014. His current research majored in High Intensity Focused Ultrasound (HIFU) based thrombolysis using multiple frequency excitations.

Publications

Journal Articles

1. **Suo, Dingjie**, Bala Govind, Andrew Antony, Yun Jing. "Microbubble mediated dual-frequency high intensity focused ultrasound thrombolysis with flow system: an *in vitro* study." (In preparation. 2017)
2. **Suo, Dingjie**, Bala Govind, Shengqi Zhang, and Yun Jing. "Numerical investigation of the inertial cavitation threshold under multi-frequency ultrasound." Ultrasonics Sonochemistry (2017).
3. **Suo, Dingjie**, Zhiyang Jin, Xiaoning Jiang, Paul A. Dayton, and Yun Jing. "Microbubble mediated dual-frequency high intensity focused ultrasound thrombolysis: An *In vitro* study." Applied Physics Letters 110, no. 2 (2017): 023703.
4. **Suo, Dingjie**, Sijia Guo, Weili Lin, Xiaoning Jiang, and Yun Jing. "Thrombolysis using multi-frequency high intensity focused ultrasound at MHz range: an *in vitro* study." Physics in medicine and biology 60, no. 18 (2015): 7403.

5. Di, Jin, Jicheng Yu, Qun Wang, Shanshan Yao, **Dingjie Suo**, Yanqi Ye, Matthew Pless, Yong Zhu, Yun Jing, and Zhen Gu. "Ultrasound-triggered noninvasive regulation of blood glucose levels using microgels integrated with insulin nanocapsules." Nano Research 10, no. 4 (2017): 1393-1402.
6. Xie, Yangbo, Chen Shen, Wenqi Wang, Junfei Li, **Dingjie Suo**, Bogdan-Ioan Popa, Yun Jing, and Steven A. Cummer. "Acoustic holographic rendering with two-dimensional metamaterial-based passive phased array." Scientific reports 6 (2016): 35437.

Conference Proceedings

1. **Suo, Dingjie**, Bala Govind, Shengqi Zhang, Yun Jing. “Numerical investigation of inertial cavitation threshold under multi-frequency ultrasound.” In Ultrasonics Symposium (IUS), 2017 IEEE International.
2. Guo, Sijia, **Dingjie Suo**, Yun Jing, Xiaoning Jiang, Jason Frank, and Weili Lin. “Thrombolysis enhanced by dual-frequency highintensity focused ultrasound.” In Ultrasonics Symposium (IUS), 2014 IEEE International.

ACKNOWLEDGEMENTS

This doctoral study would not have been possible without the continuous help from many well-wishers. Foremost, I would like to take this opportunity to express my sincere gratitude to my advisor Dr. Yun Jing, for his continuous support and help during these four years. He trusted me and my abilities from the very beginning and guided me through the obstacles that I faced during my research. I appreciate the time and effort that he spent in helping me with my papers, abstracts, and presentations. He taught me, “no mistake is stupid, just learn from it.” I could never have earned a doctoral degree without his patience and persistent guidance. I am truly fortunate to have had Dr. Jing as my adviser these four years.

I would like to express my sincere appreciation to my committee members, Dr. Xiaoning Jiang, Dr. Paul A. Dayton, and Dr. Marie Muller for their invaluable suggestions on my research. I am grateful to Dr. Xiaoning Jiang and Dr. Paul A. Dayton, for providing me the research equipment and freedom to conduct experiments in their labs. I would also like to thank Dr. Muller and the members of her research group, who never hesitated to offer me their help.

I would like to thank all the members of the Acoustics and Ultrasonics Lab, for their continuous help and the happy time that we spent together: Dr. Chen Shen, Dr. Tai-Yun Huang, Dr. Ni Sui, Ms. Juanjuan Gu, Mr. Sean Maguire, Dr. Yong Yang, Mr. Bala Govind, Mr. Yuanchen Deng, and Mr. Nikhil Gerard. Our collaborative studies and discussions will always be great nutrients to my research. I am especially thankful for the friendship that I shared with Dr. Chen Shen and Ms. Juanjuan Gu.

I would like to express my gratitude to my collaborators, Dr. Shengqi Zhang, Dr. Sibo Li, Dr. Jinwook Kim, Dr. Sijia Guo, Dr. Yangbo Xie, Dr. Jin Di, Ms. Yanqi Ye, Dr. K. Heath Martin and Ms. Gloria Nyankima for their enthusiastic and considerate attitude to our collaborative research projects.

I would like to express my thankfulness to my friends and mentors during my Ph.D. career: Dr. Fuh-Gwo Yuan, Dr. Xiang Yan, Dr. Wei Jing, Dr. Jianguo Ma, Dr. Zhuochen Wang, Mr. Wei-yi Chang, Ms. Shujin Huang, Dr. Xiao Zhang, Mrs. Shiqin Xu, Mr. Yang Gao, Dr. Fengtao Bai and Mr. Cheng Chen. Your help and guidance walked me through my tough times.

Finally, my deepest gratitude to my parents, my brother, and my wife for their generous love and support, especially during my years of studying abroad. My parents are the best examples to show, that hard-work, integrity, and kindness, can build a happy and prosperous life. Their words and deeds taught me what to do and what spirit to carry when facing different situations in life. Their unconditional love is always with me and encourages me to fulfill my dreams. I apologize for the limited time that I spent with them, in the recent years. I am thankful to my brother for staying with my parents and taking care of them, while I am far away from home. I am grateful to my wife for her love and support and for all that she has sacrificed for me to do my doctoral study. Without her encouragement, I could never have completed this research. I am delighted to share this achievement with her.

TABLE OF CONTENTS

LIST OF TABLES

LIST OF FIGURES

Chapter 1 Introduction

Stroke is the third most common cause of death in the developed countries and affects more than 0.7 million Americans every year [1, 2]. Of all strokes, about 87% in the U.S. are ischemic strokes where blood flow to a region of the brain is blocked. Ischemic stroke is regarded as one of the most deadly diseases of impetuosity because of its sudden onset without any warning [3]. Ischemic stroke can induce adult disability, loss of brain function and even death within a few hours without proper treatment [4, 5]. Studies showed that only 15% to 60% of patients are able to reach the hospital within 3 hours of the symptom onset and this percentage has not changed for the last 10 years [6-8].

The function of a blood clot is to prevent damaged blood vessels from bleeding. Blood cells, e.g. platelets will affix to the damage site and generate the initial fibrin network. After the damage is repaired, the generation of plasmin will clean up the fibrin network under normal circumstances. However, hemodynamic changes and hypercoagulability, e.g. atherosclerosis, could result in an excessive blood clotting which is also known as thrombi that are rich in platelet and fibrin network. More details about the formation of thrombi will be introduced in Chapter 2.

The frontline treatment for stroke is thrombolytic drugs. By creating plasmin, the thrombolytic drug could lyse fibrin to cleave thrombi. There are several types of thrombolytic drugs and each of them has its own limitations. The most widely used thrombolytic drug currently is the tissue-type plasminogen activator (rt-PA). However, only 1.5% of total stroke cases could receive this thrombolytic drug treatment because of the strict limitation criteria.

Recently, the HIFU based thrombolysis approach was introduced and was demonstrated for its effectiveness both *in vitro* and *in vivo* [9-13]. This HIFU based method has a number of advantages: (1) it is noninvasive and does not require tissue plasminogen activator (t-PA), therefore could reduce the cost and eliminate associated side effects; (2) much faster treatment can be achieved, e.g., 300 mg clots can be disintegrated in 90 to 300 seconds [11]; and (3) the procedure can be guided by real-time ultrasonography for targeting and treatment monitoring [11]. Overall, the HIFU based approach is a potentially superior alternative thrombolysis strategy.

This dissertation focuses on the research of noninvasive thrombolysis using multi-frequency high intensity focused ultrasound excitations for stroke treatment. The main differences between this study and previous studies are as follows: 1) this study utilized MHz range (near 1.5 MHz) ultrasound which is safer than kHz range ultrasound for stroke treatment due to the smaller focal size. 1.5 MHz ultrasound was recently adopted in a rabbit model of embolic stroke; 2) this study investigated the effect of frequency difference, duty cycle and treatment time on dual-frequency HIFU for thrombolysis; 3) while the focus of this work is dual-frequency HIFU, triple frequency HIFU was also trialed to examine its performance in thrombolysis; 4) this study showed that by adding microbubbles as thrombolysis agent, the sonothrombolysis threshold could be further lowered and the sonothrombolysis efficiency could increase; 5) not only did the study focus on experimental sonothrombolysis, but it also utilized the microbubble theoretical work to prove that multi-frequency excitation could have a lower power threshold to initiate thrombolysis.

1.1 Motivation

Time to treatment since symptom onset is a crucial factor for the management of acute ischemic stroke patients since a prolonged treatment time leads to dramatic brain cells death. Tissue plasminogen activator (t-PA) has been widely used to treat acute ischemic stroke patients and is currently the only FDA approved treatment approach for this disease. This treatment, however, suffers from a short time window as t-PA thrombolysis is only effective within 4.5 hours of symptom onset [14]. This approach is also slow and is characterized by a low recanalization rate [15]. Additionally, it could also lead adverse effects, e.g., causing cerebral hemorrhage [16, 17].

Extensive efforts have been put into improving thrombolysis efficiency and ultrasound has been proposed and demonstrated as a superior approach [11, 18-30]. There are primarily three different ultrasound based approaches for improving the treatment of ischemic stroke: 1) low intensity ultrasound in combination with t-PA; 2) low intensity ultrasound in combination with t-PA and microbubbles (MBs); 3) HIFU alone. Depending on the approach used, the mechanism for sonothrombolysis could be either stable cavitation or inertial cavitation. For example, for low intensity ultrasound approaches, stable cavitation has a greater contribution [21] whereas, for HIFU based approaches, inertial cavitation plays a more important role [11]. It was demonstrated that using low intensity ultrasound in combination with t-PA might be an efficient and safe approach for treating acute stroke [22-25]. Shaw et al. utilized 120 kHz unfocused ultrasound and found that the lytic efficiency of recombinant t-PA (rt-PA) can be increased *in vitro*. The ultrasound administrated group yielded better lysis results than that of rt-PA alone group at all rt-PA concentration levels, i.e., 1-3 μg/mL [26]. Ishibashi

et al. adopted a rabbit femoral artery model and found that the ultrasound administrated group (exposed to 490 kHz, 0.13 W/cm2 ultrasound) had a higher recanalization ratio than that of the t-PA alone group [27]. To further augment the thrombolysis efficiency, MBs were introduced in addition to 170 KHz ultrasound in a human blood clot model [28]. Shawn et al. demonstrated that echogenic liposomes together with pulsed ultrasound at 120 KHz were effective in improving lysis using t-PA [29]. Zhou and Ramaswami compared sonothrombolysis efficiencies of different ultrasound systems and concluded that similar sonothrombolysis efficiency when using t-PA and MBs can be yielded [30]. Although sonothrombolysis has been shown to be successful *in vitro* and *in vivo*, symptomatic hemorrhage was found in some clinical studies [31-33], which is possibly due to the standing wave generated inside the cranial cavity [34]. In addition, these treatment approaches still rely on t-PA and could take hours to complete and suffer from the same side effects.

Recently, the HIFU based approach is a potentially superior alternative thrombolysis strategy. The high energy required for this approach at MHz frequency (due to the strong attenuation of the skull), however, hinders potential clinical applications of this promising approach. For instance, a recent numerical study showed that, in order to achieve a peak negative pressure above the cavitation threshold at 1.5MHz on the proximal M1 through intact skulls, the required total power can be as high as 130 kW assuming continuous waves, which is challenging in an emergency clinical environment [35]. By increasing the element number, the total power can be reduced. However, a large number of elements raise technical difficulties and cost from both making the transducer

array and driving system. In addition, any strategy that could further accelerate HIFU based lysis would be greatly beneficial to the patients.

Alternatively, it has been reported that multi-frequency sonication could significantly enhance cavitation activity and even reduce the cavitation threshold [36-41] which could be an alternative approach for clot lysis since the main mechanism of HIFU based thrombolysis approaches is inertial cavitation.

1.2 Objectives

The main theme of this dissertation is the development of new non-invasive thrombolysis methods in the treatment of stroke. By adding more frequencies and microbubbles, the thrombolysis efficiency has been improved and the thrombolysis acoustic power needed has been decreased. To provide insides on the mechanism of why inertial cavitation can be enhanced by multi-frequency, microbubble dynamics and acoustic cavitation signals data have been studied. Three different approaches of HIFU thrombolysis and the mechanism of acoustic cavitation were aimed to be researched for *in vitro* applications: 1) multi-frequency static model, 2) microbubble mediated multi-frequency static model, 3) microbubble mediated multi-frequency with flow system, 4) numerical investigation of inertial cavitation.

1.3 Dissertation outline

In this dissertation, three different approaches of HIFU thrombolysis and numerical investigation of microbubble inertial cavitation are presented. Chapter 1 will be a general introduction. The background of HIFU based thrombolysis and microbubble dynamics are described in Chapter 2. All the detailed information regarding relevant theories and

modeling methods are provided in the sub chapters of Chapter 2. In Chapter 3, comprehensive study on multi-frequency HIFU thrombolysis at MHz range is presented. Chapter 4 includes the study on microbubble mediated multi-frequency HIFU thrombolysis. Numerical investigation of microbubble inertial cavitation is presented in Chapter 5. Finally, conclusion and future work are described in Chapter 6 followed by the Appendices.

Chapter 2 Background

2.1 Introduction to stroke

Stroke is a disease that happens within the brain, caused by the obstruction or partially obstruction of the arteries. It has been the third most common cause of death in the developed countries and affects more than 0.8 million Americans every year [1, 2]. Someone dies from stroke every four minutes.

There are different types of strokes. Ischemic stroke, account for 87% of all strokes, is caused when a blood clot blocks the blood flow in the brain while hemorrhagic stroke is caused by a blood vessel rupture and prevent blood flow to the brain. A transient clot may cause a transient ischemic attack or mini stroke. Despite the types of strokes, they all stop the blood vessel from carrying oxygen and nutrients to the brain which will cause the death of the brain cells and result in disability, loss of brain function and even death within a few hours without proper treatment [4, 5].

Before a further discussion of the stroke, a detail introduction of a blood clot should be addressed first. The function of blood clot is to prevent damaged blood vessels from bleeding. Blood cells, e.g. platelets will affix to the damage site and generate the initial fibrin network. After the damage is repaired, the generation of plasmin will clean up the fibrin network under normal circumstances. However, hemodynamic changes and hypercoagulability, e.g. atherosclerosis, could result in an excessive blood clotting which is also known as thrombi that are rich in platelet and fibrin network. Fibrin is the primary structural protein of the blood clot, the essential purpose of which is to stop bleeding [42]. Figure 2.1 showed the structure and mechanical properties of fibrin. The red blood cells

and platelets are trapped within the fibrin fibers that forms a viscous, sticky blood clot [42]. Figures 2.2 and 2.3 further illustrate the process of the formation of a blood clot during a blood vessel damage where TF is tissue factor and MP is microparticles [43].

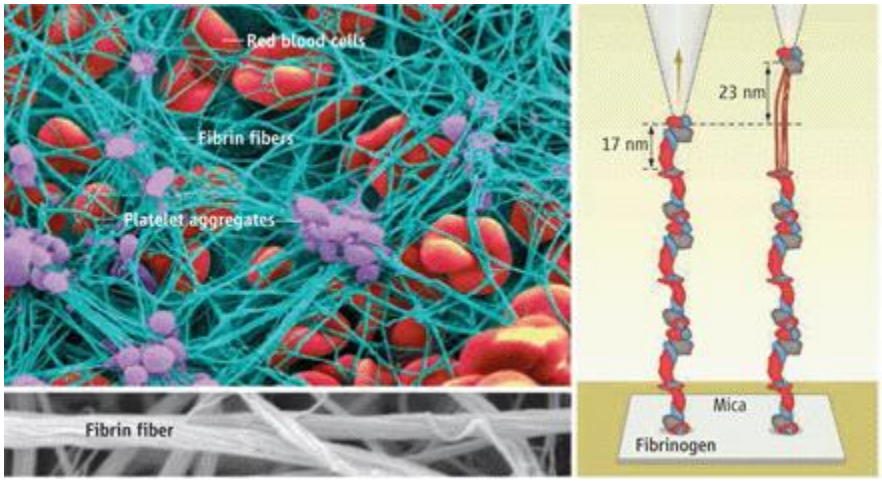

Figure 2.1 Structure and mechanical properties of fibrin [42].

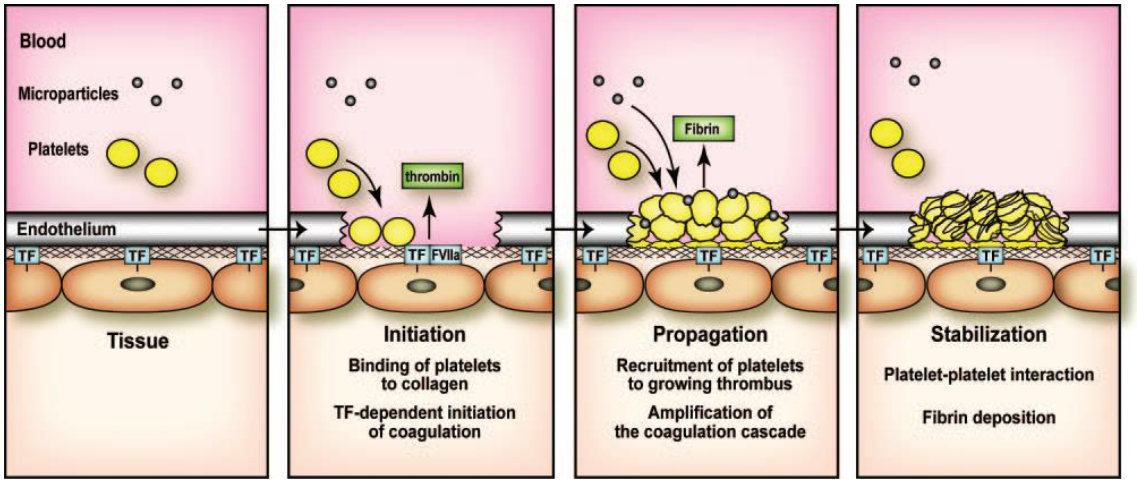

Figure 2.2 Formation of a clot at the site of blood vessel injury [43].

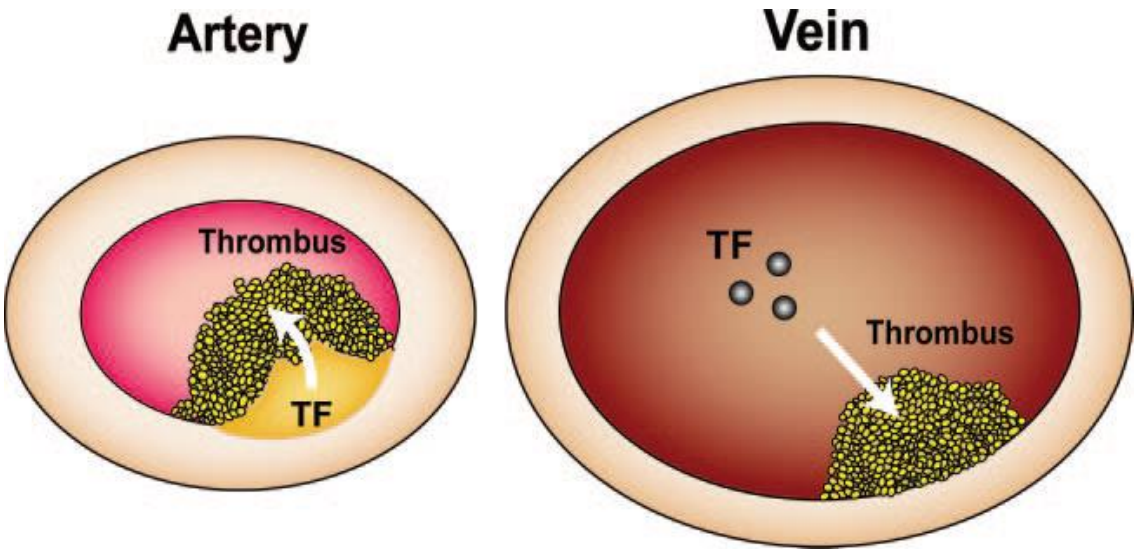

Figure 2.3 Contribution of a vessel wall and MP TF to arterial and venous thrombosis [43].

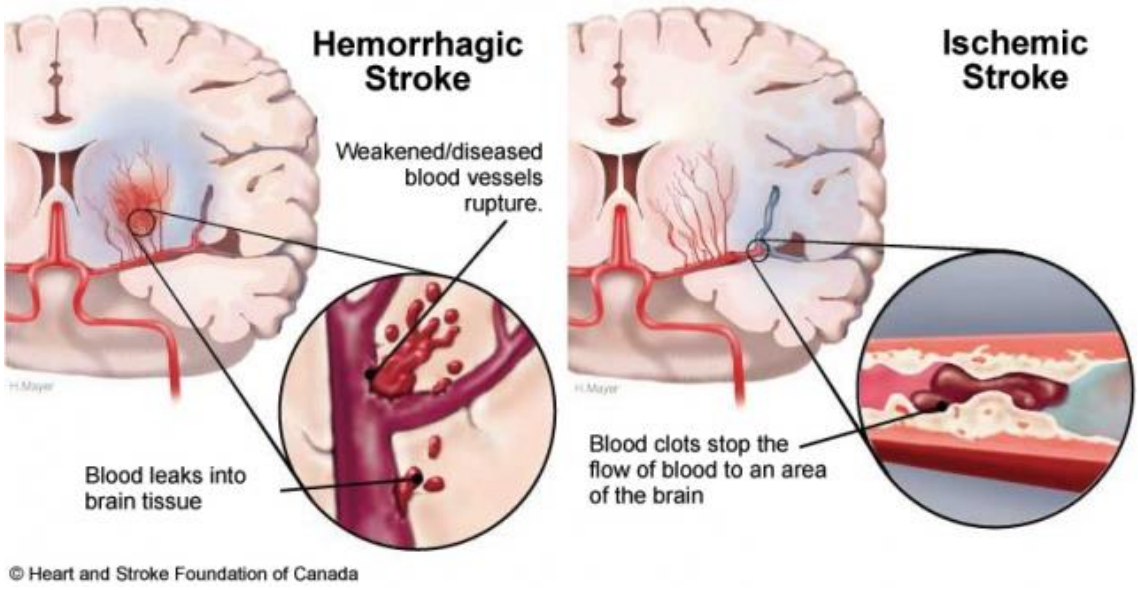

Figure 2.4 Demonstration of strokes. Hemorrhagic stroke on the left and ischemic stroke on the right.

Once the clot blocks the blood flow in the brain area, it will cause a stroke Fig. 2.4 The effects of a stroke depend on many factors as the brain manages numerous human functions and is an extraordinarily complicated organ. Every part of the brain has its own functionality and the stroke will affect the body depending on the location where it

occurs. When a stroke occurs on the right side, it might result in paralysis on the left side of the body, vision problems, quick, inquisitive behavioral style and memory loss. When it occurs on the left side, it might produce paralysis on the right side of the body, speech/language problems, slow, cautious behavioral style and memory loss (Fig. 2.5) [44].

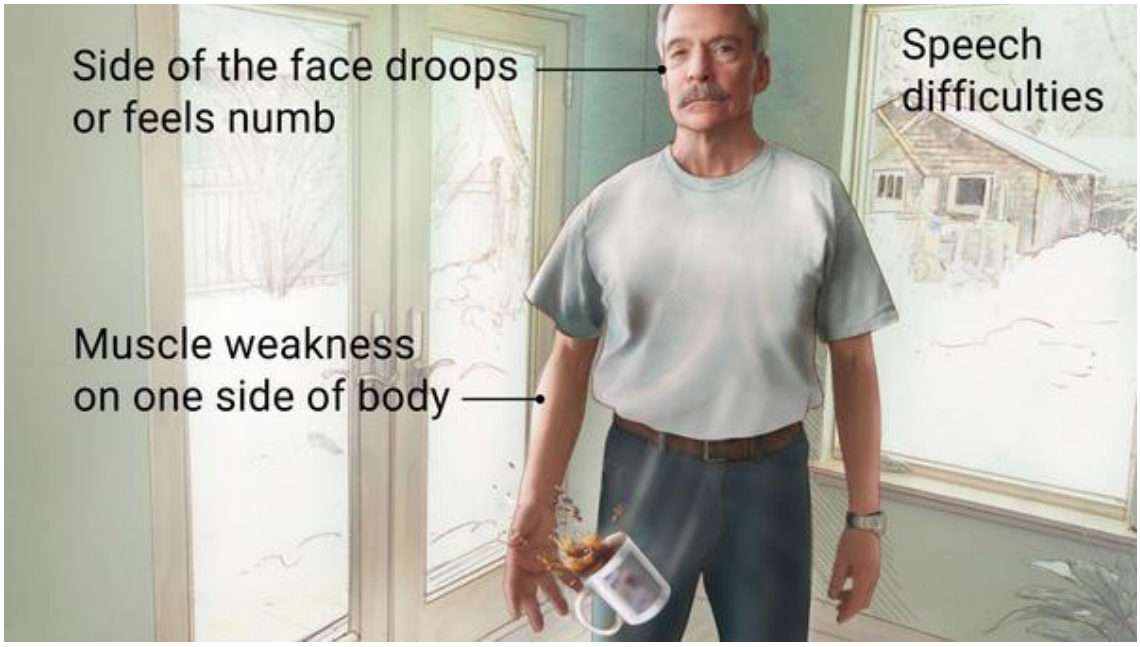

Figure 2.5 The effects of a stroke [44].

However, 80% of strokes can be prevented. The recognition of stroke when it happens is poor according to the public's knowledge of stroke warning signs. Less than half of stroke events were called 9-1-1 within 1 hour of the symptoms onset [45, 46]. Public education of stroke recognition is extremely important as researchers reported that the fibrinolytic treatment could be increased from 4.3% to 28.6% if all patients arrived within 3 hours of the stroke onset [47]. Effective community education and stroke education campaigns among middle school students would further increase the public recognition of stroke. There are 5 common stroke warning signs, sudden weakness, sudden speech

difficulty, sudden visual loss, sudden dizziness, and sudden, severe headache [48]. Over 88% of all strokes will also have one or more of face weakness, arm weakness, and speech difficulty [48].

Time to treatment since symptom onset is a crucial factor for the management of acute ischemic stroke patients since a prolonged treatment time leads to the dramatic death of brain cells. As a result, emergency evaluation and diagnosis of acute ischemic stroke are extremely important. Some procedures to evaluate the patient include emergency triage and initial evaluation, patient history, physical examination, neurological examination and stroke scale/scores, access to neurological expertise and diagnostic tests [46]. There are also several other early diagnoses, such as brain and vascular imaging, where ultrasound plays a key role.

Most of the treatments for stroke are categorized as intravenous fibrinolysis. It has been the most widely accepted therapy for acute stroke treatment since FDA approved the use of rtPA in 1996 [15, 49-55]. The time window of acceptance of the rtPA drug was 3 hours with an approximate 90 mins treatment [56]. This approach is also slow and is characterized by a low recanalization rate [15]. Additionally, it could have severe adverse effects, e.g., causing cerebral hemorrhage [16, 17]. A study showed that intracranial hemorrhage occurred in 6.4% of the patients treated with intravenous rtPA, while only 0.6% of patients who were given placebo were affected [56, 57].

The initiation of intravenous rtPA treatment time window has also been debated for a long time. With a data from 6 large intravenous rtPA tails pool, the odds ratio showed a 2.81 for within 1.5 hours of symptom onset after 3 months of the treatment and 1.55 for a time window of 1.5 to 3 hours, 1.4 within 3 to 4.5 hours and 1.15 within 4.5 to 6 hours

[58]. This indicated the fundamental importance of minimizing total ischemic time and restoring blood flow to the threatened but not yet infarcted tissue as soon as feasible. Although the maximum time window in which fibrinolytic therapy may be given in many patients has been expanded to 4.5 hours, clinical trial evidence indicates a much higher success rate if the treatment is within 1 hour [46]. Researchers also suggested that 80% of the patients suffering a stroke should receive treatment within 1 hour of being brought to the hospital [46, 59-61].

Extensive efforts have been put into improving thrombolysis. Ultrasound has been proposed and demonstrated as a superior approach [11, 18-30]. There are primarily three different ultrasound based approaches for improving the treatment of ischemic stroke: 1) low intensity ultrasound in combination with t-PA; 2) low intensity ultrasound in combination with t-PA and microbubbles (MBs); 3) HIFU alone. It was demonstrated that using low intensity ultrasound in combination with t-PA might be an efficient and safe approach for treating acute stroke [62]. The EKOS technology reported an intra-arterial or intra-clot delivery of ultrasound via a catheter (fig 2.6) [63]. Shaw et al. utilized 120 kHz unfocused ultrasound and found that the lytic efficiency of recombinant t-PA (rt-PA) can be increased *in vitro*. The ultrasound administrated group yielded better lysis results than that of rt-PA alone group at all rt-PA concentration levels, i.e., 1-3 μg/mL [26]. Ishibashi et al. adopted a rabbit femoral artery model and found that the ultrasound administrated group (exposed to 490 kHz, 0.13 W/cm2 ultrasound) had a higher recanalization ratio than that of the t-PA alone group [27]. To further augment the thrombolysis efficiency, MBs were introduced in addition to 170 KHz ultrasound in a human blood clot model [28]. Shawn et al. demonstrated that echogenic liposomes

together with pulsed ultrasound at 120 KHz were effective in improving lysis using t-PA [29]. Zhou and Ramaswami compared sonothrombolysis efficiencies of different ultrasound systems and concluded that similar sonothrombolysis efficiency when using t-PA and MBs can be yielded [30]. Although sonothrombolysis has been shown to be successful *in vitro* and *in vivo*, symptomatic hemorrhage was found in some clinical studies [31-33], which is possibly due to the standing wave generated inside the cranial cavity [34]. In addition, these treatment approaches still rely on t-PA and could take hours to complete and suffer from the same side effects. The details of ultrasound in the treatment of stroke will be further introduced in the following sessions.

2.2 Ultrasound in medicine and biology

Ultrasound has been involved in various biomedical applications due to its non-invasive property. Not only diagnostic ultrasound but also therapeutic ultrasound has been researched a lot over the past decades [64]. The principle of ultrasound diagnostic applications is that the ability of ultrasound could penetrate biological tissue and return signals with tissue information which determines the tissue properties while only causing microscopic or no damage to the tissue. To date, ultrasound imaging has been accepted as the most widely used diagnostic tool in many biomedical applications [65]. Table 2.1 showed the advantages of ultrasound imaging over other imaging methods [65]. Ultrasound provides real-time cross-sectional images while keeping the cost-effective [66]. More recently, microbubble/nanodroplet contrast agent has been added in advanced ultrasound imaging to further increase the imaging quality for specific applications [67].

The details of the microbubbles will be introduced in the next session.

The biological changes in tissue due to the interaction with ultrasound was first reported in 1927 [68]. Since then, the use of therapeutic ultrasound to treat people with pain, musculoskeletal injuries and soft tissue lesions has been over 60 years [69]. Tissue heating was the major goal at first, and it was used for soft tissue injuries [70]. Recent research has been focused on either high intensity focused ultrasound for tissue ablation or low intensity ultrasound to stimulate physiological processes [70]. The major therapeutic effects include thermal effect and non-thermal effects such as mechanical effects, cavitation, acoustic streaming, periodic acoustic pressure [70].

To understand these major effects, the fundamental theory of acoustics is then introduced in the following session.

Table 2.1 Comparison of imaging methods [65].

Modality	Ultrasound	X-ray	CT	MRI
What is imaged	Mechanical properties	Mean tissue absorption	Tissue absorption	Biochemistry (T_1 and T_2)
Access	Small windows adequate	2 sides needed	Circumferential Around body	Circumferential Around body
Spatial resolution	Frequency and axially dependent 0.3–3 mm	~1 mm	~1 mm	~1 mm
Penetration	Frequency dependent 3–25 cm	Excellent	Excellent	Excellent
Safety	Very good	Ionizing radiation	Ionizing radiation	Very good
Speed	100 frames/sec	Minutes	½ minute to minutes	10 frames/sec
Cost	$	$	$$$$	$$$$$$$$
Portability	Excellent	Good	Poor	Poor

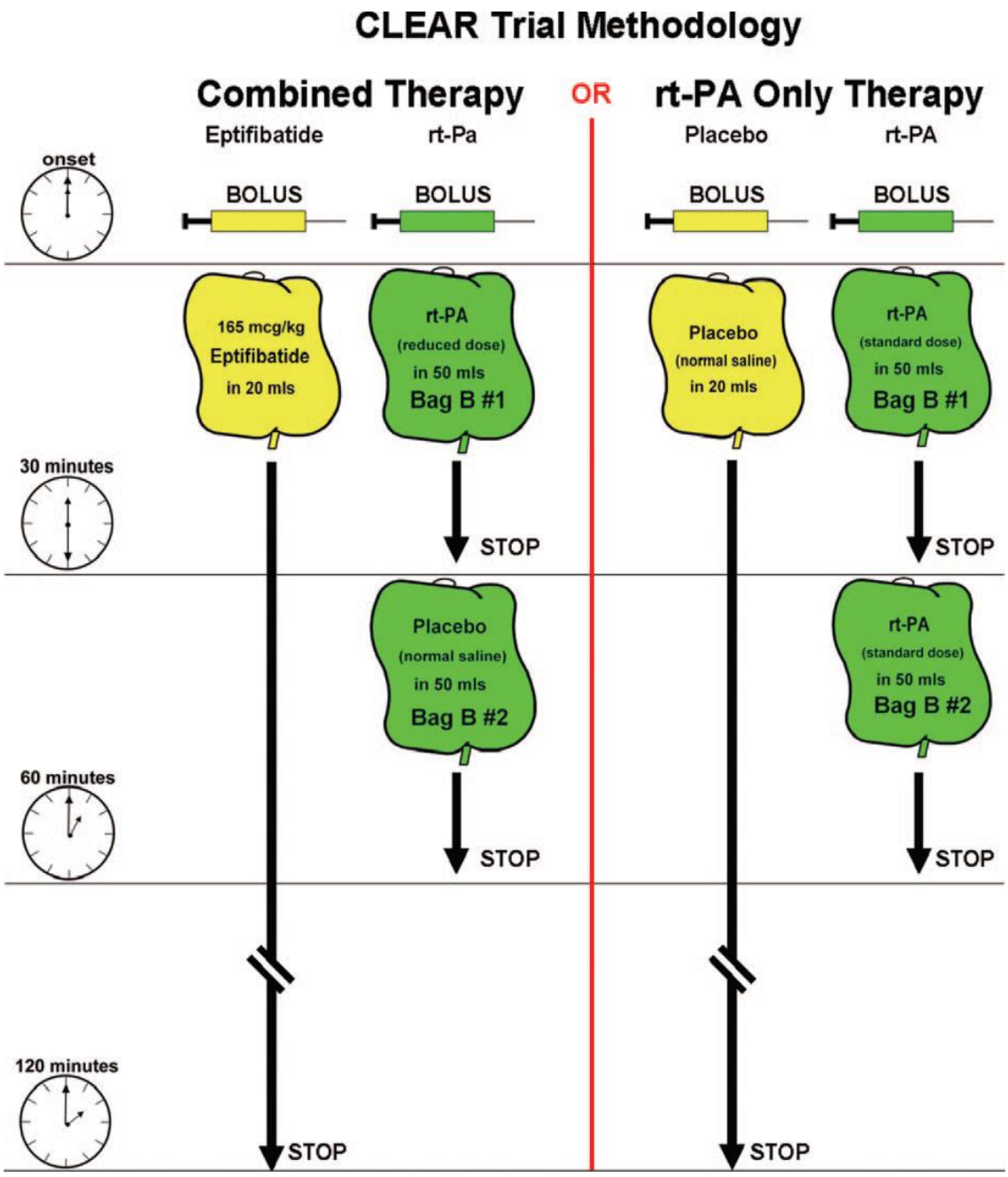

Figure 2.6 Bolus and infusion methodology for the 2 arms of the CLEAR trial [63].

2.2.1 Acoustic wave equation and propagation in tissue

When ultrasound interacts with a tissue, a portion of the sound gets reflected and absorbed, while the remaining sound is transmitted through it.

The displacement of a wave propagating in space is a function both of position and of time:

$$u = u(x,t) \tag{3.1}$$

Where u is the local particle velocity, t is time and x is the space variable along the direction of propagation of the sound waves.

Let the speed of the propagating wave be c. Then a Galilean transformation:

$$x' = x - ct \tag{3.2}$$

The wave equation could thus be transformed into:

$$u(x,t) = u(x') = f(x - ct) \tag{3.3}$$

For a one-dimensional plane wave along the x direction, according to Hooke's Law, the displacement can be derived as:

$$\frac{\partial u}{\partial x} = -\frac{p}{\rho c^2} \tag{3.4}$$

where u is the displacement of the particles in the medium, p is the acoustic pressure at position x, c is the speed of sound and ρ is mass density of the medium.

Newton's second law applied locally in the medium gives,

$$\rho \frac{\partial^2 u}{\partial t^2} = -\frac{\partial p}{\partial x} \tag{3.5}$$

Combining the equation 2.4 and equation 2.5, we can derive the one-dimensional longitudinal wave equation. This equation is only valid in homogeneous, linear, lossless media, without any acoustic sources:

$$\frac{\partial^2 u}{\partial x^2} = \frac{1}{c^2}\frac{\partial^2 u}{\partial t^2} \tag{3.6}$$

A solution to an equation of the form is:

$$u(x,t) = A\exp\left\{i\left[k(x-ct)+\varepsilon\right]\right\} \tag{3.7}$$

where A, k, and ε are constants.

When an acoustic wave propagates in a tissue, the amount of energy reflected and transmitted depends on the acoustic impedance. Most acoustic media for biomedical ultrasound is tissues which have an acoustic impedance similar to that of water (1.5×106 Pa·s/m), the acoustic impedance (z) is defined as:

$$z = \frac{p}{u} \approx \rho c \tag{3.8}$$

Impedance values of different human tissues are listed in table 2.2.

The other acoustic parameters could be calculated according to the acoustic impedance.

The pressure reflection coefficient R between tissue 1 and tissue 2 is:

$$R = \frac{z_2 - z_1}{z_2 + z_1} \tag{3.9}$$

The acoustic transmission coefficient T from tissue 1 to tissue 2 is:

$$T = \frac{2z_2}{z_2 + z_1} \tag{3.10}$$

According to the variation of acoustic impedance of diverse types of tissue, e.g. in fat and bone are different compared to the other types of tissue (table 2.2) [71]. Diagnostic and therapeutic ultrasound applications need to consider all the reflection, transmission and attenuation of all types of tissue. For example, in the treatment of stroke, the propagation of ultrasound should be transmitted through the skull, which will have a strong reflection between the skull boundaries due to the impedance mismatch. It is necessary to redesign the ultrasound beam to perform a transcranial therapy [72-75].

Another concern for ultrasound applications is safety. For diagnostic ultrasound, thermal and mechanical damage on tissue should be concerned in terms of acoustic intensity (I) and mechanical index (MI) [76, 77].

2.2.2 Acoustic intensity

Acoustic intensity describes the acoustic power applied on the unit area. It can be used to evaluate the acoustic field.

$$I = \frac{W}{Area} \tag{3.11}$$

where W is the acoustic power, and Ares is the applied area size.

Table 2.2 Acoustic properties of biomedical ultrasound media [71].

Tissue type	Wave speed (m/s)	Acoustic impedance (MRayl)	Attenuation (dB/cm/MHz)
Blood	1550	1.67	0.15-0.25
Liver	1578	1.66	0.40-1.00
Kidney	1560	1.64	
Fat	1430-1450	1.33	1.00
Muscle	1585	1.70	0.57-3.00
Brain	1540-1550	1.68	0.44
Bone	3200-4000	6.47	30
Air	333	430×10^{-6}	

Acoustic intensity is the time average of instantaneous intensity, which is given by,

$$I(t) = p(t)u(t) \tag{3.12}$$

where I(t) is instantaneous acoustic intensity, p is acoustic pressure and u is the particle oscillation velocity in the medium.

$$I = \frac{1}{T}\int_0^T p(t)u(t)dt \tag{3.13}$$

where I is the acoustic intensity and T is the period.

For a single frequency wave, the pressure is:

$$p = \rho c u \tag{3.14}$$

so, the acoustic intensity can be rewritten as:

$$I = \frac{p^2}{\rho c} = \frac{p^2}{z} = \frac{P^2}{2z} \tag{3.15}$$

Where P is the amplitude of the acoustic pressure.

2.2.3 Mechanical index

Mechanical Index is one of the most important parameters for cavitation safety concern. It is defined as the ratio of peak negative pressure (PNP) (in MPa) and the square root of fundamental frequency (f) of the acoustic wave (in MHz),

$$MI = \frac{PNP}{\sqrt{f}} \tag{3.16}$$

A higher mechanical index will induce a larger bio-effect which is destructive and harmful to the tissue [77]. The upper limits of ultrasound applications guided by the Food and Drug Administration (FDA) in the US are provided in table 2.3 [71]. The safety guideline that is issued by the British Medical Ultrasound Society in terms of the mechanical index is summarized below [78]:

For *MI* < 0.3, the applied acoustic pressure is considered low and not much bio-effect occurred.

MI > 0.3, there is a possibility of minor damage to neonatal lung or intestine, thus neonatal exposure times at these levels should be kept to a minimum.

MI > 0.7: there is the risk of inertial cavitation for the microbubble contrast agent mediated imaging (there is also a theoretical risk of cavitation in the absence of microbubble contrast agent).

The U.S. FDA regulation states that diagnostic ultrasound cannot exceed an MI of 1.9. In most diagnostic ultrasound applications, the MI is less than 1.

Table 2.3 The upper limits of ultrasound applications provided by the Food and Drug Administration in the USA (FDA) [71].

	Derated I_{SPTA} (mW/cm^2)	Derated I_{SPPA} (mW/cm^2)	Mechanical index (*MI*)	Thermal index (*TI*)
All applications except ophthalmology	720	190	1.9	6.0
Ophthalmology	50		0.23	1.0

2.3 Microbubbles and cavitation

Microbubbles were first used as ultrasound contrast agent for medical imaging enhancement by altering the image contrast between different tissue and structures [79-83] (Fig. 2.7). A broad range of evidence showed that by contributing MBs, the cavitation threshold could be further decreased as HIFU could cavitate the pre-existing MBs easily and the cavitation event would be even stronger, thereby showing a promising

enhancement of sonothrombolysis *in vitro* and *in vivo* [28, 30, 84-92] (Fig. 2.8). Petit et al. reported the cavitation inside the clot as a result of MBs penetrate through the clot[88]. Tachibana et al. announced a 51.3% fibrinolysis with MBs compare with 33.3% without MBs[28]. Meairs and Hynynen claimed that the ultrasound cavitation threshold was lowered and caused less damage to other tissue by introducing MBs[89, 91]. Zhou et al. noted that by infusion of MBs, the Siemens ultrasound system could increase the thrombolysis efficiency from 42% to 57% without the present of a temporal bone[30].

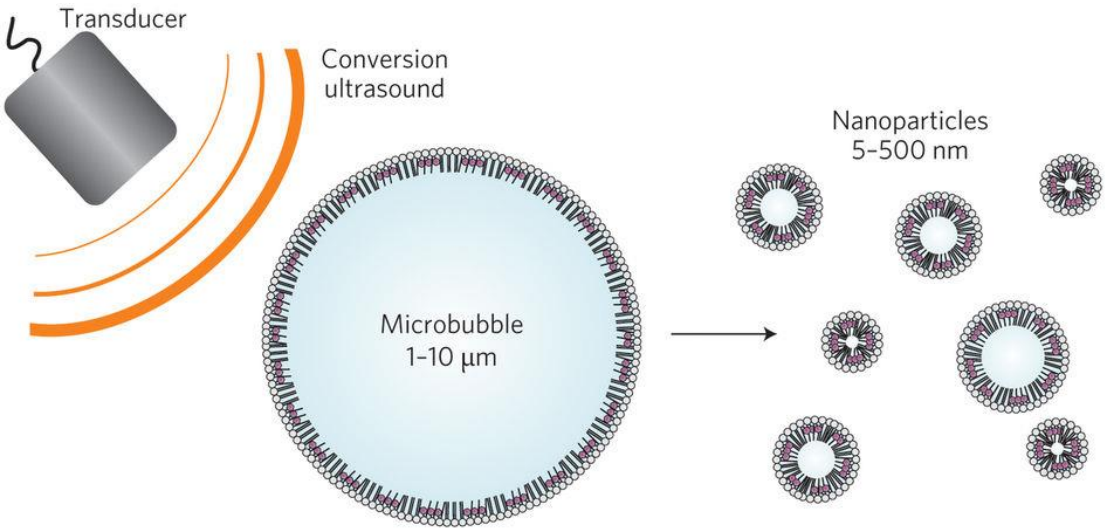

Figure 2.7 Schematic of an encapsulated microbubble and nanodroplets [83].

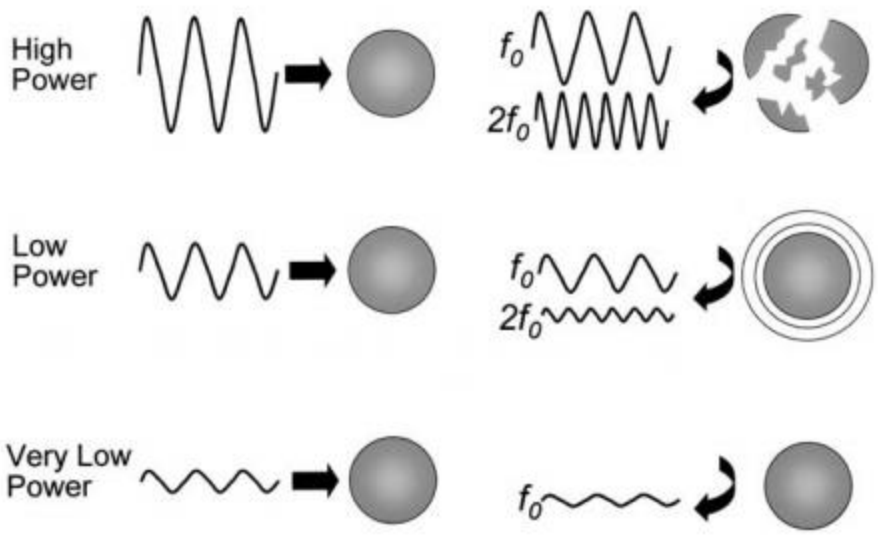

Figure 2.8 Microbubble response with different acoustic power [93].

Cavitation is the formation and activation of a gas filled bubble under acoustic excitation in a medium [94]. The gas bubble could either oscillate stably or expand gradually and eventually collapse (stable and inertial cavitation) [94]. Cavitation could lead to thermal effects as well as chemical and optical effects [95-98]. A strong acoustic field can occur during the inertial cavitation. Microscopic gas bubbles or impurities are generally present in a liquid will be forced to oscillate due to an applied high intensity acoustic field (higher than the threshold). With such low pressure, the microscopic gas bubbles will implode violently and generate high pressure and high temperature [99]. The cavitation forces and micro-jets generated during the collapse of the bubble could break the tissue and therefore could be used in tissue ablation and thrombolysis [62, 100-103]. The stable cavitation is the oscillation of microbubble in a liquid driven by an acoustic field. In stable cavitation, the applied acoustic intensity is lower than the threshold, so the bubble will oscillate stably. The bubbles in the liquid are more resistant to compression than to expansion and occur as a highly nonlinear oscillation, generating a lot of subharmonic,

ultraharmonic, harmonic and superharmonic (Fig. 2.9) [104]. The threshold upon which acoustic cavitation is initiated depends on a number of factors, including the ultrasound frequency, bubble size, and surrounding medium properties [75, 77, 105].

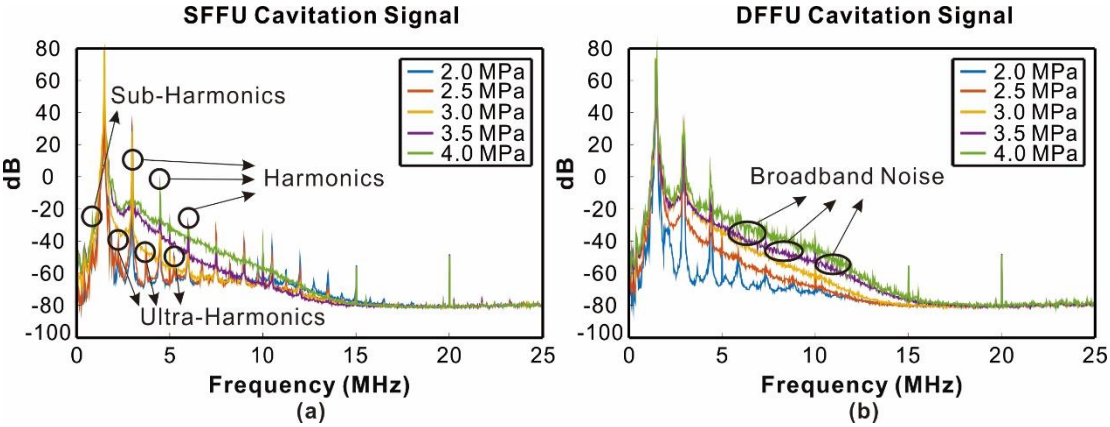

Figure 2.9 Detected cavitation signals for (a) SFFU and (b) DFFU at different pressure levels [104].

Chapter 3 Multi-frequency HIFU thrombolysis

Thrombolysis using multi-frequency high intensity focused ultrasound at MHz range: an *in vitro* study

This chapter present a new High intensity focused ultrasound (HIFU) based thrombolysis approach. HIFU has emerged as a promising drug-free treatment approach for ischemic stroke. The large amount of acoustic power required by this approach, however, poses a critical challenge to the future clinical translation. In this study, multi-frequency acoustic waves at MHz range (near 1.5 MHz) were introduced as HIFU excitations to reduce the required power for treatment as well as the treatment time. *In vitro* bovine blood clots weighing around 150 mg were treated by single-frequency and multi-frequency HIFU. The pulse length was 2 ms for all experiments except the ones where the duty cycle was changed. It was found that dual-frequency thrombolysis efficiency was statistically better than single-frequency under the same acoustic power and excitation condition. When varying the acoustic power but fixing the duty cycle at 5%, it was found that dual-frequency ultrasound can save almost 30% power in order to achieve the same thrombolysis efficiency. In the experiment where the duty cycle was increased from 0.5% to 10%, it was shown that dual-frequency ultrasound can achieve the same thrombolysis efficiency with only half of the duty cycle of single-frequency. Dual-frequency ultrasound could also accelerate the thrombolysis by a factor of 2-4 as demonstrated in this study. No significant differences were found between dual-frequencies with different frequency differences (0.025 MHz, 0.05 MHz, and 0.1 MHz) and between dual-frequency and triple-frequency. The measured cavitation doses of dual-frequency and triple-frequency excitations were at about the same level but both were significantly

higher than that of single-frequency [106].

This chapter has some of previously published material authored by Dingjie Suo as shown below. All previously published material was reprinted with permission from the publishers.

- **Suo, Dingjie**, Sijia Guo, Weili Lin, Xiaoning Jiang, and Yun Jing. "Thrombolysis using multi-frequency high intensity focused ultrasound at MHz range: an *in vitro* study." Physics in medicine and biology 60, no. 18 (2015): 7403.

3.1. Introduction

Stroke is the third most common cause of death in the developed countries and affects more than 0.7 million Americans every year [1, 2]. Of all strokes, about 87% in the U.S. are ischemic strokes where blood flow to a region of the brain is blocked. Ischemic stroke is regarded as one of the most deadly diseases of impetuosity because of its sudden onset without any warning [3]. Ischemic stroke can induce adult disability, loss of brain function and even death within a few hours without proper treatment [4, 5].

Time to treatment since symptom onset is a crucial factor for the management of acute ischemic stroke patients since a prolonged treatment time leads to dramatic brain cells death. Tissue plasminogen activator (t-PA) has been widely used to treat acute ischemic stroke patients and is currently the only FDA approved treatment approach for this disease. This treatment, however, suffers from a short time window as t-PA thrombolysis is only effective within 4.5 hours of symptom onset [14]. This approach is also slow and is characterized with a low recanalization rate [15]. Additionally, it could have severe adverse effects, e.g., causing cerebral hemorrhage [16, 17].

Extensive efforts have been put into improving thrombolysis efficiency and ultrasound has been proposed and demonstrated as a superior approach [11, 49, 62, 75, 77, 102, 107-113]. There are primarily three different ultrasound based approaches for improving the treatment of ischemic stroke: 1) low intensity ultrasound in combination with t-PA; 2) low intensity ultrasound in combination with t-PA and microbubbles (MBs); 3) HIFU alone. Depending on the approach used, the mechanism for sonothrombolysis could be either stable cavitation or inertial cavitation. For example, for low intensity ultrasound approaches, stable cavitation has a greater contribution [21] whereas for HIFU based approaches, inertial cavitation plays a more important role [11]. It was demonstrated that using low intensity ultrasound in combination with t-PA might be an efficient and safe approach for treating acute stroke [22-25]. Shaw *et al*. utilized 120 kHz unfocused ultrasound and found that the lytic efficiency of recombinant t-PA (rt-PA) can be increased *in vitro*. The ultrasound administrated group yielded better lysis results than that of rt-PA alone group at all rt-PA concentration levels, i.e., 1-3 μg/mL [26]. Ishibashi *et al*. adopted a rabbit femoral artery model and found that the ultrasound administrated group (exposed to 490 kHz, 0.13 W/cm^2 ultrasound) had a higher recanalization ratio than that of the t-PA alone group [27]. To further augment the thrombolysis efficiency, MBs were introduced in addition to 170 KHz ultrasound in a human blood clot model [28]. Shawn *et al*. demonstrated that echogenic liposomes together with pulsed ultrasound at 120 KHz were effective in improving lysis using t-PA [29]. Zhou and Ramaswami compared sonothrombolysis efficiencies of different ultrasound systems and concluded that similar sonothrombolysis efficiency when using t-PA and MBs can be yielded [30]. Although sonothrombolysis has been shown to be successful *in vitro* and *in*

vivo, symptomatic hemorrhage were found in some clinical studies [31-33], which is possibly due to the standing wave generated inside the cranial cavity [34]. In addition, these treatment approaches still rely on t-PA and could take hours to complete and suffer from the same side effects.

Recently, the HIFU based thrombolysis approach was introduced and was demonstrated for its effectiveness both *in vitro* and *in vivo* [9-13]. This HIFU based method has a number of advantages: (1) it is noninvasive and does not require t-PA, therefore could reduce the cost and eliminate associated side effects; (2) much faster treatment can be achieved, e.g., 300 mg clots can be disintegrated in 90 to 300 seconds [11]; and (3) the procedure can be guided by real-time ultrasonography for targeting and treatment monitoring [11]. Overall, the HIFU based approach is a potentially superior alternative thrombolysis strategy. The high energy required for this approach at MHz frequency (due to the strong attenuation of the skull), however, hinders potential clinical applications of this promising approach. For instance, a recent numerical study showed that, in order to achieve a peak negative pressure above the cavitation threshold at 1.5MHz on the proximal M1 through intact skulls, the required total power can be as high as 130 kW assuming continuous waves, which is challenging in an emergency clinical environment [35]. By increasing the element number, the total power can be reduced. However, a large number of elements raise technical difficulties and cost from both making the transducer array and driving system. In addition, any strategy that could further accelerate HIFU based lysis would be greatly beneficial to the patients.

Since the main mechanism of HIFU based thrombolysis approaches is inertial cavitation, one possibility to improve them is to develop an approach that is more efficient in

producing inertial cavitation. Lower frequencies (e.g., around 100 kHz) require lower power in order to achieve lysis since the inertial cavitation thresholds are lower. However, the larger focal zones could raise safety concerns. For instance, clot lysis has been demonstrated, with vessel damage, at a low frequency (0.68 MHz) in a rabbit femoral artery model [114], whereas no vessel damage was found at a higher frequency, i.e., 1.5 MHz [13, 102]. To achieve a reasonably small focal size for safety, it was suggested the operating frequency of the ultrasound should be in MHz range (e.g., 1.1 – 1.5 MHz), so that the focal width and depth may be smaller than the M1 vessel diameter [35].

Alternatively, it has been reported that multi-frequency sonication could significantly enhance cavitation activity and even reduce the cavitation threshold [36-40, 115]. Tatake and Pandit demonstrated that dual-frequency is more effective in inducing cavitation than single-frequency (16 kHz and 40 kHz, 25 kHz and 4 kHz combinations) [36]. The study by Ruo *et al.* suggested that dual-frequency (28 kHz and 0.87 MHz) could considerably increase clot mass dissolution [37]. Another study found that triple frequency (28 kHz, 1 MHz and 1.87 MHz combination) could further increase the cavitation yield [37]. Guo *et al.* and Ma *et al.* investigated the use of dual-frequency (multiple single frequency transducers and a single aperture dual frequency transducer) for tissue ablation and observed faster temperature elevation in *ex vivo* chicken breast tissue [38, 116]. A 30% reduction of inertial cavitation threshold was observed when using two neighboring frequencies (531 kHz and 565 kHz) compared with single-frequency (552 kHz) [39]. Most recently, it was noticed that the use of dual-frequency (535 kHz and 565 kHz) excitation could allow a 40% reduction on the power needed to achieve complete

thrombolysis in 300 seconds [40]. The aimed application for these two studies [39, 40] is transcutaneous thrombolysis, which justifies the usage of kHz range frequencies. The main differences between this study and [40] are as follows: 1) this study utilized MHz range (near 1.5 MHz) ultrasound which is safer than kHz range ultrasound for stroke treatment due to the smaller focal size. 1.5 MHz ultrasound was recently adopted in a rabbit model of embolic stroke [13]; 2) this study investigated the effect of frequency difference, duty cycle and treatment time on dual-frequency HIFU for thrombolysis; 3) while the focus of this work is dual-frequency HIFU, triple frequency HIFU was also trialed to examine its performance in thrombolysis.

3.2. Materials and methods

3.2.1 Clot preparation

Blood clots were prepared in a similar fashion as in [117]. Bovine blood was added into the 2.75% W/V calcium chloride solution (Fisher Scientific, Fair Lawn, NJ) as coagulant for clotting (5 ml/50 ml blood). The blood mix was drained into tygon tubes (6.35-mm ID, 7.94-mm OD) and sealed. The tubes were immersed in a 37 °C water bath for 3 hours and then stored at 4 °C for over 72 hours for complete clot generation and retraction. The clots were in cylindrical shape with a diameter at around 4 mm. Before thrombolysis experiments, the clots were immersed in 37 °C water for 1 hour and then placed in a PVC tube (4.65-mm ID, 6.55-mm OD) for thrombolysis experiments.

3.2.2 Experimental system

All experiments were conducted in a water tank (820×460×410 mm) with a 3-D translational stage (Velmex, Inc., Bloomfield, NY). The tank was filled with degased

water which was maintained at 37±0.5 °C during the entire course of each experiment by a bucket heater (720G 1000 Watts, Allied Precision Industries, Inc., Elburn, IL) and a real-time temperature controller (DSV QuickStart V3.3 Temperature controller, Dorkfood, Oakland, CA).

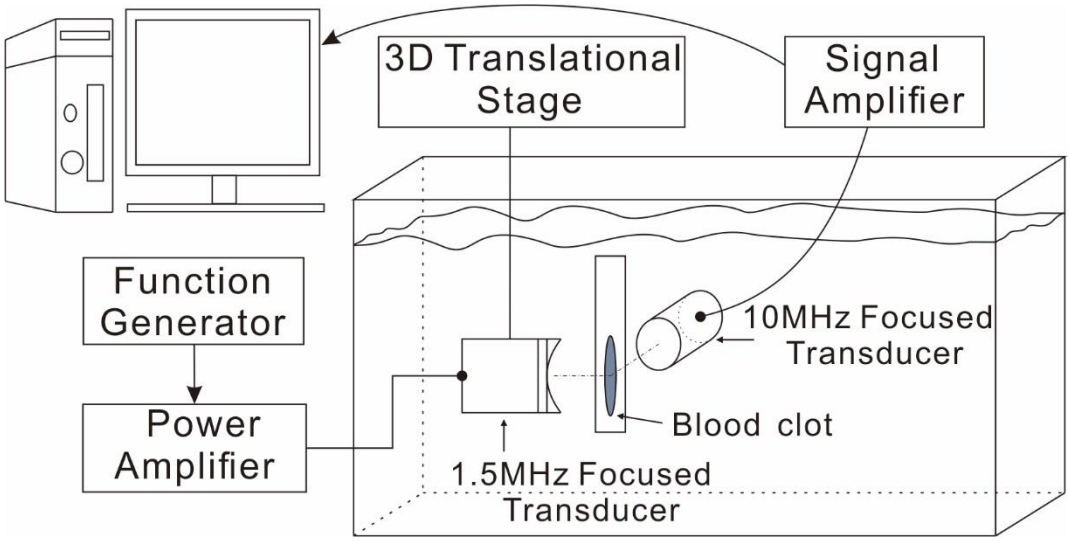

Figure 3.1 Schematic of the experimental system.

Figure 3.2 Real setup of the experimental system.

A sketch of the experimental system and the real setup are shown in Figures 3.1 and 3.2. A HIFU transducer with a nominal center frequency at 1.5 MHz (Blatek Inc., State

College, PA) was fixed on the 3-D translational stage and faced the blood clot sample. The HIFU transducer aperture diameter is 29.5 mm and the focal length is 30 mm. The -6 dB focal beam length and diameter are 9.14 mm and 1.13 mm, respectively. Another broad-band focused transducer with a center frequency at 10 MHz (Panametrics V309, Olympus, Center Valley, PA) was placed at 90° with respect to the 1.5 MHz HIFU transducer to collect the broad-band inertial cavitation signal. The focal length is 50.8 mm and the aperture diameter is 15.8 mm.

For the two transducers used in the experiment, the focal points of both transducers were located using the 3-D translational stage and a needle hydrophone (HNC-0200, ONDA, Sunnyvale, CA). During the cavitation signal collection period, the two foci were approximately coincided and located inside the PVC tube containing the blood clots.

The 1.5 MHz transducer was driven by a RF power amplifier (3100L, Electronics & Innovation, Rochester, NY) which amplified signals generated from a function generator (AFG3101, Tektronix Inc., Beaverton, OR) (Fig 3.4). Power output (1.3-4 watts) from the 1.5 MHz HIFU transducer was adjusted using the input voltage from the signal generator and calibrated by a power meter (UPM-DT-1000PA, Ohmic Instruments, St. Charles, MO) before and after each set of experiments. The peak negative pressure at the focus of the HIFU transducer was calibrated at 1.5 MHz using a hydrophone (HNA-0400, ONDA, Sunnyvale, CA) in combination with wave field modeling [118, 119]. Burst waves were used for all experiments. For all experiments except the ones where the duty cycle was varied, the pulse length was 2 ms (i.e., pulse repetition frequency was 500 Hz) and the duty cycle was 5%. The duty cycle was changed by adjusting the pulse length while maintain the same number of burst cycles.

Figure 3.3 Example of the input values from the functional generator.

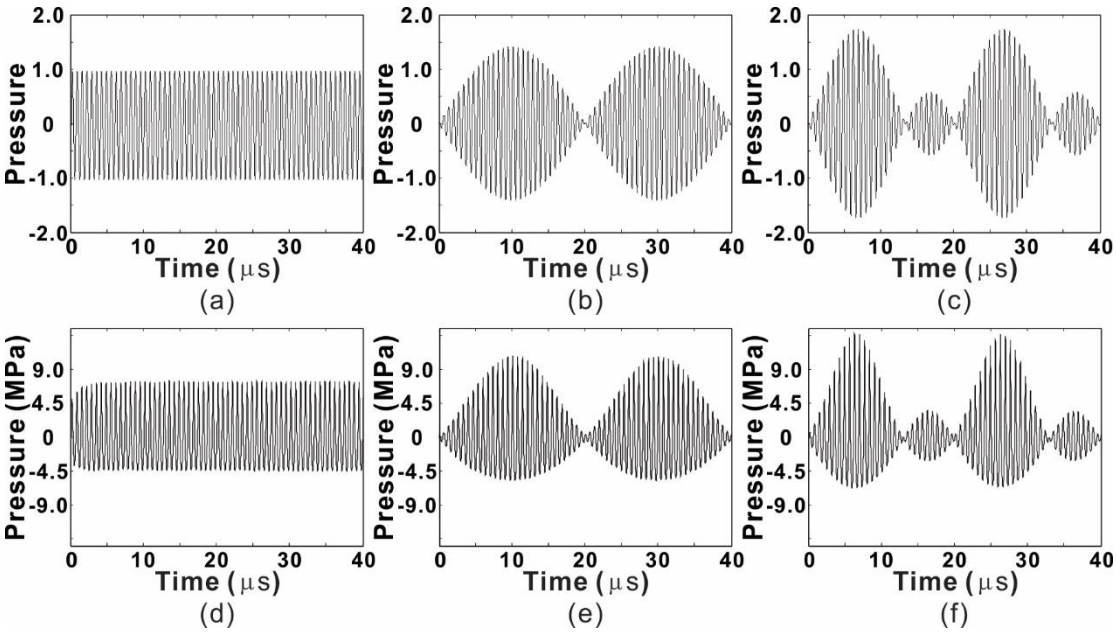

Figure 3.4 Input pressure waveforms for (a) single-, (b) dual- and (c) triple-frequency excitations. Measured pressure waveforms at the focus for (d) single-, (e) dual- and (f) triple-frequency excitations.

Single-frequency was at 1.5 MHz, dual-frequency was 1.45+1.5 MHz and triple-frequency was 1.4+1.45+1.5 MHz.

3.2.3 Experiment procedure

Each clot (Fig. 3.5 (a)) was cut into roughly 12-mm long pieces and flushed with saline solution. Each clot initially weighed 150 ± 20 mg (total number of clots used in the experiments was 250). Thereafter, the clot was pushed into the PVC tube filled with saline solution for sonication under HIFU. During the treatment, the 3-D translation stage was under the scan mode to move the HIFU transducer. The scanning step size was 2 mm to treat the entire clot and at each position the transducer stayed at rest for a period of time t/4 where t is the total treatment time. After the treatment, the debris from the PVC tube was injected onto a 100 μm filter and then flushed with saline solution and dried before weighing. A control group (five clots) was introduced and the same process was adopted except without HIFU treatment: the control group was submerged in water for 60 seconds without ultrasound.

Figure 3.5 Clot before and after treatment.

Multiple groups of experiments were performed at single frequency, dual-frequency, and triple-frequency excitations, i.e., 1.5MHz, 1.5MHz+1.475MHz, 1.5MHz+1.45MHz, 1.5MHz+1.4MHz, 1.5MHz+1.475MHz+1.45MHz, 1.5MHz+1.45MHz+1.4MHz. Dual-frequency and triple-frequency excitations were generated using ArbExpress signal generator software (ArbExpress, Tektronix Inc., Beaverton, OR) with equations shown below (examples are given for 1.5MHa+1.45MHz and 1.5MHz+1.45MHz+1.4MHz):

$$\mathrm{Sin}(1.5\times10^{6}\times2\pi)+\mathrm{Sin}(1.45\times10^{6}\times2\pi) \tag{4.1}$$

$$\mathrm{Sin}(1.5\times10^{6}\times2\pi)+\mathrm{Sin}(1.45\times10^{6}\times2\pi)+\mathrm{Sin}(1.4\times10^{6}\times2\pi) \tag{4.2}$$

Frequency difference greater than 0.1 MHz was not tried because of the relatively narrow bandwidth of the HIFU transducer. Very importantly, the output powers were adjusted to be identical among single, dual- and triple-frequency excitations for fair comparisons.

This was achieved with the assistance of the power meter. When generating the multi-frequency signals, weighting coefficients were applied to assure that each frequency produces about the same power. This is necessary because the frequency response of the HIFU transducer is not ideally flat from 1.4 to 1.5 MHz. Each group of comparison had one variable (e.g., peak negative pressure, treatment time, and duty cycle) while other parameters remained the same. Table 1 lists the relevant peak negative pressures, peak-to-peak input voltages, and the measured output powers under 5% duty cycle. Each set of treatments was repeated 5 times. Standard deviation and p-value were calculated. The p-value was computed using the T-test with one-tailed distribution in Matlab R2014a (The MathWorks, Inc., Natick, MA).

Table 3.1 Peak negative pressure (PNP), input voltage amplitude, and output power (OP) at each frequency under 5% duty cycle.

	Single-frequency					Dual-frequency					Triple-frequency	
PNP(Mpa)	4.5	5.0	5.5	6.0	6.5	4.5	5.0	5.5	6.0	6.5	5.0	5.5
P-P(mv)	470	530	590	650	710	690	767	860	963	1042	930	1050
OP(watts)	1.33	1.90	2.30	2.90	3.84	1.33	1.90	2.30	2.90	3.84	1.90	2.30

3.2.4 Cavitation dose measurement

Cavitation doses were measured at different frequencies and different peak negative pressures. The process is similar to that in [87, 120]. Briefly, the signal received by the 10 MHz focused transducer was amplified using a signal amplifier (AH-2020, ONDA, Sunnyvale, CA) and then transferred to a computer for processing. The cavitation signals were captured 10 times for each set of cavitation experiment with a three seconds interval. Each captured signal length was 30 ms which consisted of 15 bursts. Each set of cavitation experiment was therefore about 30 sec long. The sampling frequency was 50 MHz. Every single burst was extracted and then transformed into the frequency domain.

The root-mean-square (RMS) value was calculated for the spectra from 10.2 MHz to 10.4 MHz (this range was chosen to be close to the center frequency as well as to avoid the harmonics). For each capture, there will be 15 RMS values because of the 15 bursts. The mean of these 15 RMS values was then calculated. This was repeated for the 10 captures in each set of cavitation experiment, yielding 10 mean values, which was finally integrated with respect to the time to calculate the cavitation dose for the 30 sec cavitation experiment. At each frequency configuration and pressure, three cavitation experiments were conducted.

3.3. Results

Thrombolysis efficiencies with various peak negative pressures were first examined. To calculate the thrombolysis efficiency in percentage, the difference between the initial clot weight and the clot weight after treatment was divided by the initial weight. It is noted that the peak negative pressures were shown only for the 1.5 MHz single frequency ultrasound in figures. For dual-frequency and triple-frequency, the peak negative pressures were different in order to achieve the same output power. Theoretically, if the peak negative pressure of a single-frequency was p_{peak}, the highest peak negative pressures for the dual-frequency and triple-frequency should be $\sqrt{2}\, p_{peak}$ and $\sqrt{3}\, p_{peak}$, respectively (Figs. 3.4 a-c). However, due to the nonlinear distortion, the peak negative pressures at the focus for DFFU and TFFU were lower than those numbers (Figs. 3.4 d-f). More than three frequencies were not tried in this study because of the limitation of the function generator.

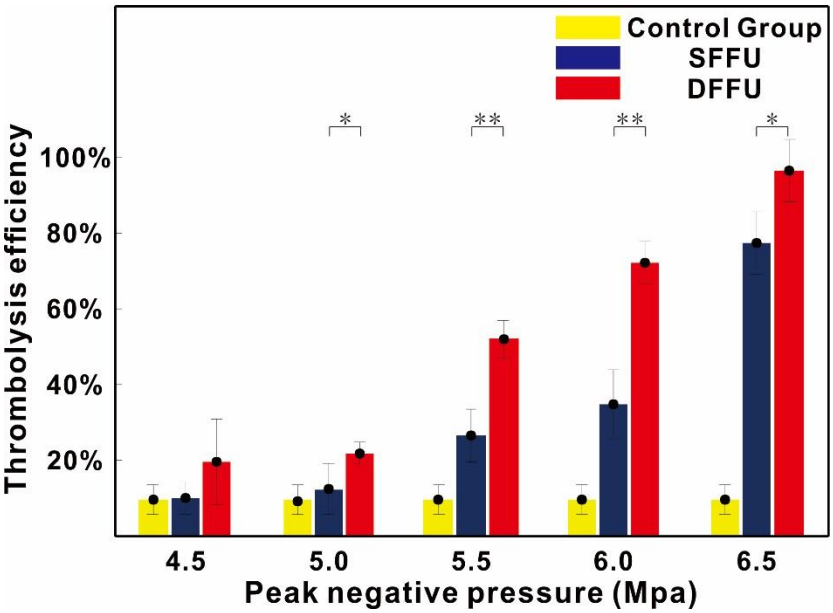

Figure 3.6 Thrombolysis efficiency v.s. peak negative pressure. The SFFU operated at 1.5 MHz and DFFU operated at 1.45+1.5 MHz. 5% duty cycle, 2 ms pulse length and 60s treatment time. (* p-value < 0.05; ** p-value < 0.001)

Figure 3.6 shows the thrombolysis efficiency with 60 seconds treatment time and 5% duty cycle. The dual-frequency focused ultrasound (DFFU) with 1.5+1.45 MHz excitation yielded a statistically better efficiency (p-value < 0.05) than single-frequency focused ultrasound (SFFU) at peak negative pressures higher than 5.0 MPa. SFFU only achieved an efficiency above 50% when the peak negative pressure was around 6.5 MPa whereas DFFU was effective at a pressure level as low as 5.5 MPa. Because the acoustic power is roughly proportional to pressure square, the DFFU was almost 30% more efficient in this case. Similar findings were reported in a previous study using kHz range dual-frequency, where dual-frequency was found to be about 40% more efficient in thrombolysis when varying the acoustic power/pressure [40]. At a peak negative pressure below 5.0 MPa, both SFFU and DFFU were not effective and the thrombolysis efficiencies were not significantly better than those of the control case. The thrombolysis efficiency of DFFU dramatically increased when the peak pressure increased from 5.0 to

5.5 MPa, implying that inertial cavitation likely had occurred. On the other hand, the thrombolysis efficiency of SFFU showed dramatic improvement when the peak pressure changed from 6.0 to 6.5 MPa.

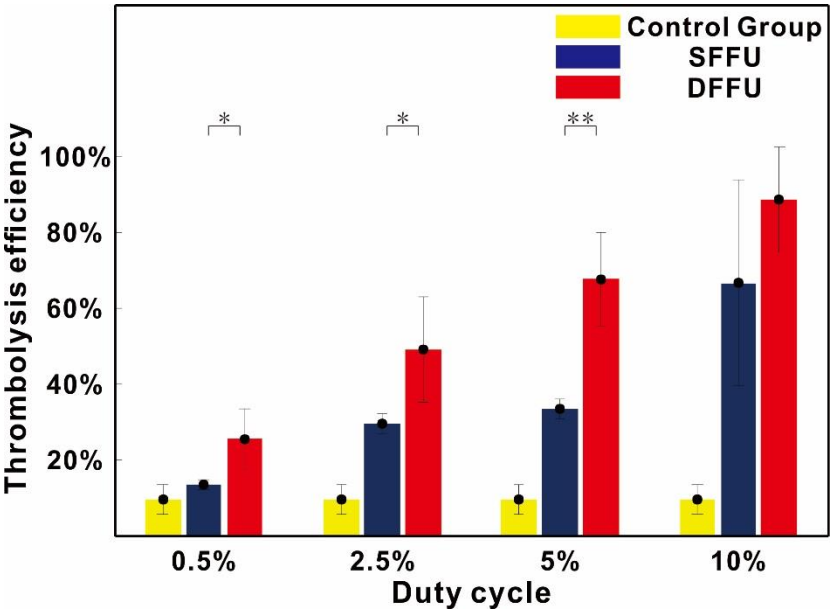

Figure 3.7 Thrombolysis efficiency v.s. duty cycle. The SFFU operated at 1.5 MHz and DFFU operated at 1.45+1.5 MHz. 60s treatment time, 5.5 MPa peak negative pressure. (* p-value < 0.05; ** p-value < 0.001)

The effect of duty cycle and pulse length on cavitation and thrombolysis was discussed previously in [121] for single-frequency excitations. The effect of duty cycle was examined here for both SFFU and DFFU. Figure 3.7 displays the relationship between thrombolysis efficiency and duty cycle at 5.5 MPa peak negative pressure with 60 seconds long sonication. 5.5 MPa peak negative pressure was chosen because at 5% duty cycle, inertial cavitation very likely occurred and lysis was clearly observed for DFFU. For both SFFU and DFFU, the thrombolysis efficiency increased with the duty cycle. DFFU thrombolysis efficiency was statistically better than that of SFFU at duty cycles lower than 10%. At 10% duty cycle, excellent thrombolysis efficiency was noted for both SFFU and DFFU. In clinical applications of thrombolysis, however, a low duty cycle will

probably be favored because the heating effect can be minimized. The heating can be particularly a problem in the skull due to the high absorption. Due to the fast increase of SFFU thrombolysis efficiency when changing the duty cycle from 5% to 10%, it is likely that the SFFU cavitation threshold pressure at 10% duty cycle was lower than 5.5 MPa but the threshold pressures at lower duty cycles were higher than 5.5 MPa. In this set of experiments, to achieve a thrombolysis efficiency above 60%, the DFFU requires a duty cycle at 5% whereas the SFFU requires a duty cycle at 10%. The required power for DFFU is therefore a half of that of SFFU, i.e., a 50% reduction.

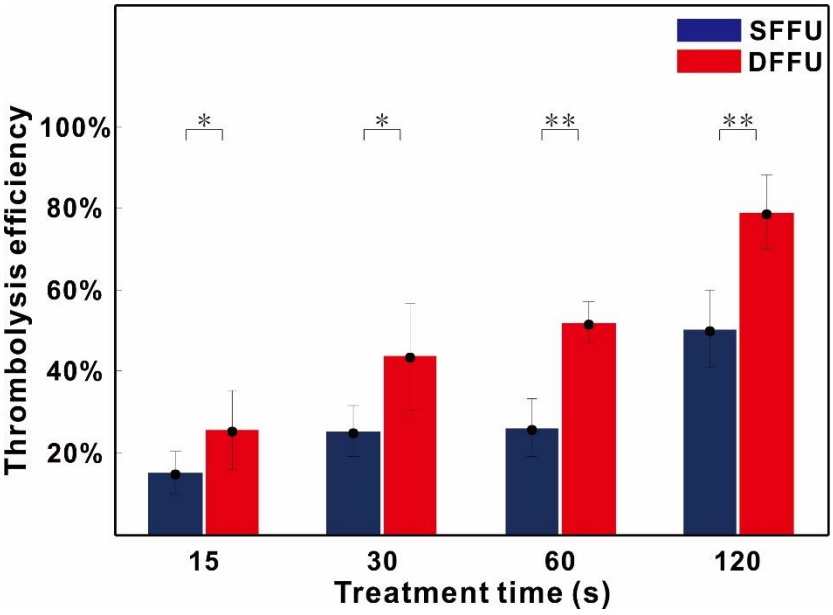

Figure 3.8 Thrombolysis efficiency v.s. treatment time. The SFFU operated at 1.5 MHz and DFFU operated at 1.45+1.5 MHz. 5% duty cycle, 2 ms pulse length and 5.5 MPa peak negative pressure. (* p-value < 0.05; ** p-value < 0.001)

The thrombolysis efficiency against treatment time is shown in Fig. 3.8. At peak negative pressure of 5.5 MPa, the average clot lysis rates for SFFU and DFFU were 1.06 mg/s and 1.72 mg/s (p-value < 0.001), respectively. DFFU was shown to be consistently better than SFFU. To achieve a same amount of efficiency (e.g., 50%), DFFU took around 30-60 sec

while SFFU took almost 120 sec. Therefore, DFFU can accelerate thrombolysis by a factor of 2-4 in this specific case.

Figure 3.9 illustrates the thrombolysis efficiency for different dual-frequency pairs under various peak negative pressures. Again, the peak negative pressure is for the single-frequency excitation under the equivalent power. The treatment time was 60 seconds and the duty cycle was 5%. Although these dual-frequencies could have distinct waveforms (Fig. 3.10), no evidence could be found as to which one would lead to better thrombolysis efficiency in a statistically significant way under the circumstance that the frequency difference is small (< 0.1MHz). Notably, at 6.5 MPa, all three dual-frequencies achieved almost 100% thrombolysis.

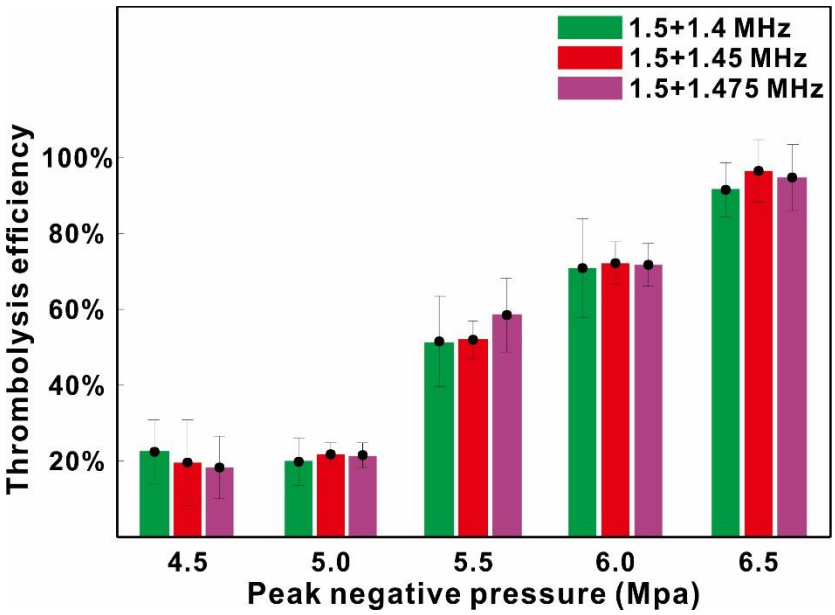

Figure 3.9 Thrombolysis efficiency for DFFU with different frequency differences. 5% duty cycle, 2 ms pulse length and 60s treatment time.

It was suspected that, the higher peak negative pressure from the dual-frequency excitation potentially led to the higher thrombolysis efficiency, since a higher negative

peak pressure could trigger inertial cavitation more easily. For this reason, triple-frequency focused ultrasound (TFFU) was also tested for thrombolysis since the highest peak pressure is even higher. The results shown in Fig. 3.11 did not reveal significantly better thrombolysis than DFFU at the two negative peak pressures tested, i.e., 5.0 and 5.5 MPa. These two pressure levels were chosen because the thrombolysis efficiency of DFFU dramatically increased from 5.0 MPa to 5.5 MPa, implying inertial cavitation likely had occurred in between these two pressures. TFFU still had statistically better thrombolysis efficiency than that of SFFU. The results suggested that, under the same acoustic power, both DFFU and TFFU could yield more efficient thrombolysis than SFFU at around or above 5.5 MPa. Although TFFU had the highest peak negative pressure among all, it did not outperform DFFU.

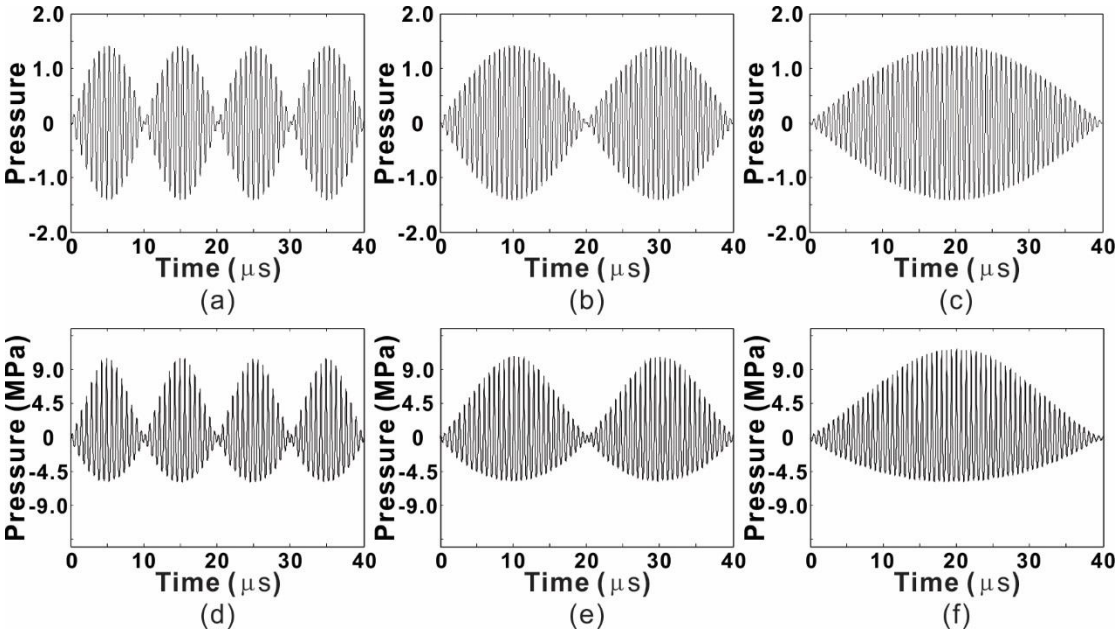

Figure 3.10 Input pressure waveforms for (a) 1.5+1.4 MHz, (b) 1.5+1.45 MHz and (c) 1.5+1.475 MHz excitations. Measured pressure waveforms at the focus for (d) 1.5+1.4 MHz, (e) 1.5+1.45 MHz and (f) 1.5+1.475 MHz excitations.

To understand the underlying mechanism of more efficient thrombolysis introduced by

DFFU and TFFU, the cavitation doses were measured at the various pressure levels under 5% duty cycle. Figure 3.12 shows typical spectra of SFFU, DFFU, and TFFU for a single burst. Results between 10.2 and 10.4 MHz were shown since these were used to calculate the cavitation dose. TFFU and DFFU had about the same amplitude which was about 5-15 dB higher than that of SFFU. Figure 3.13 showed the broadband noise that have a similar trend of figure 3.12. Figure 3.14 (a) shows the cavitation doses at different pressure levels. The cavitation doses of DFFU and TFFU were consistently higher than that of SFFU, which supports the hypothesis that the enhancement in thrombolysis is at least partly due the stronger inertial cavitation. Figure 3.14 (a) also indicates that inertial cavitation likely occurred after 6.5 MPa for SFFU and after 5.5 MPa for DFFU. The correlation between cavitation dose and thrombolysis efficiency (Fig. 3.14 (b)) showed an almost linear relationship with an R value of 0.96 which matches well with the previous study [120, 122]. The SFFU and DFFU cavitation doses were used to generate this figure.

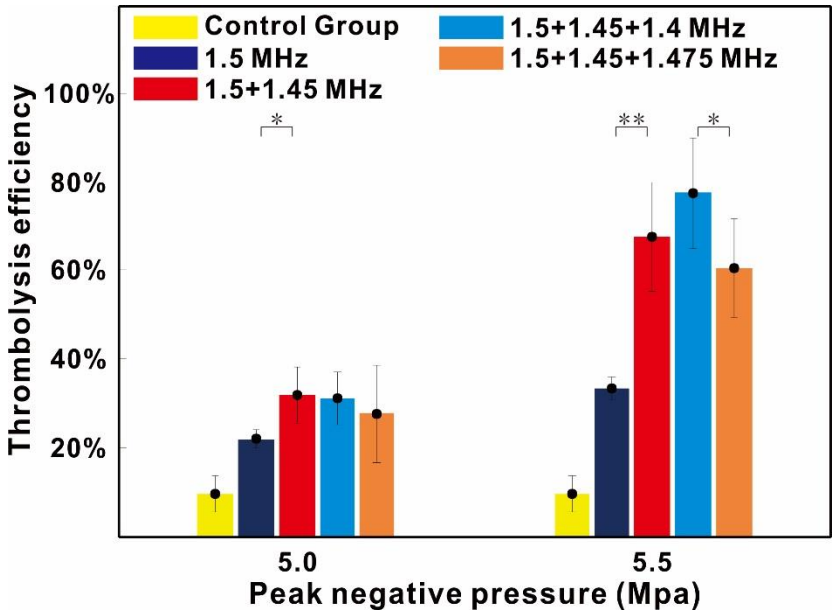

Figure 3.11 TFFU in comparison with SFFU and DFFU in terms of the thrombolysis efficiency at two different pressure levels. 5% duty cycle, 2 ms pulse length and 60s treatment time. (* p-value < 0.05; ** p-value < 0.001)

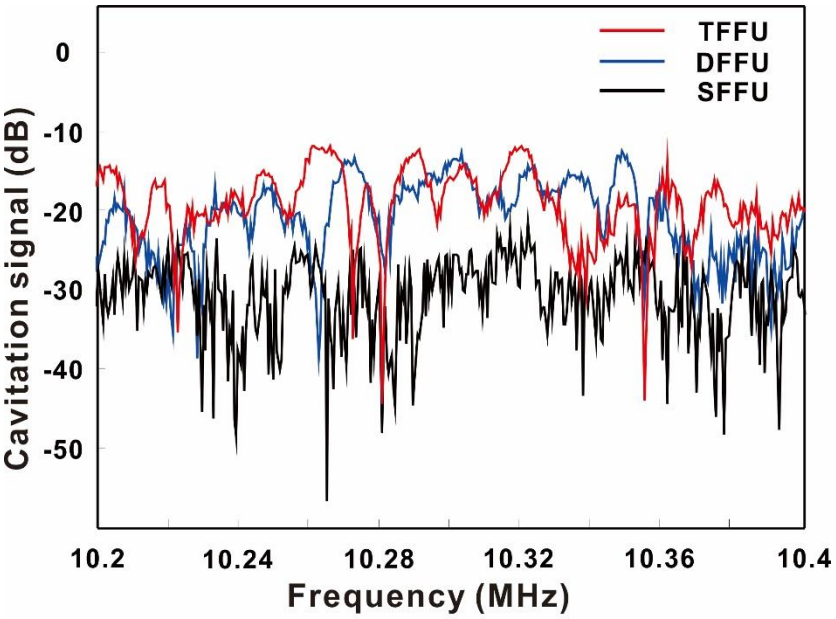

Figure 3.12 Measured cavitation signals during one burst for SFFU, DFFU, and TFFU from 10.2 MHz to 10.4 MHz. This region of the spectrum was later on used to calculate the cavitation dose.

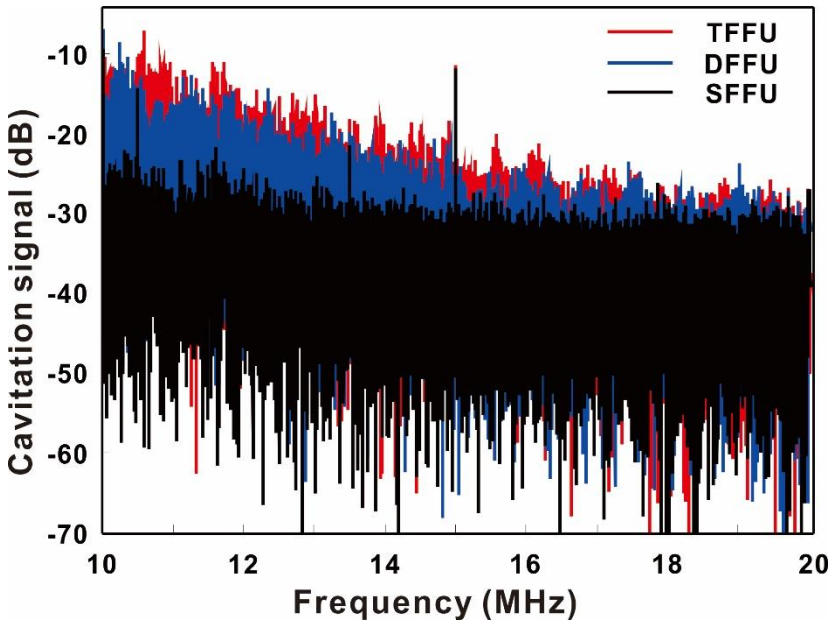

Figure 3.13 Measured cavitation signals during one burst for SFFU, DFFU, and TFFU from 10 MHz to 20 MHz. This region of the spectrum was showed the broadband noise of cavitation.

3.4. Discussions

Previous studies on HIFU alone thrombolysis have shown promising results. The high power required by this approach, however, is a serious drawback considering the future clinical translation of this approach for treating ischemic stroke. The significant thrombolysis efficiency improvement as demonstrated in this study suggested that multi-frequency sonication could potentially be a solution. Not only multi-frequency sonication could reduce the required power for achieving a certain level of thrombolysis efficiency, it could also considerably accelerate the lysis. The reason for better thrombolysis efficiency can be attributed to the stronger inertial cavitation resulted from multi-frequency sonication. Although this phenomenon has been discovered before, the mechanism is still relatively poorly understood.

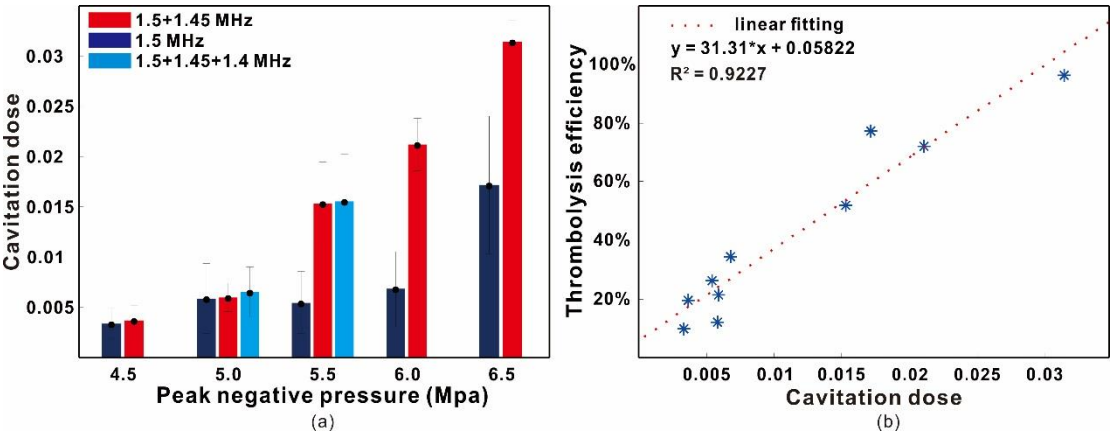

Figure 3.14 Measured cavitation signals during one burst for SFFU, DFFU, and TFFU from 10 MHz to 20 MHz. This region of the spectrum was showed the broadband noise of cavitation.

It has been argued that the stronger inertial cavitation from dual-frequency is because of the nonlinear frequency mixing [123]. This could partially explain why DFFU did not dramatically outperform SFFU at low pressure levels (Fig. 3.6), because the associated nonlinear effect is still low. The nonlinear effect causes the primary frequencies to

interact with each other, therefore resulting in waves with a wide range of frequencies. Particularly, the difference frequencies can be generated from the nonlinear wave propagation, which could yield very low cavitation threshold pressures. In addition, the generated difference frequencies could excite large size bubbles which collapse and break into a large number of small fragments (smaller bubbles) [124] and they will be excited by higher frequencies. Acoustic excitation of these smaller fragments is very efficient because these new born fragments contain little gas and are likely to collapse at a high rate [125]. However, Guo *et al.* [38] showed that, with two separate transducers operating at different frequencies (the non-confocal configuration), which effectively minimize the difference frequency and its harmonics generated at the focus, stronger inertial cavitation can still be consistently observed. Another possible reason for stronger cavitation is that the wider range of frequencies generated from the nonlinear interactions could be more energy efficient in producing cavitation as it is a random pressure, frequency dependent phenomena [125]. In other words, a wider frequency range could excite more bubbles with a wider nuclei bubble size range, resulting in stronger cavitation. On the other hand, this study did not show an advantage of using TFFU over DFFU, even though TFFU could generate a wider frequency spectrum. This could be because of the small frequency difference (<0.1 MHz) used in this study and using a greater frequency difference may show different results [37]. It should also be pointed out that Guo *et al.* also trialed TFFU (3.3 MHz + 1.5 MHz + 950 kHz) and it was not found to be more efficient than DFFU in tissue ablation [38]. The same argument could be used to explain why dual-frequencies with different frequency differences led to similar results, i.e., in all cases, the frequency differences were relatively small.

We also attempt to explain the enhanced cavitation from the perspective of peak negative pressures. A new figure (Fig. 3.15) was drawn which was edited from Figs. 3.4 (d-f) and 3.10 (d-f) with the pressures normalized by the peak negative pressure of SFFU. As indicated in Figs. 15 (a) and (b), the peak negative pressure of DFFU was higher than that of SFFU. As a result, while the SFFU did not reach the cavitation threshold, DFFU could reach the threshold because of the higher peak negative pressure. When comparing DFFU to TFFU, although TFFU had the highest peak negative pressure, it did not show any advantages over DFFU (Fig. 3.11). This could probably be understood by Figs. 3.15 (b) and (c). Suppose that the cavitation threshold pressure is 1.01, the SFFU peak negative pressure, which is at 1.0, is then barely below the threshold. When examining the waveforms of the two multi-frequency signals, it was found that for DFFU, the period of time in which the negative pressure amplitudes are above the threshold (the parts below the dash-dot line) is longer than that of TFFU, i.e., 18.7 μs vs. 14.7 μs. This might have compensated for the fact that TFFU has a higher peak negative pressure, leading to similar thrombolysis efficiency between DFFU and TFFU. The same hypothesis could be used to explain why the effect of frequency difference in DFFU is almost negligible (Fig. 3.9). As shown in Fig. 3.15 (d-f), all three waveforms with different frequency differences have about the same period of time in which the negative pressure amplitudes are above the threshold, i.e., 18.7 μs vs. 18.7 μs vs. 19.3 μs. They also have the same peak negative pressure.

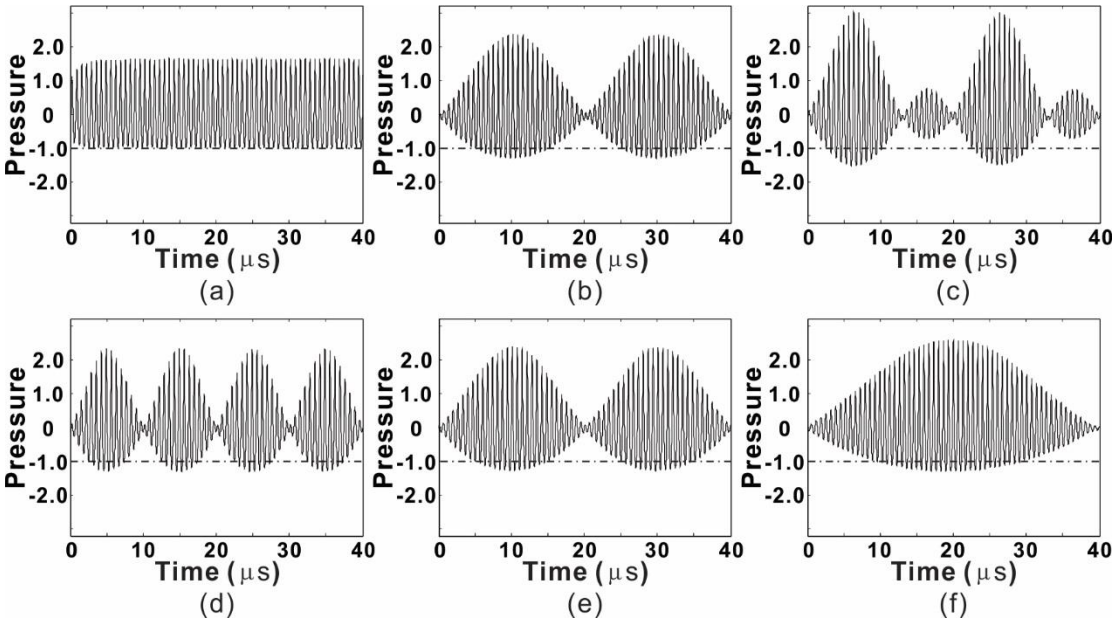

Figure 3.15 Normalized waveforms for (a) SFFU, (b) DFFU, and (c) TFFU; DFFU with different frequency differences: (d) 1.5+1.4 MHz, (e) 1.5+1.45 MHz, and (f) 1.5+1.475 MHz.

More extensive studies need to be carried out in the future in order to identify the exact mechanism of cavitation enhancement via multi-frequency sonication. One potential path is to perform bubble dynamics modeling and examine how bubble reacts to SFFU and DFFU [126]. The calculation of Zhang et al. showed that dual-frequency excitation could excite bubbles at much lower sizes to an unstable state than single-frequency does and this unstable state was more likely to cause initial cavitation [126]. They also investigated the acoustical scattering cross section and found dual-frequency approach could generate more resonances [127].

Although more extensive *in vitro* and *in vivo* studies still need to be performed in order to further evaluate the potential of the proposed approach, a few foreseeable challenges in clinical translation can be envisioned: 1) the highest operating frequency for transcranial ultrasound spherical arrays currently available is at 1 MHz [128]. To deliver 1.5 MHz

ultrasound transcranially on human, a new “brain array” will likely be needed; 2) Trans-skull delivery of 1.5 MHz ultrasound energy will be possibly inefficient due to the high absorption of the skull. However, treatment safety is the most important factor to consider and a high frequency leads to precise targeting. By using DFFU, it is expected that the acoustic energy can be more efficiently used for thrombolysis, therefore offsetting the disadvantage of high frequency absorption. Adding microbubbles (MBs) could potentially further enhance the thrombolysis efficiency as they can also reduce the cavitation threshold pressure. For ischemic stroke, however, the delivery of MBs in the local low- or no-flow environment is challenging; 3) to accurately focus ultrasound through the skull using the numerical time-reversal approach, the resolution of CT scans of the skull ideally should be much smaller than the wavelength. This is challenging at 1.5 MHz frequency because of its small wavelength. However, a recent paper showed that, as long as the resolution is smaller than about half of the wavelength, sufficiently accurate transcranial beam focusing can be achieved using a k-space method [129].

3.5. Conclusion

This paper studies the efficacy of multi-frequency HIFU for thrombolysis *in vitro*. Single-frequency, dual-frequency, and triple-frequency were compared with one another under the same acoustic output power. While a previous study investigated the use of kHz range dual-frequency HIFU for the application of subcutaneous thrombolysis [40], this study utilized MHz range frequency which is considered safer and is relevant to treating ischemic stroke patients. The experimental results demonstrated that dual-frequency HIFU is more efficient than single-frequency in thrombolysis efficiency. In a specific case, dual-frequency HIFU was found to require 30% less energy to achieve the same

thrombolysis of single-frequency HIFU. When varying the treatment time, it was found that dual-frequency HIFU can accelerate the thrombolysis by a factor of 2-4 to achieve a 50% thrombolysis efficiency. Thrombolysis efficiency improved for both dual-frequency and single-frequency when increasing the duty cycle. In addition, to achieve a thrombolysis efficiency at 60%, dual-frequency HIFU could reduce the needed power by a half. When increasing the frequency difference of dual-frequencies from 0.025 MHz to 0.1 MHz, the thrombolysis efficiency did not show significant changes. The use of triple-frequency HIFU also did not show clear advantages over dual-frequency HIFU albeit it still outperformed single-frequency HIFU. The measured inertial cavitation dose showed that multi-frequency HIFU had stronger cavitation activities than that of single-frequency HIFU, explaining the more efficient lysis. In the future, we will continue our work and demonstrate the effectiveness of multi-frequency HIFU for thrombolysis through *ex vivo* human skulls and *in vivo*. The exact mechanism of enhanced thrombolysis through multi-frequency excitations also remains to be the subject of our future study.

Chapter 4 Microbubble mediated thrombolysis

Microbubble mediated dual-frequency high intensity focused ultrasound thrombolysis: an *In vitro* study

This chapter present new thrombolysis technique. High intensity focused ultrasound (HIFU) has recently emerged as a promising alternative approach for thrombolysis. However, the high acoustic energy required by HIFU could elicit thermal damage bioeffects, impeding the clinical translation of this technique. This paper investigates the use of dual-frequency focused ultrasound (DFFU) mediated by microbubbles (MBs) to minimize the acoustic power required for thrombolysis *in vitro*. It was found that MBs, with sufficient concentration, could significantly lower the power threshold for thrombolysis for both DFFU and single-frequency focused ultrasound (SFFU). In addition, SFFU needs about 96%-156% higher energy to achieve the same thrombolysis efficiency as that of DFFU. The thrombolysis efficiency is also found to increase with the duty cycle. The measured cavitation signals reveal that the enhanced inertial cavitation is likely responsible for the improved thrombolysis under DFFU and MBs [104].

This chapter has some of previously published material authored by Dingjie Suo as shown below. All previously published material was reprinted with permission from the publishers.

- **Suo, Dingjie**, Zhiyang Jin, Xiaoning Jiang, Paul A. Dayton, and Yun Jing. "Microbubble mediated dual-frequency high intensity focused ultrasound thrombolysis: An *In vitro* study." Applied Physics Letters 110, no. 2 (2017): 023703.

- **Suo, Dingjie**, Bala Govind, Andrew Antony, Yun Jing. “Microbubble mediated dual-frequency high intensity focused ultrasound thrombolysis with flow system: an in vitro study.” (In preparation. 2017)

4.1 Introduction

To date, the only FDA approved treatment for acute ischemic stroke is intravenous injection of tissue plasminogen activator (tPA). However, this technique is only effective within 4.5 hours of the symptom onset. Furthermore, the use of tPA can exacerbate intracerebral hemorrhage [130]. Finally, this technique is characterized with a low recanalization rate [131] as the chronic components of the thrombi have fibrous network which are stiff, retracted, and not responsive to thrombolytic drugs [132, 133]. Even when recanalization is successful, the procedure may take up to several hours with lytic agents.

Ultrasound has been suggested to be a potential alternative approach for recanalization. Ultrasound could be used in combination with tPA or contrast agents [134], or even as a stand-alone treatment [11-13]. When combined with tPA, ultrasound can increase the recanalization rate at diagnostic intensities [18] but could also be associated with an increased symptomatic hemorrhage [33, 135, 136]. Researchers have also demonstrated *in vivo* and *in vitro* that relatively short-pulsed, high intensity focused ultrasound (HIFU) alone can mechanically disintegrate a clot within minutes, thanks to inertial cavitation [10-12, 137, 138]. Although this technique is drug free (therefore avoiding the associated side effects), non-invasive, and yields rapid lysis, there are still issues that need to be addressed before HIFU can be applied in a clinical setup for treating acute stroke patients.

Frequencies must be in the MHz range for safe treatment of stroke using HIFU because a higher frequency yields a smaller focal size, reducing the risk of tissue erosion outside the desired region [13, 139]. However, due to the strong attenuation of the skull as well as high inertial cavitation thresholds at high frequencies, a large amount of acoustic power is required for thrombolysis through an intact skull at a frequency over 1 MHz [35]. To achieve this, advanced transducer arrays are required for beam focusing through the skull [35], which are complicated and expensive, reducing the likelihood of clinical translation. In addition, a large amount of acoustic power delivered at high frequencies not only raises concern for brain tissue damage around the focus, but also could potentially overheat the skull and damage neighboring tissue. One existing solution is to use microbubbles (MBs) since they are known to be able to considerably lower the required acoustic power for initiating cavitation [140]. Notably, recent studies have shown that MBs and ultrasound mediated thrombolysis can be effective *in vitro* and *in vivo* without using thrombolytic drugs [134, 138, 141-144] and without apparent side effects. The ability of MBs to reduce the acoustic power, however, could be compromised by the fact that the delivery of MBs in the local low- or no-flow environment is very challenging, although clinical studies have shown that intravenous microbubbles can accelerate thrombolysis under ultrasound [145]. To further reduce the power required by HIFU for thrombolysis, additional methods other than using MBs should be developed.

Recent studies from a few groups including ours showed that dual-frequency focused ultrasound (DFFU) holds great potential in enhancing ablation efficacy, thrombolysis efficiency, and cavitation [40, 106, 146-150]. Liu and Hsieh found that single element

transducers with dual frequency could enhance both inertial and stable cavitation [146]. Recent papers by Guo *et al* [149] and Yang *et al* [150] reported that the detected inertial cavitation signal was stronger for DFFU than single-frequency focused ultrasound (SFFU). Other researchers also observed a nearly doubled thrombolysis efficiency at certain power levels during thrombolysis experiments [40, 106]. In this study, we investigate an approach for HIFU-based clot dissolution, where DFFU and MBs are combined to enhance the inertial cavitation and therefore the thrombolysis efficiency.

4.2 Materials and methods

4.2.1 Static model

Bovine blood clots were prepared using the same method as described in [106]. Before experiments, the clots were immersed in 37 °C water for 30 minutes and then drained into a 1 ml latex free syringe (Becton Dickinson and Company, Franklin Lakes, NJ) (4.65-mm ID, 6.55-mm OD) with saline solution for thrombolysis. The experimental system was similar to that in [106] and is shown in Figs. 4.1 and 4.2. All experiments were conducted in a water tank filled with degassed water at 37 ± 0.5 °C. A three-dimensional (3-D) translational stage (Velmex, Inc., Bloomfield, NY) was used to move a 1.5 MHz HIFU transducer (Blatek Inc., State College, PA) to target the clot. The aperture diameter and focal length are 29.5 mm and 30 mm, respectively. A 10 MHz (Panametrics V309, Olympus, Center Valley, PA) broad-band focused transducer (50.8 focal length and 15.8 aperture diameter) was placed orthogonal to the axial direction of the HIFU transducer to collect the inertial cavitation signal. The two transducer focal points coincided within the clot. An RF power amplifier (3100L, Electronics & Innovation, Rochester, NY) was used to amplify signals generated from a function

generator (AFG3101, Tektronix Inc., Beaverton, OR). A high-intensity hydrophone (HNA-0400, ONDA, Sunnyvale, CA) was used to calibrate the peak negative pressure (PNP) at the focus of the HIFU transducer. Burst waves were used with a pulse length 100 us and 10% duty cycle except for the ones where the duty cycle was varied.

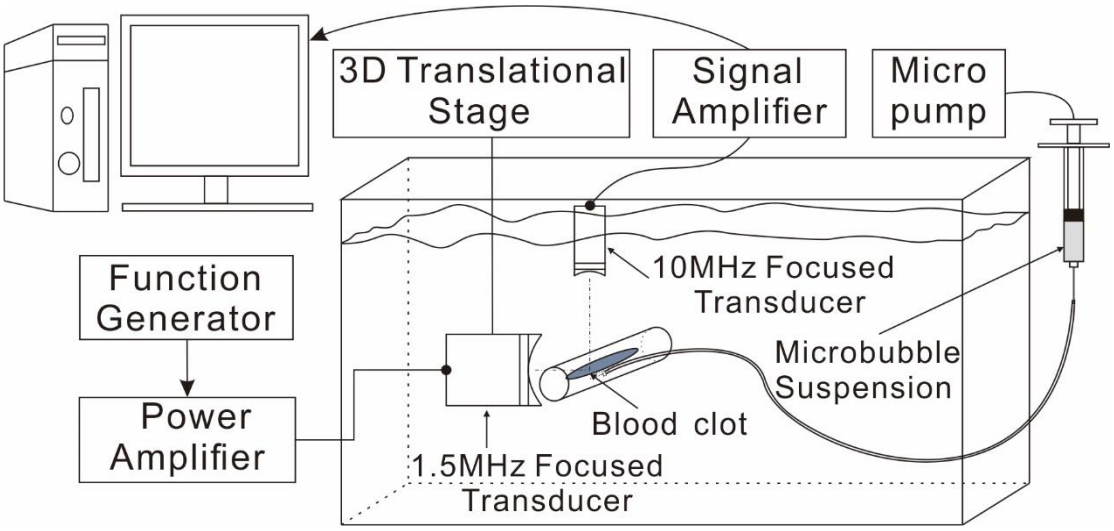

Figure 4.1 Schematic of the experimental system.

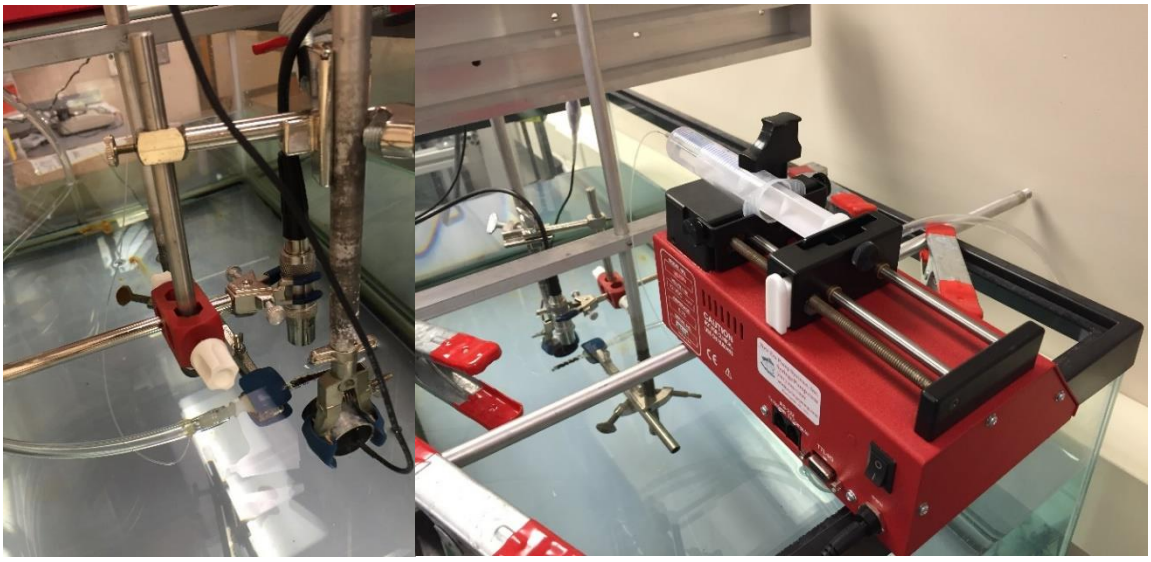

Figure 4.2 Real setup of the experimental system.

MBs were produced from lipid solutions as described in [151]. Before experiments, the MBs were activated using a shaker for 45 secs (Bristol-Myers Squibb Medical Imaging. Inc. N. Billerica, MA). The radius of the MB was 0.9 ± 0.45 μm at a concentration of 1×10^{10} MBs/ml after activation. 1 ml MBs was dissolved into 10 ml, 100 ml, and 1000 ml saline solution in order to vary the concentration from 1×10^{9} MBs/ml to 1×10^{7} MBs/ml. The MBs were subsequently drawn into a 30-ml syringe (Henke Sass Wolf, Tuttlingen, Germany) which was installed on a micropump (DUAL-NE-1010_US, New Era Pump System Inc., Farmingdale, NY). The micropump was configured to have a flow rate of 100 μl/min during the whole process [152]. For each experiment, the pump was turned on for 30 secs before the ultrasound was activated and was kept on until the end of the experiment. The syringe containing MBs was shaken manually after each experiment to stop MBs from concentrating on the surface of the suspension.

Each clot was blotted and weighted (170 ± 20 mg) before experiments. The total number of clots used in the experiments was n=105. The clots were pushed into the syringes filled with saline solution. The syringes containing the clots were then connected with the pump system using a narrow tube through which the MBs were delivered to the clot site. The exit of the narrow tube was located beside the center of the clot along its axial direction (the tube was not inserted into the clot). Each clot was cut into roughly 17-mm long and 4-mm in diameter and was flushed with saline solution. During the treatment, the HIFU transducer was moved by the 3-D translational stage at 3 mm step size along the length of the clot to treat the entire clot. The system paused at each location for a period of time t/4 for each step, where t is the total treatment time. After the treatment, the debris from the syringe was injected onto a 100 μm filter and blotted gently before

weighing using tissue wipers. The control group experiments were conducted the same way except that HIFU was not activated. All thrombolysis experiments were repeated 5 times and the standard deviation and p-value were calculated using a T-test with one-tailed distribution. The single frequency excitation had a center frequency at 1.5 MHz while the dual-frequency one had two center frequencies at 1.5MHz and 1.45MHz [106]. The two frequencies were chosen because of the relatively narrow bandwidth of the HIFU transducer and also the fact that no significant differences were found between dual-frequency excitations with different frequency differences (e.g., 1.5MHz+1.475MHz, 1.5MHz+1.45MHz, and 1.5MHz+1.4MHz). The output powers at different input levels were calibrated by a power meter (UPM-DT-1000PA Ohmic Instruments St Charles MO) prior to the experiment to ensure that the output powers were the same for SFFU and DFFU.

The cavitation signal was processed after it was received by the 10 MHz focused transducer and amplified by a signal amplifier (AH-2020, ONDA, Sunnyvale, CA). For each cavitation detection experiment, cavitation signals were captured every 10 secs and a total of 10 signal samples were taken. The length of each capture was 4 ms which consisted of 4 bursts at a sampling rate of 50 MHz. Each signal was transformed into the frequency domain and all 10 signal samples of that one experiment were averaged. Finally, every 100 points (a 25 KHz range in the frequency domain) of the averaged data were substituted with their root-mean-square value to generate a clear frequency-domain figure. The process of signal processing is showed in Figure 4.3. The thrombolysis efficiency was calculated using the clot weight loss percentage [106]. An efficiency of 100% indicates a complete thrombolysis.

Various PNPs were firstly examined by fixing the other acoustic parameters. The PNPs shown in figures below only represent those of SFFU. The DFFU results are always compared with those of SFFU under the same power, but with different PNPs. To achieve the same output power, the PNPs for DFFU was about 30-40% higher as demonstrated in our previous study [106]. The I_{sppa} for all achieved PNPs were 159 W/cm^2, 257 W/cm^2, 364 W/cm^2, 551 W/cm^2, and 733 W/cm^2. The I_{spta} could approximately be calculated using $I_{spta} = I_{sppa} \times$ ducy cycle. For 10% duty cycle, the corresponding I_{spta} were 15.9 W/cm^2, 25.7 W/cm^2, 36.4 W/cm^2, 55.1 W/cm^2, and 73.3 W/cm^2, respectively.

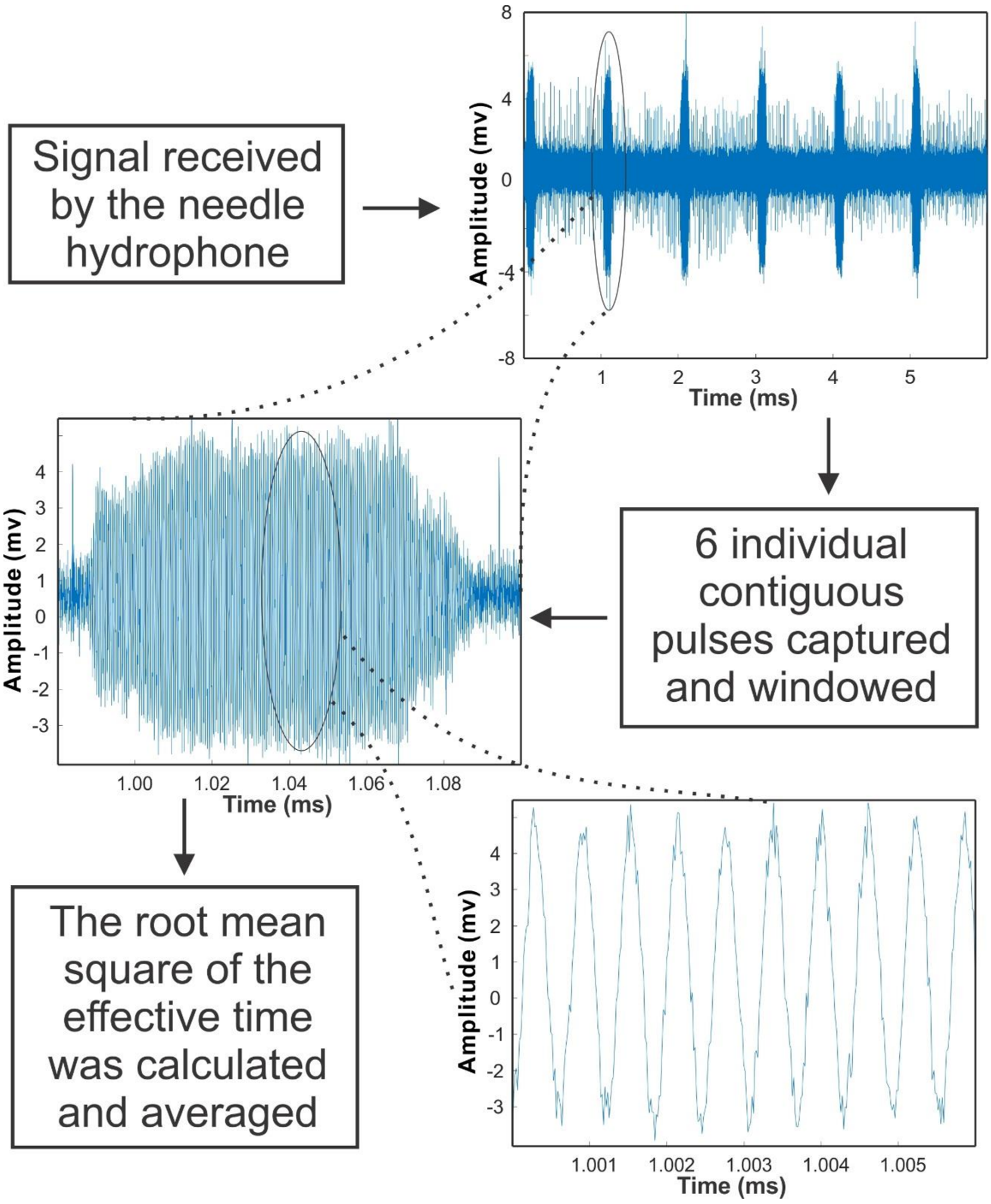

Figure 4.3 Schematic of the data processing

4.2.2 Flow system model

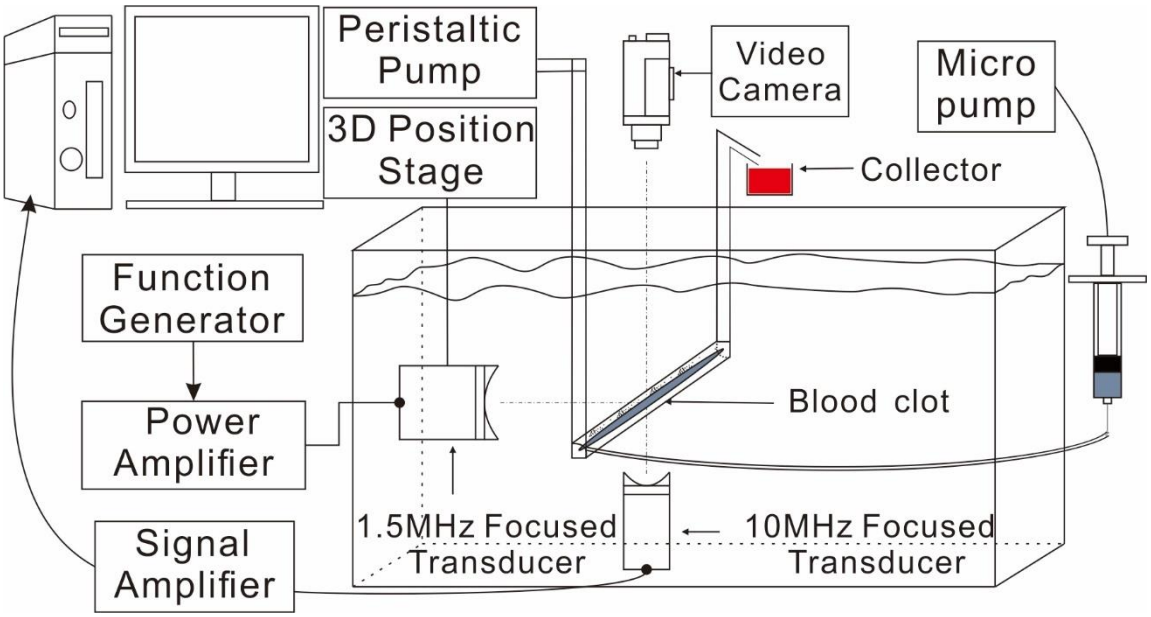

Figure 4.4 Schematic of the flow system experimental setup

Figure 4.5 Real setup of the experimental system.

The blood clots for the flow system are prepared in a similar fashion as in [117]. Bovine blood is added into the 2.75% W/V calcium chloride solution (Fisher Scientific, Fair Lawn, NJ) as coagulant for clotting (5 ml/50 ml blood). The blood mix is drained into tygon tubes (1/8-in ID, 3/16-in OD) with a thread inside and sealed. Each tubing length is set to 11 cm. The tubes are thereafter immersed in a 37 °C water bath for 3 hours and then stored at 4 °C for over 72 hours for complete clot generation and retraction. The

clots are in cylindrical shape with a diameter at around 3 mm after coagulant with a length of each clot is 10 cm. Before thrombolysis experiments, the clots are immersed in 37 °C water for 1 hour and then loaded to the clot holder for thrombolysis experiments.

The setup for the experiment is customized in an attempt to visually investigate the transient mass loss by a combination during HIFU-induced thrombolysis. A peristaltic pump is used to produce a flow rate was 0.4ml/s, which gives a flow rate of 23 cm/s to 94 cm/s at the clot site depend on the clot size. The flow area at the clot site is calculated as the radius of the clot the value varies from 1.2-1.5 mm. This simulates the flow of fluid in a blood vessel. The schematic of the experiment setup and the real setup are shown in figures 4.4 and 4.5. The tube is held by a 3-D printed fixture which facilitates the circulation of water in the tube as shown in figure 4.5. To quantify the mass loss, Digital Image Processing is used. A camera is mounted on the x-stage of the 3-axis stage and directly above the tank in which is immersed the clot and its supporting fixtures. During the experiment, the camera has the 10-cm clot in its field of view. As it slides along the x-axis synchronously with the clot, it records the dissipative action of the HIFU transducer on the blood clot at intervals of 0.8 cm along the clot's length and at approximately 30 frames/second. This approach is used for varying combinations of ultrasound pressure amplitude and input frequency. Visibly, the effect of each of these combinations is different and this rate of dissipation needs to be quantified. During post-processing, the color image in each frame is converted to a binary (black/white) image with appropriate thresholds to isolate the clot silhouetted against the lighter background of the tank's floor. The pixels embodied by the clot progressively dwindle in number and at each instance, this is compared to their number in the original, untreated clot as shown in Figures 4.6 (a)

and (b). A median filter is then used to remove the little variance due to noise. This establishes a quantitative assessment of the trend in the clot's mass loss for cases mediated by microbubble injection and those without microbubble injection. Sample results shown in Figures 4.6 (c) and (d) confirm that the use of dual-frequency ultrasound is decisively more effective than single-frequency ultrasound.

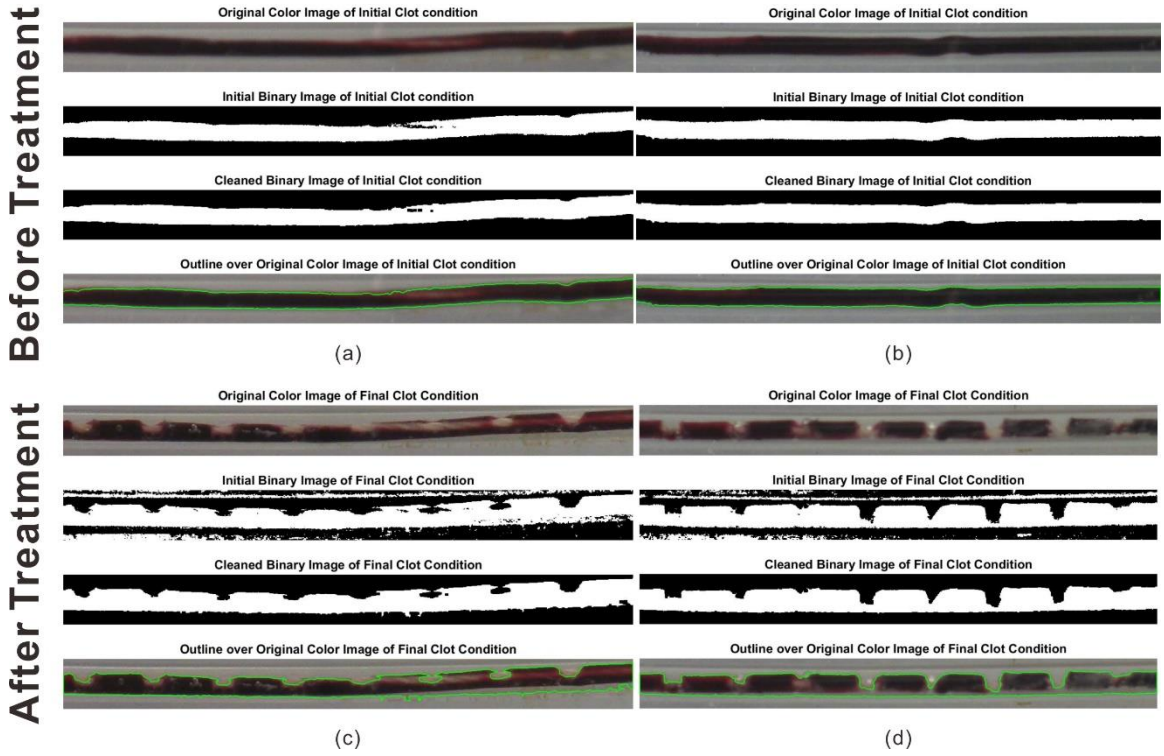

Figure 4.6 Imaging processing steps that show the clot lysis. (a) and (b), clot condition before treatment; (c) and (d) clot condition after treatment.

4.3 Results

Figure 4.7 shows the thrombolysis efficiencies with 10^9 MBs/ml, 3 min treatment time and 10% duty cycle. Figures 4.7 (a) and (b) indicate that, DFFU excitation could achieve an efficiency above 25% at a pressure level as low as 2.5 MPa and the efficiency was 11% higher than the control group. On the other hand, SFFU could only achieve about

the same efficiency at a pressure level between 3.5 and 4.0 MPa. In terms of energy, SFFU needs about 96%-156% higher acoustic energy since the energy is roughly proportional to pressure square. It should be noted from Fig. 4.7 (b) that once the pressure threshold for thrombolysis is achieved, e.g., around 2.5 MPa for DFFU and around 3.0 MPa for SFFU, there is a dramatic increase in thrombolysis efficiency which indicates that inertial cavitation possibly occurred and this will be later confirmed by our passive cavitation experiments. Beyond the threshold, the thrombolysis efficiency gradually increases with the pressure level. Except for the case where both SFFU and DFFU were ineffective at 2.0 MPa, DFFU was at least 28% more efficient than SFFU at each pressure level. The highest contrast was found at 2.5 MPa, where DFFU is 86% more efficient than SFFU (25% thrombolysis efficiency vs.14% thrombolysis efficiency). The thrombolysis power threshold for DFFU was about 30% lower than SFFU (2.5 MPa vs. 3.0 MPa). Note that this is only an approximation since the exact pressure/power thresholds were not measured in this study.

Figure 4.8 shows the effect of MB concentration (0 MBs/ml, 10^7 MBs/ml, 10^8 MBs/ml and 10^9 MBs/ml) on thrombolysis efficiencies for both SFFU and DFFU at 2.5 MPa PNP. At 0 MBs/ml concentration (without MBs) and also 10^7 MBs/ml, neither SFFU nor DFFU had any effect on the clot which indicates none of them reached the threshold for thrombolysis. The SFFU thrombolysis efficiency was similar to that of the control group whereas DFFU thrombolysis efficiency increased progressively with the growing MBs concentration starting from 10^7 MBs/ml. This is possibly due to the fact that more MBs lead to more cavitation nuclei and stronger inertial cavitation activities [153].

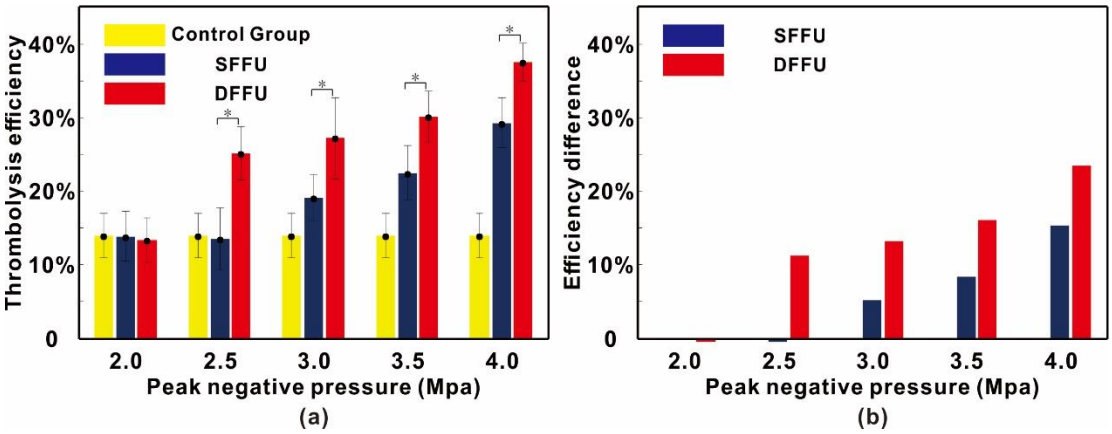

Figure 4.7 Thrombolysis efficiency v.s. PNP. Acoustic parameters: 109 MBs/ml MB concentration, 10% duty cycle, 100 us pulse length and 3 mins treatment time. (a) Thrombolysis efficiency; (b) Thrombolysis efficiencies of SFFU and DFFU minus the thrombolysis efficiency of the control group. (*p-value < 0.005)

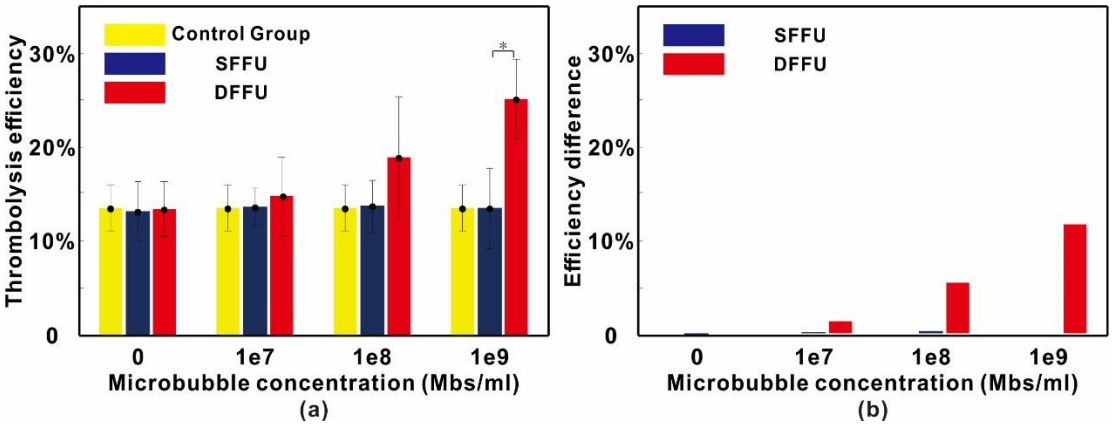

Figure 4.8 Thrombolysis efficiency v.s. MB concentration. Acoustic parameters: 2.5 MPa PNP, 10% duty cycle, 100 us pulse length and 3 mins treatment time. (a) Thrombolysis efficiency; (b) Thrombolysis efficiencies of SFFU and DFFU minus the thrombolysis efficiency of the control group. (*p-value < 0.005)

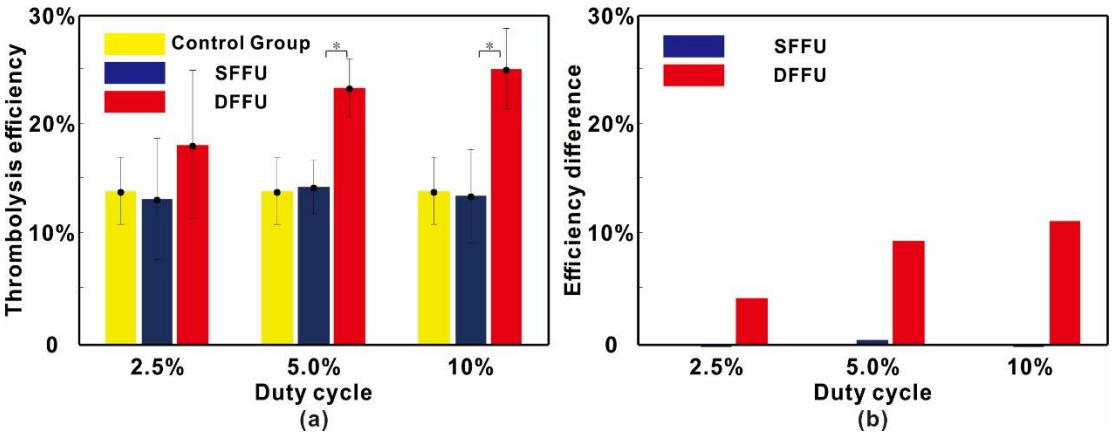

Figure 4.9 Thrombolysis efficiency v.s. duty cycle. Acoustic parameters: 109 MBs/ml MB concentration, 2.5 MPa negative peak pressure, 100 us pulse length and 3 mins treatment time. (a) Thrombolysis efficiency; (b) Thrombolysis efficiencies of SFFU and DFFU minus t the thrombolysis efficiency of the control group. (*p-value < 0.005)

The effect of duty cycle was also examined for both SFFU and DFFU. The duty cycle was varied by adjusting the pulse length/pulse repetition period and three values of duty cycle were tested, i.e., 2.5%, 5%, and 10%, corresponding to 250 Hz, 500 Hz, and 1KHz for the pulse repetition frequency. Figure 4.9 illustrates the relationship between thrombolysis efficiency and duty cycle at 2.5 MPa PNP and the MB concentration of 10^9 MBs/ml. At this pressure level, the thrombolysis efficiency of SFFU was similar with the control group for duty cycle less than 10% and there was no appreciable difference between the results of the three duty cycles tested. In contrast, the thrombolysis efficiency of DFFU increased with the growing duty cycle. The increase was more significant when the duty cycle changed from 2.5% to 5% than from 5% to 10%. This suggests that 5% duty cycle could be potentially a good choice for thrombolysis as it is less energy-consuming than the 10% duty cycle and it causes less heating in the tissue.

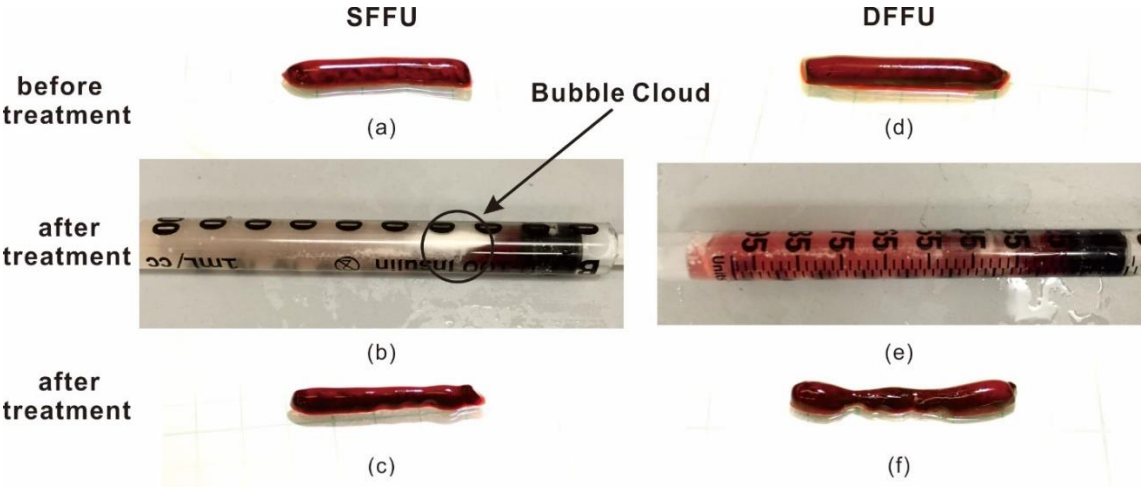

Figure 4.10 Blood clot before and after treatment at 2.5 Mpa with 10 % duty cycle and 109 MBs/ml MB concentration.

Figure 4.10 shows the clot before and after treatment. It is clear that at 2.5 MPa, the bubble cloud still exists after the treatment of SFFU which indicates the pressure is lower than the bubble cavitation. However, after the treatment of DFFU, no bubble cloud left and the dents on the clot (Fig 4.10 (f)) is larger than the dents on Figure 4.10 (c).

The results of the flow system will be further analyzed and will be presented in our next paper. The results should consist of one figure of the clot lysis size with an error bar at different treatment power. One figure of the clot loss percentage against the time line at different treatment power. One figure of the clot lysis rate comparation of SFFU and DFFU during the one-minute treatment.

4.4 Discussion

The acoustic attenuation of the syringe tube was tested after the experiment, the setup is showed in figure 4.11. Thereafter, the signal collected from the hydrophone is showed in figure 4.12. The acoustic pressure amplitude is attenuated because of the existence of the tubing. Figures 4.12 (a) and (b) show the acoustic pressure in time domain without tubing

and with tubing while (c) and (d) show the acoustic pressure in frequency domain. As can been seen from the figure that the pressure amplitude for a signal with tubing could be 6 dB lower than a signal without tubing. In terms of energy, it will be 50% energy loss.

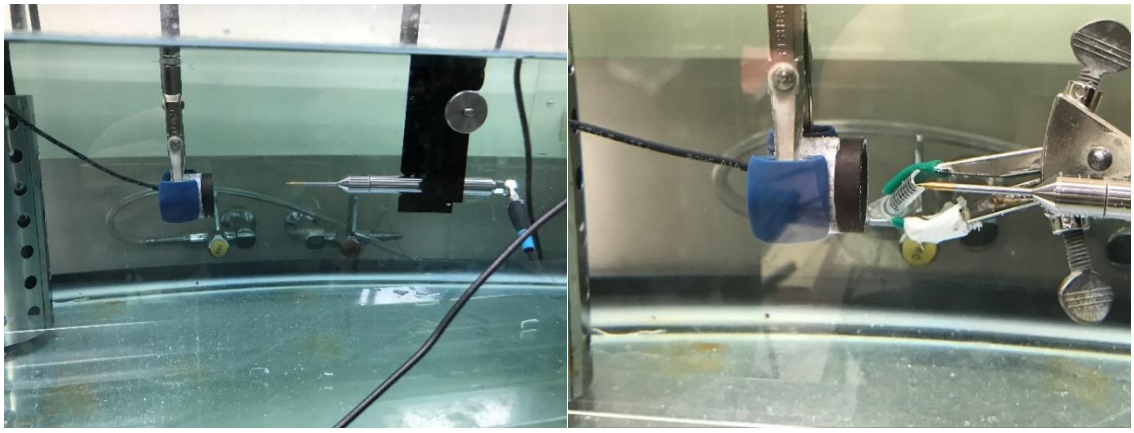

Figure 4.11 The setup of acoustic attenuation caused by the syringe tube.

To understand the underlying mechanism of enhanced thrombolysis efficiency of DFFU, the cavitation signal was measured at various power levels at 10% duty cycle. Figure 4.13 presents the wide-band cavitation spectra of SFFU and DFFU. The detected signals for low pressure levels (e.g., 2 MPa) clearly show the harmonics, sub-, and ultra-harmonics which are due to nonlinear wave propagation and stable cavitation, respectively. At higher pressure levels, sub- and ultra-harmonics disappeared and broadband noise arise due to the inertial cavitation. The results show that ultra-harmonics could be observed for SFFU at PNPs lower than 3.0 MPa and DFFU at PNPs lower than 2.5 MPa, implying most of MBs were undergoing stable cavitation. The detected broadband noise for SFFU surged as the pressure increased from 2.5 MPa to 3.0 MPa, indicating the onset of inertial cavitation. The same phenomena happened for DFFU as the pressure transitioned from 2.0 MPa to 2.5 MPa. These cavitation results are well-correlated with the previously

demonstrated thrombolysis results at different pressure levels, suggesting that the enhanced thrombolysis is likely due to the enhanced inertial cavitation. The stronger inertial cavitation is possibly due to the nonlinear frequency mixing originated from the two fundamental frequencies and a higher negative peak pressure of DFFU [106].

Figure 4.14 shows the broad band noise that collected during the flow system experiments. The inertial cavitation of SFFU yields between 3.0 MPa and 3.5 MPa while the DFFU yields between 2.5 MPa and 3.0 MPa. The results, again, correlated with the experimental thrombolysis results and affirm our hypothesis that DFFU has a lower cavitation threshold.

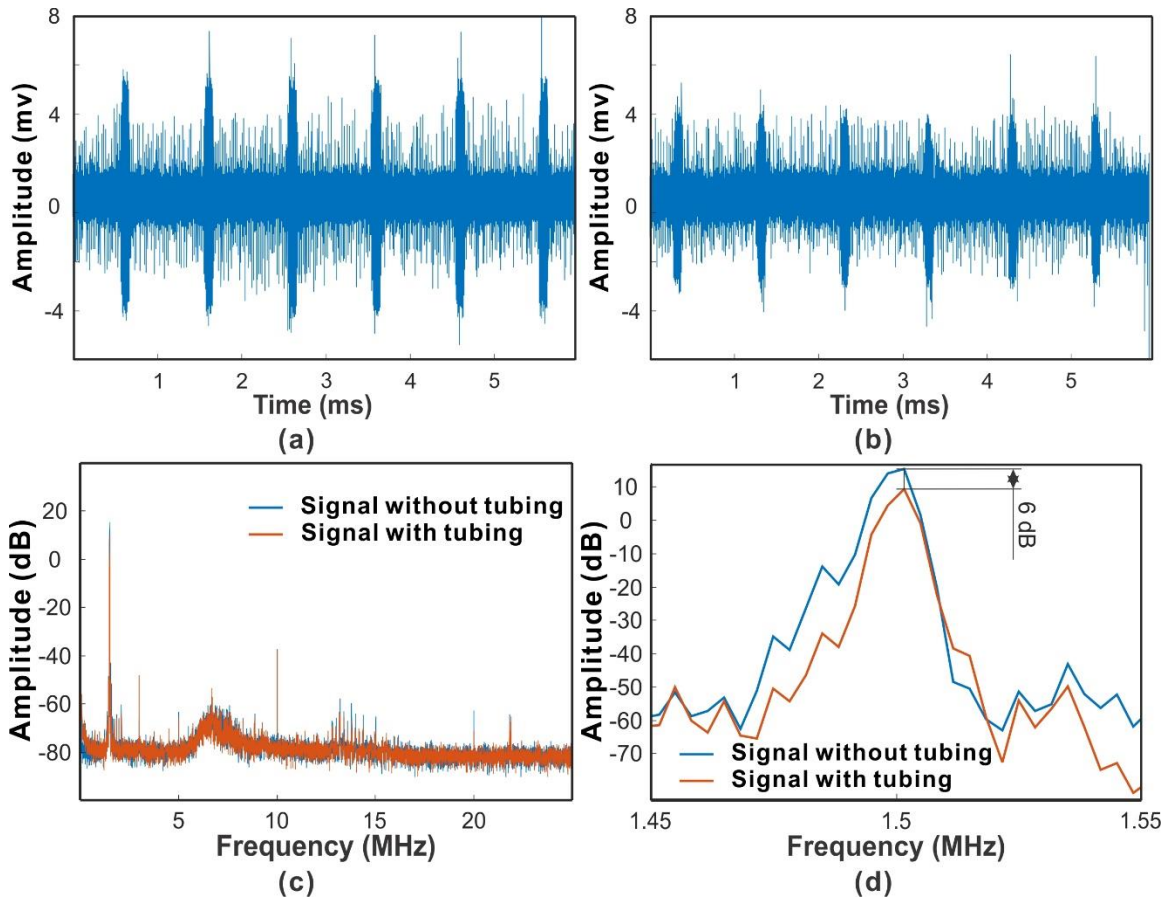

Figure 4.12 The acoustic pressure attenuation because of the existence of the tubing. (a) and (b), acoustic pressure in time domain without tubing and with tubing. (c) and (d), acoustic pressure in frequency domain.

4.5 Summary

In conclusion, this paper demonstrated *in vitro* thrombolysis using SFFU and DFFU mediated with MBs. While it is known that DFFU and MBs can individually reduce the power threshold for thrombolysis, this study reveals that these two techniques combined can further reduce the power required for thrombolysis and enhance the thrombolysis efficiency. The detected cavitation signal indicated that the enhanced inertial cavitation is likely responsible for the enhanced thrombolysis efficiency. Our approach that integrates DFFU and MBs for enhancing inertial cavitation, not only is useful for thrombolysis, but can also find utility in tissue ablation, drug delivery, and lipid extraction [154]. Our future work will further investigate the usefulness of DFFU for thrombolysis in more realistic situations including the *in vitro* flow model and *in vivo* model, where blood flow and tissue attenuation can be taken into account.

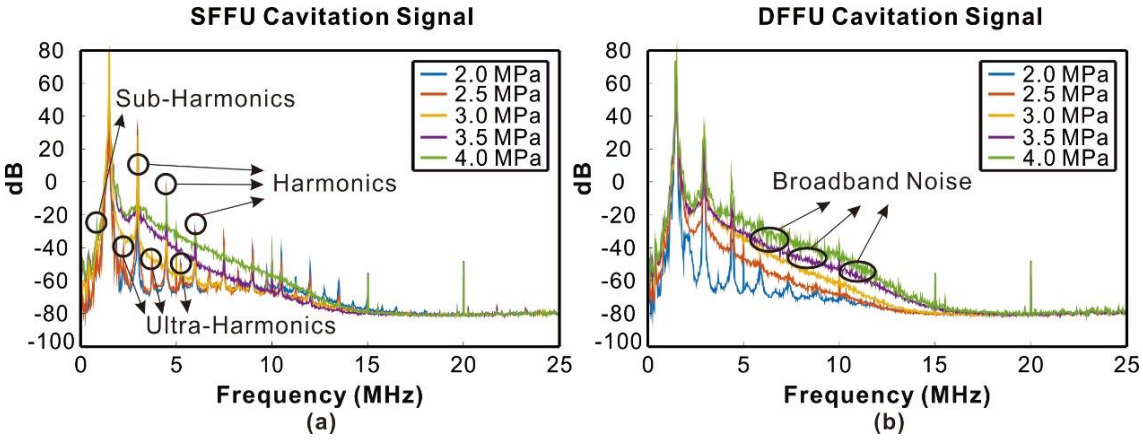

Figure 4.13 Detected cavitation signals for (a) SFFU and (b) DFFU at different pressure levels.

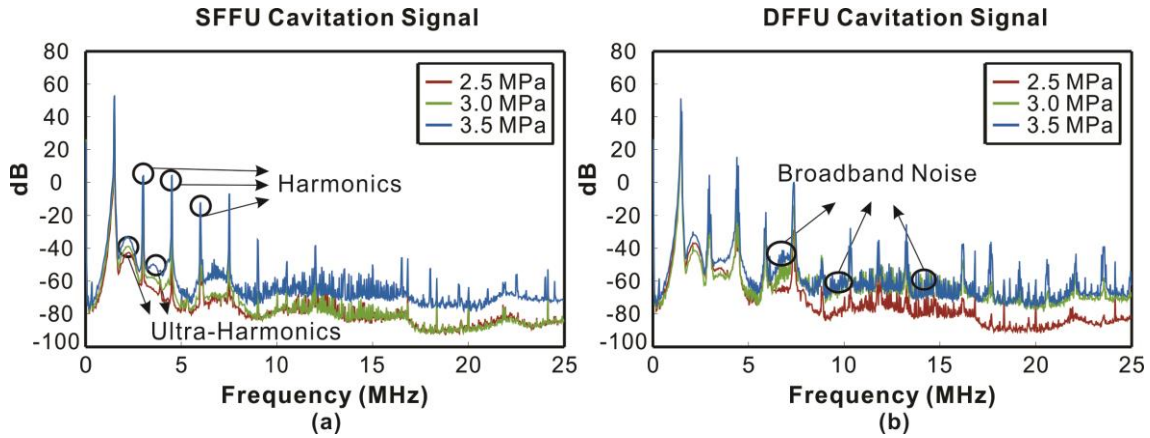

Figure 4.14 Detected cavitation signals for (a) SFFU and (b) DFFU at different pressure levels with flow system.

Chapter 5 Numerical investigation of cavitation

Numerical investigation of the inertial cavitation threshold under multi-frequency ultrasound

This chapter present numerical modeling of microbubble behavior under ultrasound. Through the introduction of multi-frequency sonication in High Intensity Focused Ultrasound (HIFU), enhancement of efficiency has been noted in several applications including thrombolysis, tissue ablation, sonochemistry, and sonoluminescence. One key experimental observation is that multi-frequency ultrasound can help lower the inertial cavitation threshold, thereby improving the power efficiency. However, this has not been well corroborated by the theory. In this paper, a numerical investigation on the inertial cavitation threshold of microbubbles (MBs) under multi-frequency ultrasound irradiation is conducted. The relationships between the cavitation threshold and MB size at various frequencies and in different media are investigated. The results of single-, dual and triple frequency sonication show reduced inertial cavitation thresholds by introducing additional frequencies which is consistent with previous experimental work. In addition, no significant difference is observed between dual frequency sonication with various frequency differences. This study, not only reaffirms the benefit of using multi-frequency ultrasound for various applications, but also provides a possible route for optimizing ultrasound excitations for initiating inertial cavitation [155].

This chapter has some of previously published material authored by Dingjie Suo as shown below. All previously published material was reprinted with permission from the publisher.

- **Suo, Dingjie**, Bala Govind, Shengqi Zhang, and Yun Jing. "Numerical

investigation of the inertial cavitation threshold under multi-frequency ultrasound." Ultrasonics Sonochemistry (2017).

5.1 Introduction

High intensity focused ultrasound (HIFU) has been used in multiple clinical trials as a promising non-invasive surgery modality [111, 113, 156, 157]. HIFU is known to be able to elicit thermal and mechanical effects. Mechanical effects consist of cavitation, radiation force, shear stress and acoustic streaming. Cavitation is the formation and activity of a gas filled bubble under acoustic excitation in a medium [94]. The gas bubble could either oscillate stably or expand gradually and eventually collapse (stable and inertial cavitation) [94]. Cavitation could lead to thermal effects as well as chemical and optical effects [95-98]. The cavitation forces and micro-jets generated during the collapse of the bubble could break the tissue and therefore could be used in tissue ablation and thrombolysis [62, 100-103]. The threshold upon which acoustic cavitation is initiated depends on a number of factors, including the ultrasound frequency, bubble size, and surrounding medium properties [75, 77, 105].

There are numerous models that can predict the dynamics of a single microbubble (MB) under ultrasound excitation, which produce the bubble radius response and radiated pressure. These models have been used for various studies in the field of HIFU or other areas of ultrasound. The Rayleigh-Plesset (R-P) equation [158] has been widely used as a basis for computational study of bubble dynamics by assuming an incompressible liquid. This was extended by Chen *et al*. who developed a method for predicting bubble growth with large density ratios and interfaces between different media [159]. Chahine and Hsiao investigated a 3-D non-spherical model for a zero-thickness shell using a non-

dimensional form of the Rayleigh-Plesset differential equation [160]. Farny *et al*. studied the heating effect of HIFU and found a correlation between the heat generation and cavitation signal [161]. Keller and Miksis first introduced the surrounding liquid compressibility and then developed a model suitable for large amplitude oscillation [162]. Katiyar *et al*. modeled the subharmonics for free bubble and encapsulated bubble oscillations. They reported that the subharmonics would either monotonically increase or decrease within a particular range of ratios of the excitation frequency to the natural frequency of the bubble [163]. Yasui *et al*. simulated the broad band noise generated from bubble cavitation under experimental conditions using the Keller-Miksis model [164]. Wang and Yuan utilized the R-P equation to describe a radially symmetric free bubble in the acoustic field and found a correlation between acoustic cavitation and microalga cells disruption [165]. Mancia *et al.* inspected the bubble responses by changing the surrounding medium properties and waveform parameters using the Keller-Miksis model. They analyzed the surrounding medium stress and strain and found that stiffer tissues were less likely to be damaged by acoustic irradiation [115]. Yang and Church investigated the gas bubble cavitation threshold in soft tissue by extending the Keller-Miksis model to take the shear modulus of the media into account [166, 167]. Bader and Holland further employed the Yang and Church model to predict the expansion of nuclei under histotripsy pulses [110].

Multi-frequency sonication [36-40, 104, 106, 168] has recently been reported as a promising method to enhance cavitation activities and reduce the cavitation threshold. Avvaru and Pandit found that the measured cavitation signal from the hydrophone can be increased by introducing a second and third frequencies, indicating an enhanced

cavitation activity [169]. Guedra *et al*. found that the cavitation signal power generated from a dual frequency excitation was twice as high as that generated from a single frequency excitation [170]. Guo *et al.* reported a faster temperature rise in *ex vivo* chicken tissue when treated with multi-frequency ultrasound compared with single-frequency excitation [38]. Previous research from our and other groups also showed better thrombolysis efficiencies and stronger inertial cavitation signals when using multi-frequency HIFU excitation as opposed to the conventional single frequency excitation [40, 104, 106].

The mechanism of multi-frequency excitation for enhancing the inertial cavitation is still poorly understood, though experimental and numerical studies have been actively pursed to shed light on why multi-frequency is advantageous. Saletes *et al*. showed that dual-frequency could enhance the cavitation activity while reducing the heating in their HIFU cavitation experiments [123] and later on in their dual-frequency thrombolysis experiments [40]. Zhang *et al*. [126] reported on the critical bubble radii dividing stable and unstable regions of bubbles under dual-frequency acoustic excitation. The critical bubble radii are strongly affected by the amplitudes of dual-frequency acoustic excitation rather than the frequencies of the excitation. Zhang and Li numerically calculated the scattering cross section for single bubbles under dual frequency excitations [148]. They found that dual-frequency could increase the acoustic scattering cross section over a broad range of bubble size because of more resonances. To enhance the effect, the energy allocated to the two frequency components should be almost identical and the ratio of the two frequencies should be relatively large [148]. They further investigated the mass transfer and mass diffusion of gas bubble under dual frequency excitation [147, 171].

In contrast to what [126, 147, 148, 171-175] have studied, this paper aims to estimate the inertial cavitation threshold under multi-frequency sonication by solving bubble dynamics equations, which provides a more direct evidence as to why the additional frequencies can facilitate the enhancement of inertial cavitation. While our primary interests are multi-frequency based thrombolysis and thermal ablation, the results from this study may also have implications for sonoluminescence and drug delivery.

5.2 Numerical model

The methodology employed in the numerical prediction of transient bubble radial response is based on the Yang and Church model [166]. This model considers the effects of medium elasticity on a single microbubble's oscillation and will be briefly revisited here. In this investigation, the spherical bubble behaves as if it was in an unbounded viscoelastic medium. In the spherical co-ordinate system, the equation of continuity takes the following form

$$\frac{\partial \rho}{\partial t} + \frac{\partial (\rho v_r)}{\partial t} + \frac{2\rho v_r}{r} = 0, \tag{5.1}$$

where ρ is the density of the medium, v_r is the radial velocity, and r is the dimension along the radial axis. Conservation of radial momentum in a spherically symmetric radial direction yields

$$\rho\left(\frac{\partial v_r}{\partial t} + v_r \frac{\partial v_r}{\partial r}\right) = -\frac{\partial p}{\partial r} + \frac{\partial \tau_r}{\partial r} + \frac{2}{r}[\tau_r - \tau_\theta]. \tag{5.2}$$

Here, p is the pressure, τ_r is the stress in the radial direction, and τ_θ is the stress in the polar direction. In terms of surface tension σ and gas pressure P_g, the pressure in the medium can be expressed as $p = p_g - \frac{2\sigma}{R} + \tau_r$ for a transient bubble radius R.

Furthermore, at the initial time, at the interface of the bubble and surrounding medium, i.e. at a radial position R_0, the derivative $\frac{dR}{dt}$ would be zero. Also, at $R = \infty$, the pressure would equal that of the free fluid.

Yang and Church suggested that in the near field of the bubble, it is safe to approximate that only effects of compression and expansion are perceptible while the surrounding medium remains incompressible [166]. The Bernoulli momentum equation would then account for the radial pressure inside the bubble as

$$v_r = -\frac{R\dot{R}}{r^2} \tag{5.3}$$

and

$$p_{internal} = p_s - \rho_0\left(R\ddot{R} + \frac{3}{2}\dot{R}^2\right) + \frac{\rho_0}{r}\left(R^2\dot{R}\right)' - \frac{\rho_0}{2}\frac{R^4\dot{R}^2}{r^4} + \tau_r|_R^r + 3\int_R^r \frac{\tau_r}{r}dr, \tag{5.4}$$

where p_s is the pressure at the bubble surface and $\ddot{R}$ is the acceleration of the bubble wall. The linear acoustic field equation is used in the far field. This assumption is strengthened by the expectation that density variation, stress and nonlinear convection terms bear little effect in the far-field. Therefore, as a linear superposition of incoming and outgoing waves, the velocity potential can be expressed as

$$\varphi_{external} = \frac{1}{r}\left[\varphi_1\left(t - \frac{r}{c}\right) + \varphi_2\left(t + \frac{r}{c}\right)\right], \tag{5.5}$$

where c is the speed of sound in the medium. Consequently, in terms of equilibrium pressure p_0 and medium density ρ_0, the pressure is given by

$$p_{external} = p_0 - \rho_0\frac{\partial\varphi_{external}}{\partial t}. \tag{5.6}$$

Therefore, to achieve an asymptotic solution at the gas-medium interface, the far-field approximation at its relative zero radial co-ordinate approaches the near-field approximation at its relative infinite radial co-ordinate. The two solutions are then matched and we have

$$R\ddot{R} + \frac{3}{2}\dot{R}^2 = \frac{p_s - p_0}{\rho} + \frac{1}{c}\left[2\varphi_2'' + \left(R^2\dot{R}\right)''\right] - \frac{\tau_r(R,t)}{\rho} + 3\int_R^r \frac{\tau_r}{r}dr. \tag{5.7}$$

On neglecting smaller derivatives beyond the second order, the pressure at a large radial distance is $p_\infty = p_0 - 2\frac{\rho}{c}\frac{\mathrm{d}^2\varphi_2}{\mathrm{d}t^2} + \tau_r(R,t) - 3\int_R^\infty \frac{\tau_r}{r}dr$. This expression simplifies eqn. (5.7) to the Rayleigh equation given by

$$R\ddot{R} + \frac{3}{2}R^2 = \frac{p_s - p_\infty}{\rho} \tag{5.8}$$

This can be further expressed as

$$\left(1 - \frac{\dot{R}}{c}\right)R\ddot{R} + \frac{3}{2}\left(1 - \frac{\dot{R}}{3c}\right)\dot{R}^2 = \left(1 + \frac{\dot{R}}{c}\right)\frac{p_s - p_\infty}{\rho} + \frac{R}{\rho c}\frac{d}{dt}[p_s - p_\infty] \tag{5.9}$$

where

$$p_s = p_g - \frac{2\sigma}{R} + \tau_r(R,t) \tag{5.10.a}$$

$$p_s - p_\infty = p_g - \frac{2\sigma}{R} - p_0 + \left(2\frac{\rho}{c}\right)\frac{\mathrm{d}^2\varphi_2}{\mathrm{d}t^2} + 3\int_R^\infty \frac{\tau_r}{r}dr, \tag{5.10.b}$$

and the term

$$P_A g(t) = \left(2\frac{\rho}{c}\right)\frac{\mathrm{d}^2\varphi_2}{\mathrm{d}t^2} \tag{5.10.c}$$

is the driving pressure.

The stress components are calculated in the near field, assuming that the associated stress terms vanish in the far field. The shear stress, in terms of radial strain γ_r, dynamic

viscosity μ, and shear modulus G is then given by $\tau_r = 2(G\gamma_r + \mu\dot{\gamma}_r)$. Furthermore, in the near-field, $\dot{\gamma}_r = \frac{\partial}{\partial r}\left(\frac{R^2\dot{R}}{r^2}\right)$. This implies that $\gamma_r = \frac{2}{3}r^3({R_0}^3 - R^3)$. This result yields

$$\frac{d}{dt}\left(3\int_R^r \frac{\tau_r}{r}\,dr\right) = -4G\frac{{R_0}^3\dot{R}}{R^4} - 4\mu\left(\frac{\ddot{R}}{R} - \frac{\dot{R}}{R^2}\right) \tag{5.11}$$

Here, ideal gas behavior is assumed. Therefore, p_g equals $p_{g_0}\left(\frac{R_0}{R}\right)^{3\lambda}$ where λ is the polytropic index. In terms of the driving pressure $P_A g(t)$, two simplifications arise

$$p_S - p_\infty = p_g - \frac{2\sigma}{R} - p_0 + P_A g(t) - \left[\frac{4G\left(R^3 - {R_0}^3\right)}{3R^3} + 4\mu\left(\frac{\dot{R}}{R}\right)\right] \tag{5.12}$$

and

$$\frac{d}{dt}[p_S - p_\infty] = \frac{dp_g}{dt} + \frac{2\sigma\dot{R}}{R^2} + P_A\frac{dg(t)}{dt} - 4G\frac{{R_0}^3\dot{R}}{R^4} - 4\mu\left(\frac{\ddot{R}}{R} - \frac{\dot{R}^2}{R^2}\right) \tag{5.13}$$

These expressions for $p_S - p_\infty$ and $\frac{d}{dt}[p_S - p_\infty]$ are substituted into Eq. (5.9) to extract an equation of $\ddot{R}$ which is subsequently solved for R, the radial response of the bubble. In this study, the initial bubble radii vary from $R_0 = 0.2\ \mu m$ to $R_0 = 10.2\ \mu m$ and the initial gas-tissue interfacial velocity is assumed to be zero. This range of initial bubble radii is chosen as prior analysis of gas bubbles in fluids is focused in a radius range of 1 μm to 10 μm [109, 166, 167]. This consideration helps in the validation of results using a given criteria for cavitation. The solution is implemented using an inherently non-stiff ordinary differential equation solver (ode45) in MATLAB (R2016b). The variation of bubble radius as a function of time in fluid and soft tissue is manifested as a non-linear oscillation. The investigation considers two criteria, $R_{max} = 2R_0$ and a bubble-wall velocity of $\frac{dR}{dt} = c$ for inertial cavitation threshold calculation [166, 167].

In the case of single frequency,

$$P_A g(t) = P_0 \sin(2\pi f_1 t). \tag{5.14}$$

In the case of dual-frequency,

$$P_A g(t) = \frac{P_0}{\sqrt{2}} \sin(2\pi f_1 t) + \frac{P_0}{\sqrt{2}} \sin(2\pi f_2 t). \tag{5.15}$$

In the case of triple frequency,

$$P_A g(t) = \frac{P_0}{\sqrt{3}} \sin(2\pi f_1 t) + \frac{P_0}{\sqrt{3}} \sin(2\pi f_2 t) + \frac{P_0}{\sqrt{3}} \sin(2\pi f_3 t)\,. \tag{5.16}$$

Here, P_0 is a pressure amplitude, and f_1, f_2 and f_3 represent the frequency components in Hz. The pressure P_0 is progressively increased in the simulation for each bubble size in order to identify the corresponding inertial cavitation threshold. The factors $\sqrt{2}$ and$\sqrt{3}$ are necessary as they ensure the equal power between these three different excitations. In the simulation, the equilibrium pressure, $p_0 = 1.01 \times 10^5\ Pa$, density, $\rho = 1060\ kg/m^3$, speed of sound in water, $c = 1540\ m/s$, polytropic index, $\lambda = 1.4$, rigidity, G, assumes a value of zero, viscosity of water is $\mu = 0.001\ Pa \cdot s$, viscosity of blood is $\mu = 0.005\ Pa \cdot s$. In water, $\sigma = 0.072\ N/m$ and in blood, surface tension $\sigma = 0.056\ N/m$. These properties are similar to those referenced in [77]. To simulate the microbubbles' response in soft tissue ($\mu = 0.005\ Pa \cdot s, \sigma = 0.056\ N/m$), three shear moduli of 0.5 MPa , 1.5 MPa and 2.5 MPa are considered.

5.3 Numerical results

The normalized waveforms of three different excitations are shown in Fig. 5.1. The single frequency is 1.5 MHz , the dual-frequency is 1.5 MHz +1.45 MHz and the triple-frequency is 1.5 MHz +1.45 MHz +1.4 MHz . These frequencies are chosen because they were used in

our previous experimental studies [104, 106]. The linear combination of multi-frequency components having the same amount of energy has decisive effects. Neglecting the distortion in nonlinear wave propagation, in general, the dual-frequency excitation is predicted to reach a peak negative pressure of $\sqrt{2}$ times that of a single frequency excitation while a triple-frequency excitation could reach a peak negative pressure of $\sqrt{3}$ times that of a single-frequency excitation, if they were to have the same acoustic energy [106].

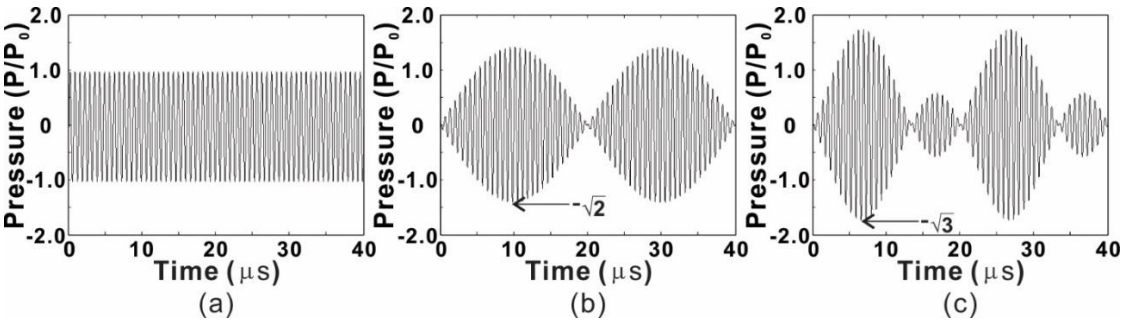

Figure 5.1 Normalized waveforms of single-, dual-, and triple-frequency excitations.

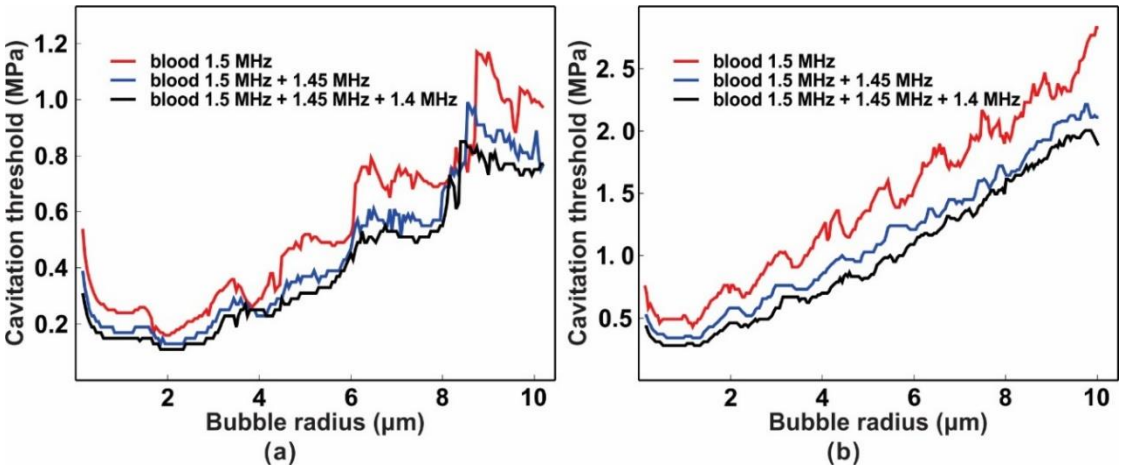

Figure 5.2 Inertial cavitation thresholds of single-, dual-, and triple-frequency excitations. (a) the criterion of R_max=2R_0 and (b) the criterion of dR/dt=c.

The initial analysis considers acoustic signals, the components of which have equal power amplitude. The behavior of MBs in blood is first simulated as it would have greater physiological implications, especially for thrombolysis. Figures 5.2 (a) and (b) show the cavitation pressure thresholds corresponding to single-, dual-, and triple-frequency excitation for both criteria. The result suggests the minima cavitation threshold occurs around 2 μm where the nature frequency of the microbubble is the same as the driving frequency [166]. When the bubble oscillates around its resonant frequency, the need of the driving pressure to reach the criterion will be lower than the bubble not oscillates at its resonant frequency [176]. When comparing Figs. 5.2 (a) and (b), the criterion of $\frac{dR}{dt} = c$ is shown to yield higher thresholds which is consistent with [167]. The results show that the power needed to initiate inertial cavitation continuously decreases with the increase in the number of individual frequency components. It is noted that the change in cavitation pressure from single-frequency excitation to dual-frequency excitation is more dramatic than that from dual-frequency excitation to triple-frequency excitation, which is consistent with our previous experimental findings [106].

Figures 5.3 (a) and (b) show a comparison of inertial cavitation thresholds for microbubble oscillation in blood and water when subjected to a single frequency excitation of $1.5 MHz$, to two combinations of dual-frequency excitations, one of $1.5 MHz + 1.4 MHz$, and another of $1.5 MHz + 1.45 MHz$. It is observed that blood shows higher pressure thresholds than water in all three cases due to their disparate values of viscosity and surface tension. These results are consistent with those in [166]. Visibly, there are several troughs on the cavitation threshold line which indicate that the driving frequency could possibly approach the natural frequency of the MB or multiples thereof.

One thing needs to be noted here is that the frequency difference does not have an appreciable impact, i.e., $1.5\,MHz+1.45\,MHz$ have almost the same cavitation threshold as $1.5\,MHz+1.4MHz$, which is once again consistent with our previous experimental findings [106].

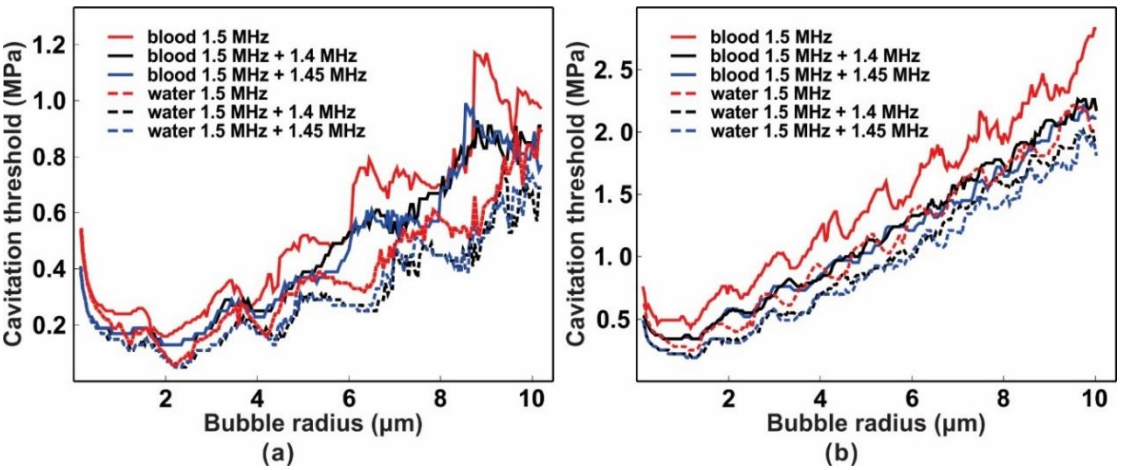

Figure 5.3 Inertial cavitation thresholds with single frequency and different dual-frequencies in water and blood. (a) the criterion of R_max=2R_0 and (b) the criterion of dR/dt=c.

Cavitation threshold characteristics from Figs. 5.4 (a) (c) and (b) (d) show that adding a frequency significantly lower than the primary frequency could considerably reduce the cavitation threshold especially for bubble radii larger than 4 μm and this difference seems to grow with increasing initial bubble radius. Figures 5.4 (a) and (c) suggest that the cavitation threshold of dual-frequency that contains a low frequency component (500 KHz) could be less than the combination of two neighboring frequencies, i.e., $1.5\,MHz+1.45\,MHz$ and $1.5\,MHz+1.4\,MHz$. A $500\,KHz$ acoustic signal alone would significantly lower the cavitation threshold (Figs 5.4 (b) and (d)). This agrees with the widely-accepted theory that lower frequency could initiate cavitation easier. As expected,

the combination of 500 KHz and 550 KHz further lowers the cavitation threshold from that of a single 500 KHz component.

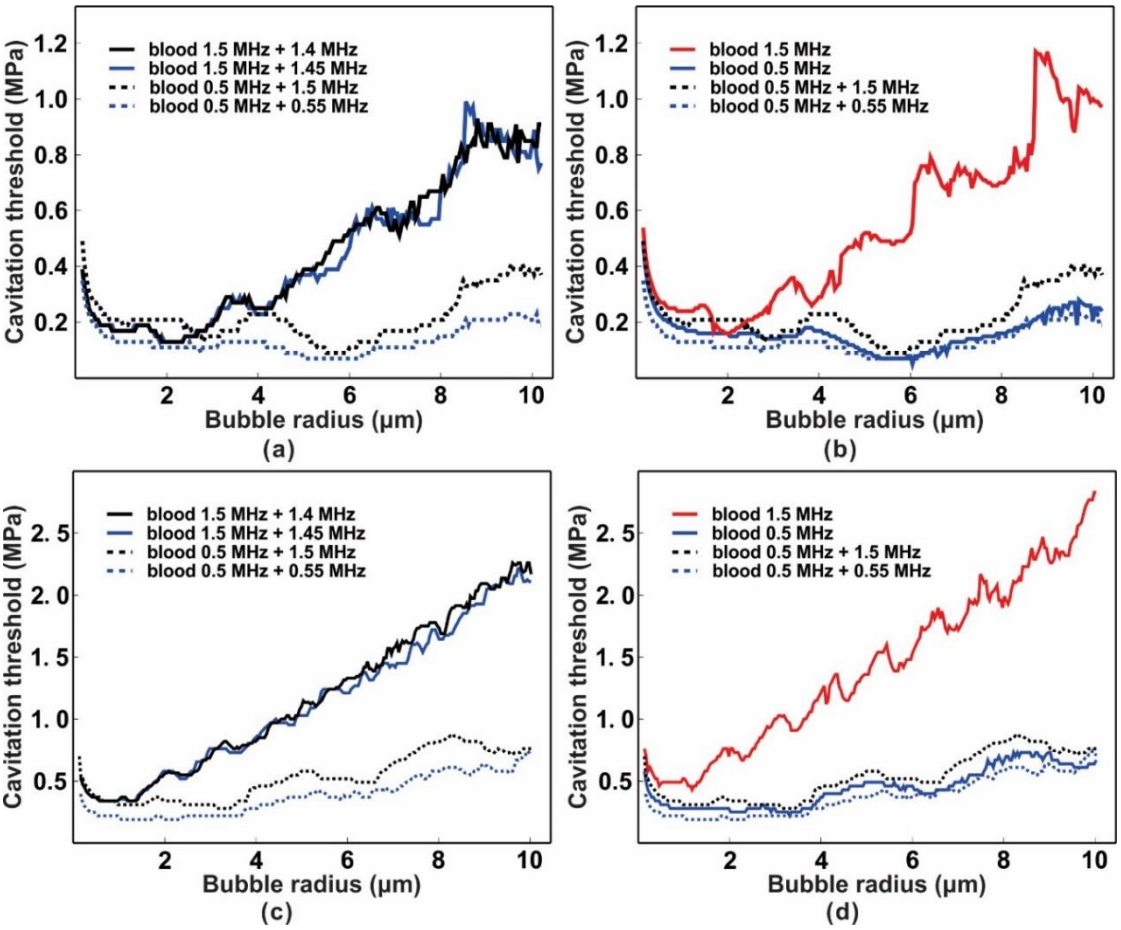

Figure 5.4 Inertial cavitation threshold changes with the addition of low frequencies: (a) (c) show different dual-frequency combinations; (b) (d) show the cavitation thresholds of high frequency, low frequency and the combination of them. (a) (b) the criterion of $R_{max} = 2R_0$ and (c) (d) the criterion of $\frac{dR}{dt} = c$.

Interestingly, Figs. 5.4 (b) and (d) show that the effect of a linear combination of the mixed signal consisting of 500 KHz and 1.5 MHz. components is less in comparison with the effect caused by a signal of 500 KHz alone. Remarkably, it fails to support the general idea of the advantage of dual-frequency excitation. To explain this, the waveforms and radius responses of this 500 KHz +1.5 MHz signal compared with 500

kHz alone would need to be investigated. A single bubble's radius response corresponding to driving pressure (Figs. 5.5 (a) and (b)) are shown in Figs. 5.5 (c) and (d) respectively. The initial bubble radius is 1 μm for both cases. As indicated, the amplitude of the dual-frequency excitation wave is not $\sqrt{2}$ times the amplitude of the single frequency excitation at $500\,KHz$. In fact, the $1.5\,MHz$ signal has a periodicity thrice that of the $500\,KHz$ signal. Hence, when combined, these two frequencies could potentially diminish the advantage of dual-frequency. In this specific case, resulting inertial cavitation pressure is about the same as that derived from a single $500\,KHz$ sonication. Another salient feature of this dual-frequency combination is that the duration of peak negative pressure is shorter than single frequency and could further explain why the threshold of $500\,KHz + 1.5\,MHz$ signal is higher than that of the $500\,KHz$ signal.

Next, another parameter is considered to account for the inertial cavitation threshold of the microbubbles, which is the power allocation of individual components in the multi-frequency signal. By understanding the trade-offs in terms of the energy of each frequency component, a strategic determination of the cavitation effect of the combination can be made. The response is modeled considering an equal effective power of each mixed signal. A comparison of three such combinations is shown in Figs. 5.6 (a) and (b). No significant difference is shown from the perspective of cavitation threshold for the criterion of $R_{max} = 2R_0$. However, for the criterion of $\frac{dR}{dt} = c$, the equal power allocation case has a higher cavitation threshold which needs to be validated with cavitation experiments in the future.

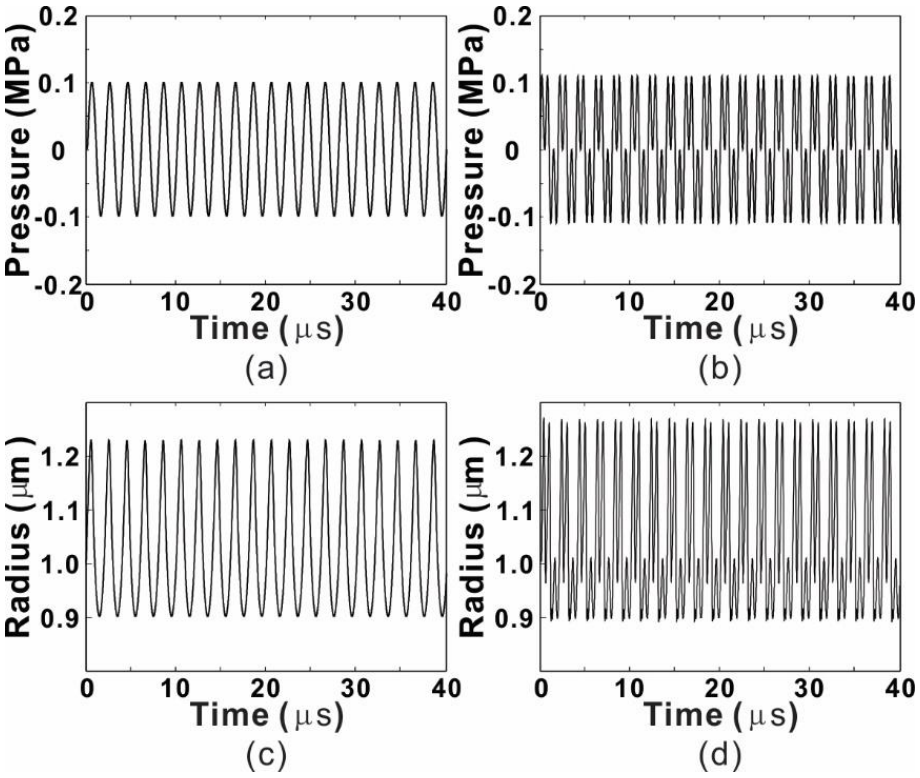

Figure 5.5 Pressure waveforms for (a) 500 KHz and (b) 500 KHz + 1.5MHz . (c) and (d) are the corresponding bubble radius responses.

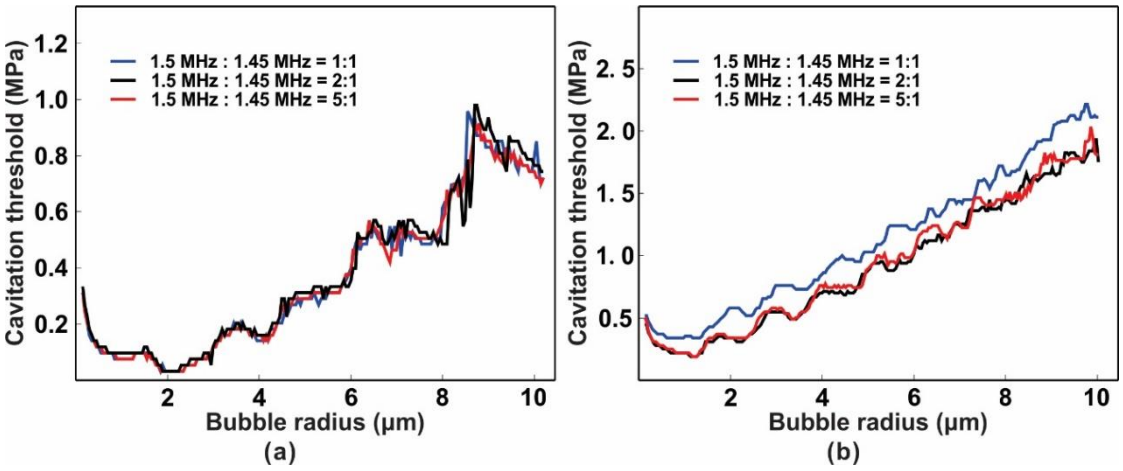

gure 5.6 Inertial cavitation thresholds of dual-frequency excitations with different power allocations. The background medium is blood. (a) the criterion of R_max=2R_0 and (b) the criterion of dR/dt=c.

Calculations are then performed for examining the effect of dual-frequency sonication in soft tissue as this could have implications for tissue ablation using dual-frequency [38].

Figure 5.7 illustrates the effect of shear modulus (G) of $0.5\,MPa$, $1.5\,MPa$ and $2.5\,MPa$. The shear modulus is a property of the surrounding medium. In all cases considered here, the thresholds in general increase with the elasticity. Dual frequency seems to be more advantageous as G increases (this is more evident when comparing results at 0.5 MPa and 1.5 MPa), suggesting that dual frequency may outperform single frequency to a better extent within higher shear modulus soft tissues. It is noted that the minimum cavitation threshold shifts to larger radii as the shear modulus G increases, which is consistent with the results showed in [166]. For example, the minimum cavitation threshold occurs around $8\,\mu m$ for a G = 1.5 MPa while it is around 4 to 5 μm for G = 0.5 MPa (Figs. 5.7 (a) and (b)).

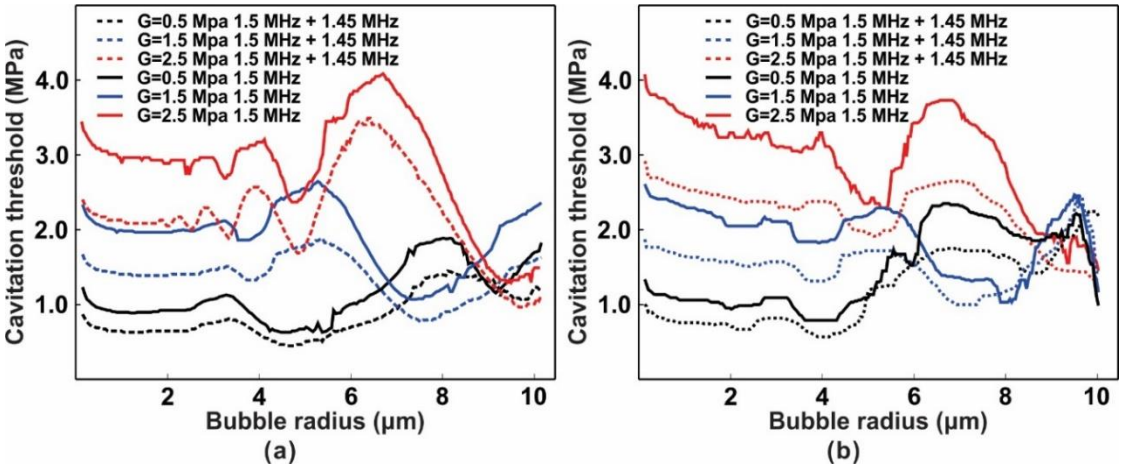

Figure 5.7 Inertial cavitation thresholds for single- and dual-frequency in soft tissue with different shear moduli. (a) the criterion of R_max=2R_0 and (b) the criterion of dR/dt=c.

5.4 Conclusion

The numerical methodology utilized in this study affirms and explains the enhanced inertial cavitation of microbubbles subjected to multi-frequency ultrasound excitation. The Yang and Church model is employed in this study to model non-linear bubble

oscillation in a viscoelastic medium. The simulation results indicate that, given equal initial bubble size, a multi-frequency excitation will in general results in lower cavitation threshold than a single-frequency excitation and reduces the requisite power for this effect. It should be noted that, bubble dynamics models become less reliable at very large pressure values as we have used in this study. Therefore, the results from this study are qualitative rather than quantitative. Nevertheless, it is believed that these results are sufficient in providing some theoretical basis in explaining why multi-frequency excitations are better for initiating inertial cavitation as we and other researchers have consistently observed in various experiments [37, 104, 106, 112].

One nuance is that the inclusion of a low-frequency component drastically reduces the threshold and this has increased influence with growing initial radii of microbubbles. In some cases, the combination could however, be less effective when component frequencies are multiples of one another and could be less potent than the sonication using a single frequency component alone. This unexpected phenomenon should be experimentally validated in the future. Another observation is that the variance in power amplitudes of similar individual frequencies in the mixed signal could cause either insignificant or appreciable change in the threshold, depending upon which cavitation criterion is used.

On further investigation, it is found that dual-frequency excitations perform better than single frequency excitations not only in fluid, but also in soft tissue. Additionally, the advantage of dual-frequency excitations seems to become more evident with the increase of the surrounding medium shear modulus. This is particularly important as it would offer some guidance in designing sonication protocols for tissue ablation. Finally, it should be

pointed out that nonlinear distortion of the acoustic waveforms (due to the nonlinear nature of the acoustic medium) is not considered throughout the paper. The harmonics contained in the acoustic pressure waveform could potentially have a non-trivial effect on the bubble dynamics and will be studied in the future.

Chapter 6 Concluding remarks and future work

6.1 Conclusions and contributions

This dissertation demonstrated the efficacy of multifrequency thrombolysis over the conventional single frequency approach, through a series of in vitro and numerical studies. The research followed a step by step process that first develops an experiment platform, then investigates this new approach with different parameters and finally theoretically validates its numerical model.

Single-frequency, dual-frequency, and triple-frequency were compared with one another under the same acoustic output power. We first utilized MHz range frequency which was considered safe and was relevant in the treatment of ischemic stroke. The experimental results demonstrated that dual-frequency HIFU was more efficient than single-frequency, for thrombolysis. We further studied *in vitro* thrombolysis using SFFU and DFFU mediated with MBs. While it was known that DFFU and MBs could individually reduce the power threshold for thrombolysis, this study revealed that these two techniques combined, could further reduce the power required for thrombolysis and enhance efficiency. The detected cavitation signal indicated that the enhanced inertial cavitation is responsible for the enhancement. Our approach that integrated DFFU and MBs, for improving inertial cavitation, was not only useful for thrombolysis, but could also find utility in tissue ablation, drug delivery, and lipid extraction [154]. Thereafter, the numerical methodology utilized in this study reaffirmed and explained the enhanced inertial cavitation of microbubbles subjected to multi-frequency ultrasound excitation. We also confirmed that the inclusion of a low-frequency component drastically reduces

the threshold, and this had increased the influence with growing initial radii of microbubbles. On further investigation, it was found that dual-frequency excitations performed better than single frequency excitations not only in the fluid but also in soft tissue. Additionally, the advantage of dual-frequency excitations seemed to become more evident with the increase of the shear modulus of the surrounding medium. This could be particularly important as it would offer some guidance in designing sonication protocols for tissue ablation.

6.2 Future work

To further explore the potentials of multi-frequency thrombolysis, some future work is suggested based on the present dissertation:

1. Future research through *ex vivo* of human skulls and *in vivo* of animals could further demonstrate the effectiveness of multi-frequency HIFU for thrombolysis. Figure 6.1 shows an example of the *in vivo* animal study. For the *ex vivo* tests, flow system that mimics the blood flow should be considered. Of all the studies, nanodroplets could be considered as an alternative of MBs, as they are small enough to penetrate through the gap between cells or even the cell membrane [151, 177, 178]. The results of SFFU and DFFU treatment should be compared to support our hypothesis that DFFU can achieve the same thrombolysis with a lower power level. The debris from the experiments should be collected and further analyzed as a size distribution. Rt-PA could be considered in the future experimental studies as it could lyse the debris efficiently and will further lower the power required. This could be potentially important when considering the acoustic energy attenuation of the skull.

2. Real-time guided therapy should be further investigated with imaging approaches using either MRI or ultrasound. Passive cavitation detection is an alternative to the real-time guide method [115, 179, 180]. Real-time therapy monitoring could improve the safety and efficiency of thrombolysis. *e.g.* with a passive cavitation detection imaging system, the thrombolysis therapy could result in a precise, effective recanalization process with a minimal risk of collateral vessel damage.
3. The exact mechanism of enhanced thrombolysis through multi-frequency excitations holds scope for future study. The inertial cavitation that generated from the excitations could also form a shock wave that would potentially enhance the mechanical impact on the thrombi. A fast camera that could look into the bubble behavior under acoustic wave excitation could be employed to investigate the current numerical models [181]. Further numerical and experimental studies focusing on bubble cloud behavior under acoustic excitations should be carried out as most applications will use a large amount of MBs rather than a single bubble. The generation of daughter bubbles should also be considered in the bubble cloud study as well as the interactions between the bubbles [164, 182]. The optimization of the driving dual frequency acoustic waveforms should be considered in the future microbubble cavitation simulation. Different acoustic parameters should be examined in the simulation such as the choice of the two center frequencies, and the phase difference between the two frequencies.
4. The nonlinear distortion of the acoustic waveforms (due to the nonlinear nature of the acoustic medium) should be considered in the numerical model. The harmonics contained in the acoustic pressure waveform could have a non-trivial

effect on the bubble dynamics and should be studied in the future. Two approaches could be considered in the future: first, applying the real waveform that is detected through a hydrophone as the input parameter in the numerical model; second, calculating the pressure waveform using the KZK or similar approaches to replace the ideal input waveforms [118, 183-188].

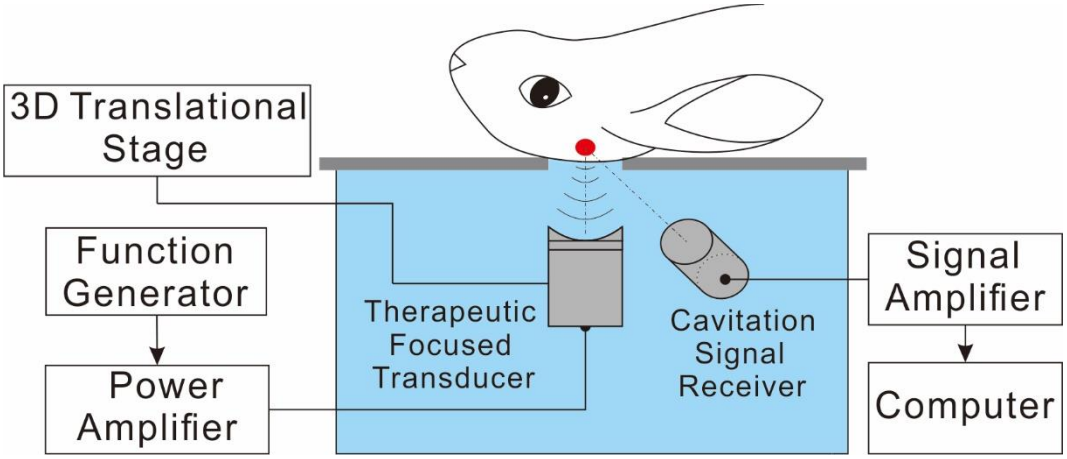

Figure 6.1 Schematic of the *in vivo* animal experiment setup.

Bibliography

1. Lloyd-Jones, D., et al., Heart disease and stroke statistics—2010 update A report from the American Heart Association. Circulation, 2010. **121**(7): p. e46-e215.
2. Towfighi, A., B. Ovbiagele, and J.L. Saver, Therapeutic milestone stroke declines from the second to the third leading organ-and disease-specific cause of death in the United States. Stroke, 2010. **41**(3): p. 499-503.
3. Engelter, S., et al., Life–threatening orolingual angioedema during thrombolysis in acute ischemic stroke. Journal of neurology, 2005. **252**(10): p. 1167-1170.
4. Bonita, R., et al., The global stroke initiative. The Lancet Neurology, 2004. **3**(7): p. 391-393.
5. González, R.G., et al., Acute ischemic stroke. 2011: Springer.
6. Tong, D., et al., Times From Symptom Onset to Hospital Arrival in the Get With The Guidelines–Stroke Program 2002 to 2009. Temporal Trends and Implications, 2012. **43**(7): p. 1912-1917.
7. Itrat, A., et al., Telemedicine in prehospital stroke evaluation and thrombolysis: Taking stroke treatment to the doorstep. JAMA Neurology, 2016. **73**(2): p. 162-168.
8. Acute Stroke Care in the US. Results from 4 Pilot Prototypes of the Paul Coverdell National Acute Stroke Registry, 2005. **36**(6): p. 1232-1240.
9. Westermark, S., et al., Effect of externally applied focused acoustic energy on clot disruption in vitro. Clinical science, 1999. **97**: p. 67-71.
10. Rosenschein, U., et al., Ultrasound Imaging–Guided Noninvasive Ultrasound Thrombolysis Preclinical Results. Circulation, 2000. **102**(2): p. 238-245.

11. Maxwell, A.D., et al., Noninvasive thrombolysis using pulsed ultrasound cavitation therapy–histotripsy. Ultrasound in medicine & biology, 2009. **35**(12): p. 1982-1994.

12. Maxwell, A.D., et al., Noninvasive treatment of deep venous thrombosis using pulsed ultrasound cavitation therapy (histotripsy) in a porcine model. Journal of vascular and interventional radiology, 2011. **22**(3): p. 369-377.

13. Burgess, A., et al., High-intensity focused ultrasound (HIFU) for dissolution of clots in a rabbit model of embolic stroke. PloS one, 2012. **7**(8): p. e42311.

14. Group, T.N.I.o.N.D.a.S.r.S.S., Tissue plasminogen activator for acute ischemic stroke, in N Eng J Med 1995. p. 8.

15. Eggers, J., et al., Effect of ultrasound on thrombolysis of middle cerebral artery occlusion. Annals of neurology, 2003. **53**(6): p. 797-800.

16. Investigators, T.I., Effects of tissue plasminogen activator and a comparison of early invasive and conservative strategies in unstable angina and non Q wave myocardial infarction: Results of the TIMI IIIb trial. Circulation, 1994. **89**: p. 1545-1556.

17. Wolpert, S., et al., Neuroradiologic evaluation of patients with acute stroke treated with recombinant tissue plasminogen activator. The rt-PA Acute Stroke Study Group. American Journal of Neuroradiology, 1993. **14**(1): p. 3-13.

18. Alexandrov, A.V., et al., Ultrasound-enhanced systemic thrombolysis for acute ischemic stroke. New England Journal of Medicine, 2004. **351**(21): p. 2170-2178.

19. Atar, S., et al., Ultrasonic thrombolysis: catheter-delivered and transcutaneous applications. European Journal of Ultrasound, 1999. **9**(1): p. 39-54.

20. Tachibana, K. and S. Tachibana, Prototype therapeutic ultrasound emitting catheter for accelerating thrombolysis. Journal of ultrasound in medicine, 1997. **16**(8): p. 529-535.

21. Datta, S., et al., Correlation of cavitation with ultrasound enhancement of thrombolysis. Ultrasound in medicine & biology, 2006. **32**(8): p. 1257-1267.

22. Daffertshofer, M. and M. Hennerici, Ultrasound in the treatment of ischaemic stroke. The Lancet Neurology, 2003. **2**(5): p. 283-290.

23. Behrens, S., et al., Potential use of therapeutic ultrasound in ischemic stroke treatment. Echocardiography, 2001. **18**(3): p. 259-263.

24. Daffertshofer, M. and M. Hennerici, Sonothrombolysis: experimental evidence. 2006.

25. Daffertshofer, M., et al., Efficacy of sonothrombolysis in a rat model of embolic ischemic stroke. Neuroscience letters, 2004. **361**(1): p. 115-119.

26. Shaw, G.J., et al., Tissue plasminogen activator concentration dependence of 120 kHz ultrasound-enhanced thrombolysis. Ultrasound in medicine & biology, 2008. **34**(11): p. 1783-1792.

27. Ishibashi, T., et al., Can transcranial ultrasonication increase recanalization flow with tissue plasminogen activator? Stroke, 2002. **33**(5): p. 1399-1404.

28. Tachibana, K. and S. Tachibana, Albumin microbubble echo-contrast material as an enhancer for ultrasound accelerated thrombolysis. Circulation, 1995. **92**(5): p. 1148-1150.

29. Shaw, G.J., et al., Ultrasound-enhanced thrombolysis with tPA-loaded echogenic liposomes. Thrombosis research, 2009. **124**(3): p. 306-310.

30. Zhou, Y. and R. Ramaswami, Comparison of Sonothrombolysis Efficiencies of Different Ultrasound Systems. Journal of Stroke and Cerebrovascular Diseases, 2014. **23**(10): p. 2730-2735.

31. Tsivgoulis, G., Safety and efficacy of ultrasound-enhanced thrombolysis: a comprehensive review and meta-analysis of randomized and nonrandomized studies. Stroke, 2010. **41**: p. 280-287.

32. Molina, C.A., Transcranial ultrasound in clinical sonothrombolysis (TUCSON) trial. Ann. Neurol., 2009. **66**: p. 28-38.

33. Daffertshofer, M., et al., Transcranial low-frequency ultrasound-mediated thrombolysis in brain ischemia increased risk of hemorrhage with combined ultrasound and tissue plasminogen activator: results of a phase II clinical trial. Stroke, 2005. **36**(7): p. 1441-1446.

34. Baron, C., et al., Simulation of intracranial acoustic fields in clinical trials of sonothrombolysis. Ultrasound in medicine & biology, 2009. **35**(7): p. 1148-1158.

35. Pajek, D. and K. Hynynen, The design of a focused ultrasound transducer array for the treatment of stroke: a simulation study. Physics in medicine and biology, 2012. **57**(15): p. 4951.

36. Iernetti, G., et al., Enhancement of high-frequency acoustic cavitation effects by a low-frequency stimulation. Ultrasonics sonochemistry, 1997. **4**(3): p. 263-268.

37. Feng, R., et al., Enhancement of ultrasonic cavitation yield by multi-frequency sonication. Ultrasonics sonochemistry, 2002. **9**(5): p. 231-236.

38. Guo, S., Y. Jing, and X. Jiang, Temperature rise in tissue ablation using multi-frequency ultrasound. Ultrasonics, Ferroelectrics, and Frequency Control, IEEE Transactions on, 2013. **60**(8): p. 1699-1707.

39. Gilles, B., et al., Reduction of ultrasound inertial cavitation threshold using bifrequency excitation. Applied physics letters, 2006. **89**(9): p. 094106.

40. Saletes, I., et al., In vitro demonstration of focused ultrasound thrombolysis using bifrequency excitation. BioMed research international, 2014. **2014**.

41. Di, J., et al., Ultrasound-triggered noninvasive regulation of blood glucose levels using microgels integrated with insulin nanocapsules. Nano Research, 2017. **10**(4): p. 1393-1402.

42. Weisel, J.W., Enigmas of Blood Clot Elasticity. Science, 2008. **320**(5875): p. 456-457.

43. Mackman, N., R.E. Tilley, and N.S. Key, Role of the Extrinsic Pathway of Blood Coagulation in Hemostasis and Thrombosis. Arteriosclerosis, Thrombosis, and Vascular Biology, 2007. **27**(8): p. 1687-1693.

44. Sim, S.K.K., A.A. Talib, and J.M. Taib, Upper Limb Post Stroke Rehabilitation Performance Monitoring Tools using Optical Mouse.

45. Mosley, I., et al., Stroke symptoms and the decision to call for an ambulance. Stroke, 2007. **38**(2): p. 361-366.

46. Jauch, E.C., et al., Guidelines for the Early Management of Patients With Acute Ischemic Stroke. A Guideline for Healthcare Professionals From the American Heart Association/American Stroke Association, 2013. **44**(3): p. 870-947.

47. Investigators, C.A.S.P.R., Prioritizing interventions to improve rates of thrombolysis for ischemic stroke. Neurology, 2005. **64**(4): p. 654-659.

48. Kleindorfer, D.O., et al., Designing a message for public education regarding stroke. Stroke, 2007. **38**(10): p. 2864-2868.

49. Scott, P.A., et al., Attitudes and Beliefs of Michigan Emergency Physicians Toward Tissue Plasminogen Activator Use in Stroke. Stroke, 2010. **41**(9): p. 2026-2032.

50. Wahlgren, N., et al., Thrombolysis with alteplase for acute ischaemic stroke in the Safe Implementation of Thrombolysis in Stroke-Monitoring Study (SITS-MOST): an observational study. The Lancet, 2007. **369**(9558): p. 275-282.

51. Wardlaw, J.M., et al., Thrombolysis for acute ischaemic stroke. Cochrane Database Syst Rev, 2009. **4**(CD000213).

52. Chung, H., R.R. Camejo, and D. Barnett, Alteplase for the treatment of acute ischaemic stroke: NICE technology appraisal guidance. Heart, 2007. **93**(12): p. 1616-1618.

53. Sharma, M., et al., Acute stroke: evaluation and treatment. Evid Rep Technol Assess (Summ), 2005. **127**: p. 1-7.

54. Saver, J.L., et al., The “golden hour” and acute brain ischemia. Stroke, 2010. **41**(7): p. 1431-1439.

55. Hill, M.D., A.M. Buchan, and C.A.f.S.E.S. Investigators, Thrombolysis for acute ischemic stroke: results of the Canadian Alteplase for Stroke Effectiveness Study. Canadian Medical Association Journal, 2005. **172**(10): p. 1307-1312.

56. Group, S.S., Tissue plasminogen activator for acute ischemic stroke. N Eng J Med., 1995. **333**: p. 1581-1587.

57. Kwiatkowski, T.G., et al., Effects of tissue plasminogen activator for acute ischemic stroke at one year. New England Journal of Medicine, 1999. **340**(23): p. 1781-1787.

58. ATLANTIS, T., Association of outcome with early stroke treatment: pooled analysis of ATLANTIS, ECASS, and NINDS rt-PA stroke trials. The Lancet, 2004. **363**(9411): p. 768-774.

59. Alberts, M.J., et al., Recommendations for the establishment of primary stroke centers. Jama, 2000. **283**(23): p. 3102-3109.

60. Szoeke, C.E., et al., Acute stroke thrombolysis with intravenous tissue plasminogen activator in an Australian tertiary hospital. The Medical Journal of Australia, 2003. **178**(7): p. 324-328.

61. Grotta, J., Lubeluzole treatment of acute ischemic stroke. Stroke, 1997. **28**(12): p. 2338-2346.

62. Bader, K.B., G. Bouchoux, and C.K. Holland, Sonothrombolysis, in Therapeutic Ultrasound. 2016, Springer. p. 339-362.

63. Pancioli, A.M., et al., The combined approach to lysis utilizing eptifibatide and rt-PA in acute ischemic stroke. Stroke, 2008. **39**(12): p. 3268-3276.

64. Cobbold, R.S., Foundations of biomedical ultrasound. 2006: Oxford University Press.

65. Szabo, T.L., Diagnostic ultrasound imaging: inside out. 2004: Academic Press.

66. Silverman, R.H., High - resolution ultrasound imaging of the eye – a review. Clinical & experimental ophthalmology, 2009. **37**(1): p. 54-67.

67. Klibanov, A.L., Microbubble contrast agents: targeted ultrasound imaging and ultrasound-assisted drug-delivery applications. Investigative radiology, 2006. **41**(3): p. 354-362.

68. Wood, R.W. and A.L. Loomis, XXXVIII. The physical and biological effects of high-frequency sound-waves of great intensity. The London, Edinburgh, and Dublin philosophical magazine and journal of science, 1927. **4**(22): p. 417-436.

69. Baker, K.G., V.J. Robertson, and F.A. Duck, A review of therapeutic ultrasound: biophysical effects. Physical therapy, 2001. **81**(7): p. 1351-1358.

70. Ter Haar, G., Therapeutic ultrasound. European Journal of Ultrasound, 1999. **9**(1): p. 3-9.

71. Hoskins, P.R., K. Martin, and A. Thrush, Diagnostic ultrasound: physics and equipment. 2010: Cambridge University Press.

72. Behrens, S., et al., Transcranial ultrasound-improved thrombolysis: diagnostic vs. therapeutic ultrasound. Ultrasound in medicine & biology, 2001. **27**(12): p. 1683-1689.

73. Smirnov, P. and K. Hynynen, Design of a HIFU array for the treatment of deep venous thrombosis: a simulation study. Phys. Med. Biol, 2017. **62**: p. 6108-25.

74. Cain, C.A., et al., Histotripsy: Transcranial applications. The Journal of the Acoustical Society of America, 2016. **140**(4): p. 3030-3030.

75. Vlaisavljevich, E., et al., Effects of tissue stiffness, ultrasound frequency, and pressure on histotripsy-induced cavitation bubble behavior. Physics in medicine and biology, 2015. **60**(6): p. 2271.

76. Ahmadi, F., et al., Bio-effects and safety of low-intensity, low-frequency ultrasonic exposure. Progress in biophysics and molecular biology, 2012. **108**(3): p. 119-138.

77. Apfel, R.E. and C.K. Holland, Gauging the likelihood of cavitation from short-pulse, low-duty cycle diagnostic ultrasound. Ultrasound in medicine & biology, 1991. **17**(2): p. 179-185.

78. Hill, C.R., J.C. Bamber, and G.R. ter Haar, Physical principles of medical ultrasonics. 2004, ASA.

79. Shi, W.T. and F. Forsberg, Ultrasonic characterization of the nonlinear properties of contrast microbubbles. Ultrasound in medicine & biology, 2000. **26**(1): p. 93-104.

80. Goertz, D.E., et al., Nonlinear intravascular ultrasound contrast imaging. Ultrasound in medicine & biology, 2006. **32**(4): p. 491-502.

81. Dollet, B., et al., Nonspherical oscillations of ultrasound contrast agent microbubbles. Ultrasound in medicine & biology, 2008. **34**(9): p. 1465-1473.

82. Lanza, G.M., Theranostic agents: From micro to nano in seconds. Nat Nano, 2015. **10**(4): p. 301-302.

83. Huynh, E., et al., In situ conversion of porphyrin microbubbles to nanoparticles for multimodality imaging. 2015. **10**: p. 325.

84. Hitchcock, K.E. and C.K. Holland, Ultrasound-assisted thrombolysis for stroke therapy better thrombus break-up with bubbles. Stroke, 2010. **41**(10 suppl 1): p. S50-S53.

85. de Saint Victor, M., et al., Properties, characteristics and applications of microbubbles for sonothrombolysis. Expert opinion on drug delivery, 2014. **11**(2): p. 187-209.

86. Holland, C., Ultrasound Contrast Agents Accelerate Sonothrombolysis. Ultrasound in Medicine and Biology, 2015. **41**(4): p. S94.

87. Datta, S., et al., Ultrasound-enhanced thrombolysis using Definity® as a cavitation nucleation agent. Ultrasound in medicine & biology, 2008. **34**(9): p. 1421-1433.

88. Petit, B., et al., Sonothrombolysis: the contribution of stable and inertial cavitation to clot lysis. Ultrasound in medicine & biology, 2015. **41**(5): p. 1402-1410.

89. Meairs, S., A. Alonso, and M.G. Hennerici, Progress in sonothrombolysis for the treatment of stroke. Stroke, 2012. **43**(6): p. 1706-1710.

90. Gao, S., et al., Improvements in cerebral blood flow and recanalization rates with transcranial diagnostic ultrasound and intravenous microbubbles after acute cerebral emboli. Investigative radiology, 2014. **49**(9): p. 593-600.

91. Hynynen, K., et al., The threshold for brain damage in rabbits induced by bursts of ultrasound in the presence of an ultrasound contrast agent (Optison®). Ultrasound in medicine & biology, 2003. **29**(3): p. 473-481.

92. Lindner, J.R., Microbubbles in medical imaging: current applications and future directions. Nature Reviews Drug Discovery, 2004. **3**(6): p. 527-533.

93. Kaufmann, B.A., K. Wei, and J.R. Lindner, Contrast echocardiography. Current problems in cardiology, 2007. **32**(2): p. 51-96.

94. Peregrine, D., The Acoustic Bubble. By TG LEIGHTON. Academic Press, 1994. 613 pp.£ 95. ISBN 0-12-441920-8. Journal of Fluid Mechanics, 1994. **272**: p. 407-408.

95. Flint, E.B. and K.S. Suslick, The temperature of cavitation. Science, 1991. **253**(5026): p. 1397.

96. Suslick, K.S., et al., Acoustic cavitation and its chemical consequences. Philosophical Transactions of the Royal Society of London A: Mathematical, Physical and Engineering Sciences, 1999. **357**(1751): p. 335-353.

97. Flannigan, D.J. and K.S. Suslick, Plasma formation and temperature measurement during single-bubble cavitation. Nature, 2005. **434**(7029): p. 52-55.

98. Vogel, A., S. Busch, and U. Parlitz, Shock wave emission and cavitation bubble generation by picosecond and nanosecond optical breakdown in water. The Journal of the Acoustical Society of America, 1996. **100**(1): p. 148-165.

99. Wang, Z., Dual-frequency Ultrasound Transducers for Medical Imaging. 2016.

100. Brujan, E., The role of cavitation microjets in the therapeutic applications of ultrasound. Ultrasound in medicine & biology, 2004. **30**(3): p. 381-387.

101. Kennedy, J.E., High-intensity focused ultrasound in the treatment of solid tumours. Nature reviews cancer, 2005. **5**(4): p. 321-327.

102. Wright, C., K. Hynynen, and D. Goertz, In vitro and in vivo high intensity focused ultrasound thrombolysis. Investigative radiology, 2012. **47**(4): p. 217.

103. Köhler, M.O., et al., Volumetric HIFU ablation under 3D guidance of rapid MRI thermometry. Medical physics, 2009. **36**(8): p. 3521-3535.

104. Suo, D., et al., Microbubble mediated dual-frequency high intensity focused ultrasound thrombolysis: An In vitro study. Applied Physics Letters, 2017. **110**(2): p. 023703.

105. Helfield, B., et al., Fluid viscosity affects the fragmentation and inertial cavitation threshold of lipid-encapsulated microbubbles. Ultrasound in medicine & biology, 2016. **42**(3): p. 782-794.

106. Suo, D., et al., Thrombolysis using multi-frequency high intensity focused ultrasound at MHz range: an in vitro study. Physics in medicine and biology, 2015. **60**(18): p. 7403.

107. Guo, S., et al. Thrombolysis enhanced by dual-frequency highintensity focused ultrasound. in Ultrasonics Symposium (IUS), 2014 IEEE International. 2014. IEEE.

108. Maxwell, A.D., et al., Cavitation clouds created by shock scattering from bubbles during histotripsy. The Journal of the Acoustical Society of America, 2011. **130**(4): p. 1888-1898.

109. Holland, C.K. and R.E. Apfel, An improved theory for the prediction of microcavitation thresholds. IEEE transactions on ultrasonics, ferroelectrics, and frequency control, 1989. **36**(2): p. 204-208.

110. Bader, K.B. and C.K. Holland, Predicting the growth of nanoscale nuclei by histotripsy pulses. Physics in medicine and biology, 2016. **61**(7): p. 2947.

111. Hynynen, K., et al., MR imaging-guided focused ultrasound surgery of fibroadenomas in the breast: A feasibility study 1. Radiology, 2001. **219**(1): p. 176-185.

112. Sokka, S., T. Gauthier, and K. Hynynen, Theoretical and experimental validation of a dual-frequency excitation method for spatial control of cavitation. Physics in medicine and biology, 2005. **50**(9): p. 2167.

113. McDannold, N., et al., Transcranial MRI-guided focused ultrasound surgery of brain tumors: Initial findings in three patients. Neurosurgery, 2010. **66**(2): p. 323.

114. Hynynen, K. and N. McDannold, MRI-guided focused ultrasound for local tissue ablation and other image-guided interventions. 2006.

115. Mancia, L., et al., Predicting Tissue Susceptibility to Mechanical Cavitation Damage in Therapeutic Ultrasound. Ultrasound in Medicine & Biology, 2017.

116. Ma, J., et al., Design, fabrication, and characterization of a single-aperture 1.5-MHz/3-MHz dual-frequency HIFU transducer. Ultrasonics, Ferroelectrics, and Frequency Control, IEEE Transactions on, 2013. **60**(7): p. 1519-1529.

117. Cui, H. and X. Yang, Laser enhanced high-intensity focused ultrasound thrombolysis: An in vitro study. The Journal of the Acoustical Society of America, 2013. **133**(2): p. EL123-EL128.

118. Jing, Y., M. Tao, and G.T. Clement, Evaluation of a wave-vector-frequency-domain method for nonlinear wave propagation. The Journal of the Acoustical Society of America, 2011. **129**(1): p. 32-46.

119. Jing, Y., J. Cannata, and T. Wang, Experimental verification of transient nonlinear acoustical holography. The Journal of the Acoustical Society of America, 2013. **133**(5): p. 2533-2540.

120. Chen, W.-S., et al., Inertial cavitation dose and hemolysis produced in vitro with or without Optison®. Ultrasound in medicine & biology, 2003. **29**(5): p. 725-737.

121. Meunier, J.M., et al., Duty cycle dependence of ultrasound enhanced thrombolysis in a human clot model. Ultrasound in medicine & biology, 2007. **33**(4): p. 576-583.

122. Hwang, J.H., et al., Correlation between inertial cavitation dose and endothelial cell damage in vivo. Ultrasound in medicine & biology, 2006. **32**(10): p. 1611-1619.

123. Saletes, I., B. Gilles, and J.-C. Bera, Promoting inertial cavitation by nonlinear frequency mixing in a bifrequency focused ultrasound beam. Ultrasonics, 2011. **51**(1): p. 94-101.

124. Brennen, C.E., Fission of collapsing cavitation bubbles. Journal of Fluid Mechanics, 2002. **472**: p. 153-166.

125. Ciuti, P., et al., Study into mechanisms of the enhancement of multibubble sonoluminescence emission in interacting fields of different frequencies. Ultrasonics sonochemistry, 2003. **10**(6): p. 337-341.

126. Zhang, Y., et al., Instability of interfaces of gas bubbles in liquids under acoustic excitation with dual frequency. Ultrasonics sonochemistry, 2015. **23**: p. 16-20.

127. Zhang, Y. and S. Li, Acoustical scattering cross section of gas bubbles under dual-frequency acoustic excitation. Ultrasonics Sonochemistry, 2015.

128. Chauvet, D., et al., Targeting accuracy of transcranial magnetic resonance-guided high-intensity focused ultrasound brain therapy: a fresh cadaver model Laboratory investigation. Journal of Neurosurgery, 2013. **118**(5): p. 1046-1052.

129. Jing, Y., F.C. Meral, and G.T. Clement, Time-reversal transcranial ultrasound beam focusing using a k-space method. Physics in Medicine and Biology, 2012. **57**(4): p. 901-917.

130. Barber, P., et al., Why are stroke patients excluded from TPA therapy? An analysis of patient eligibility. Neurology, 2001. **56**(8): p. 1015-1020.

131. Saqqur, M., et al., Site of arterial occlusion identified by transcranial Doppler predicts the response to intravenous thrombolysis for stroke. Stroke, 2007. **38**(3): p. 948-954.

132. Weisel, J., Structure of fibrin: impact on clot stability. Journal of Thrombosis and Haemostasis, 2007. **5**(s1): p. 116-124.

133. Bader, K.B., et al., Efficacy of histotripsy combined with rt-PA in vitro. Physics in Medicine and Biology, 2016. **61**(14): p. 5253.

134. Culp, W.C., et al., Successful microbubble sonothrombolysis without tissue-type plasminogen activator in a rabbit model of acute ischemic stroke. Stroke, 2011. **42**(8): p. 2280-2285.

135. Tsivgoulis, G., et al., Safety and efficacy of ultrasound-enhanced thrombolysis a comprehensive review and meta-analysis of randomized and nonrandomized studies. Stroke, 2010. **41**(2): p. 280-287.

136. Molina, C.A., et al., Transcranial ultrasound in clinical sonothrombolysis (TUCSON) trial. Annals of neurology, 2009. **66**(1): p. 28-38.

137. WESTERMARK, S., et al., Effect of externally applied focused acoustic energy on clot disruption in vitro. Clinical science, 1999. **97**(1): p. 67-71.

138. Yang, W. and Y. Zhou, Effect of Pulse Repetition Frequency of High-Intensity Focused Ultrasound on In Vitro Thrombolysis. Ultrasonics Sonochemistry, 2016.

139. Hynynen, K. and N. McDannold, MRI-guided focused ultrasound for local tissue ablation and other image-guided interventions, in Emerging Therapeutic Ultrasound. 2006, World Scientific. p. 167-218.

140. Tran, B.C., et al., Microbubble-enhanced cavitation for noninvasive ultrasound surgery. IEEE transactions on ultrasonics, ferroelectrics, and frequency control, 2003. **50**(10): p. 1296-1304.

141. Brown, A.T., et al., Microbubbles improve sonothrombolysis in vitro and decrease hemorrhage in vivo in a rabbit stroke model. Investigative radiology, 2011. **46**(3).

142. Petit, B., et al., In vitro sonothrombolysis of human blood clots with BR38 microbubbles. Ultrasound in medicine & biology, 2012. **38**(7): p. 1222-1233.

143. Culp, W.C., et al., Successful Microbubble Sonothrombolysis Without Tissue Plasminogen Activator in a Rabbit Model of Acute Ischemic Stroke. Circulation, 2010. **122**(Suppl 21): p. A12635-A12635.

144. Chen, R., et al., In vivo sonothrombolysis of ear marginal vein of rabbits monitored with high-frequency ultrasound needle transducer. Journal of medical and biological engineering, 2013. **33**(1): p. 103.

145. Perren, F., et al., Microbubble potentiated transcranial duplex ultrasound enhances IV thrombolysis in acute stroke. Journal of thrombosis and thrombolysis, 2008. **25**(2): p. 219-223.

146. Liu, H.-L. and C.-M. Hsieh, Single-transducer dual-frequency ultrasound generation to enhance acoustic cavitation. Ultrasonics sonochemistry, 2009. **16**(3): p. 431-438.

147. Zhang, Y., Rectified mass diffusion of gas bubbles in liquids under acoustic field with dual frequencies. International Communications in Heat and Mass Transfer, 2012. **39**(10): p. 1496-1499.

148. Zhang, Y. and S. Li, Acoustical scattering cross section of gas bubbles under dual-frequency acoustic excitation. Ultrasonics sonochemistry, 2015. **26**: p. 437-444.

149. Guo, S., Y. Jing, and X. Jiang, Temperature rise in tissue ablation using multi-frequency ultrasound. IEEE transactions on ultrasonics, ferroelectrics, and frequency control, 2013. **60**(8): p. 1699-1707.

150. Yang, X. and J. Jo, Enhanced cavitation by using two consecutive ultrasound waves at different frequencies. Applied physics letters, 2014. **105**(19): p. 193701.

151. Lindsey, B.D., J.D. Rojas, and P.A. Dayton, On the relationship between microbubble fragmentation, deflation and broadband superharmonic signal production. Ultrasound in medicine & biology, 2015. **41**(6): p. 1711-1725.

152. Jinwook Kim, B.D.L., Wei-Yi Chang, Xuming Dai, Joseph M. Stavas, Paul A. Dayton, Xiaoning Jiang, Laser-Generated-Focused Ultrasound Transducers for

Microbubble-Mediated, Dual-Excitation Sonothrombolysis, in IEEE International Ultrasonics Symposium. 2016.

153. Lai, C.-Y., et al., Quantitative relations of acoustic inertial cavitation with sonoporation and cell viability. Ultrasound in medicine & biology, 2006. **32**(12): p. 1931-1941.

154. Wang, M., et al., Disruption of microalgal cells using high-frequency focused ultrasound. Bioresource technology, 2014. **153**: p. 315-321.

155. Suo, D., et al., Numerical investigation of the inertial cavitation threshold under multi-frequency ultrasound. Ultrasonics Sonochemistry, 2018. **41**(Supplement C): p. 419-426.

156. Kennedy, J., G. Ter Haar, and D. Cranston, High intensity focused ultrasound: surgery of the future? The British journal of radiology, 2014.

157. Wu, F., et al., Pathological changes in human malignant carcinoma treated with high-intensity focused ultrasound. Ultrasound in medicine & biology, 2001. **27**(8): p. 1099-1106.

158. Prosperetti, A., A generalization of the Rayleigh–Plesset equation of bubble dynamics. The Physics of Fluids, 1982. **25**(3): p. 409-410.

159. Chen, X.-P., C.-W. Zhong, and X.-L. Yuan, Lattice Boltzmann simulation of cavitating bubble growth with large density ratio. Computers & Mathematics with Applications, 2011. **61**(12): p. 3577-3584.

160. Chahine, G.L. and C.-T. Hsiao, Modeling microbubble dynamics in biomedical applications. Journal of Hydrodynamics, Ser. B, 2012. **24**(2): p. 169-183.

161. Farny, C.H., R.G. Holt, and R. Roy, The correlation between bubble-enhanced HIFU heating and cavitation power. Biomedical Engineering, IEEE Transactions on, 2010. **57**(1): p. 175-184.

162. Keller, J.B. and M. Miksis, Bubble oscillations of large amplitude. The Journal of the Acoustical Society of America, 1980. **68**(2): p. 628-633.

163. Katiyar, A., K. Sarkar, and F. Forsberg, Modeling subharmonic response from contrast microbubbles as a function of ambient static pressure. The Journal of the Acoustical Society of America, 2011. **129**(4): p. 2325-2335.

164. Yasui, K., et al., Numerical simulations of acoustic cavitation noise with the temporal fluctuation in the number of bubbles. Ultrasonics sonochemistry, 2010. **17**(2): p. 460-472.

165. Wang, M. and W. Yuan, Modeling bubble dynamics and radical kinetics in ultrasound induced microalgal cell disruption. Ultrasonics sonochemistry, 2016. **28**: p. 7-14.

166. Yang, X. and C.C. Church, A model for the dynamics of gas bubbles in soft tissue. The Journal of the Acoustical Society of America, 2005. **118**(6): p. 3595-3606.

167. Church, C.C., C. Labuda, and K. Nightingale, A theoretical study of inertial cavitation from acoustic radiation force impulse imaging and implications for the mechanical index. Ultrasound in medicine & biology, 2015. **41**(2): p. 472-485.

168. Guédra, M., C. Inserra, and B. Gilles, Accompanying the frequency shift of the nonlinear resonance of a gas bubble using a dual-frequency excitation. Ultrasonics Sonochemistry, 2017. **38**: p. 298-305.

169. Avvaru, B. and A.B. Pandit, Experimental investigation of cavitational bubble dynamics under multi-frequency system. Ultrasonics sonochemistry, 2008. **15**(4): p. 578-589.

170. Guédra, M., et al. Numerical investigations of single bubble oscillations generated by a dual frequency excitation. in Journal of Physics: Conference Series. 2015. IOP Publishing.

171. Zhang, Y., D. Billson, and S. Li, Influences of pressure amplitudes and frequencies of dual-frequency acoustic excitation on the mass transfer across interfaces of gas bubbles. International Communications in Heat and Mass Transfer, 2015.

172. Zhang, Y., et al., Acoustic wave propagation in bubbly flow with gas, vapor or their mixtures. Ultrasonics Sonochemistry, 2017.

173. Zhang, Y., et al., Effects of mass transfer on damping mechanisms of vapor bubbles oscillating in liquids. Ultrasonics Sonochemistry, 2018. **40**(Part A): p. 120-127.

174. Zhang, Y. and Y. Zhang, Chaotic oscillations of gas bubbles under dual-frequency acoustic excitation. Ultrasonics Sonochemistry, 2017.

175. Zhang, Y., Y. Gao, and X. Du, Stability mechanisms of oscillating vapor bubbles in acoustic fields. Ultrasonics Sonochemistry, 2018. **40**: p. 808-814.

176. Lauterborn, W. and T. Kurz, Physics of bubble oscillations. Reports on Progress in Physics, 2010. **73**(10): p. 106501.

177. Abbaspourrad, A., et al., Microfluidic fabrication of stable gas-filled microcapsules for acoustic contrast enhancement. Langmuir, 2013. **29**(40): p. 12352-12357.

178. Mullin, L.B., L.C. Phillips, and P.A. Dayton, Nanoparticle delivery enhancement with acoustically activated microbubbles. IEEE transactions on ultrasonics, ferroelectrics, and frequency control, 2013. **60**(1): p. 65-77.

179. Steven, P.A., et al., The response of MRI contrast parameters in in vitro tissues and tissue mimicking phantoms to fractionation by histotripsy. Physics in Medicine & Biology, 2017. **62**(17): p. 7167.

180. Mfoumou, E., et al., Time-dependent hardening of blood clots quantitatively measured in vivo with shear-wave ultrasound imaging in a rabbit model of venous thrombosis. Thrombosis research, 2014. **133**(2): p. 265-271.

181. Johansen, K., et al., Deconvolution of acoustically detected bubble-collapse shock waves. Ultrasonics, 2017. **73**(Supplement C): p. 144-153.

182. De Giacomo, A., et al., Cavitation dynamics of laser ablation of bulk and wire-shaped metals in water during nanoparticles production. Physical Chemistry Chemical Physics, 2013. **15**(9): p. 3083-3092.

183. Hamilton, M.F. and D.T. Blackstock, Nonlinear acoustics. Vol. 1. 1998: Academic press San Diego.

184. Averkiou, M.A. and R.O. Cleveland, Modeling of an electrohydraulic lithotripter with the KZK equation. The Journal of the Acoustical Society of America, 1999. **106**(1): p. 102-112.

185. Jing, Y. and J. Cannata. Experimental verification of a wave-vector-frequency-domain nonlinear acoustic model. in Proceedings of Meetings on Acoustics ICA2013. 2013. ASA.

186. Jing, Y., M. Tao, and J. Cannata, An improved wave-vector frequency-domain method for nonlinear wave modeling. IEEE transactions on ultrasonics, ferroelectrics, and frequency control, 2014. **61**(3): p. 515-524.

187. Jing, Y., T. Wang, and G.T. Clement, A k-space method for moderately nonlinear wave propagation. IEEE transactions on ultrasonics, ferroelectrics, and frequency control, 2012. **59**(8): p. 1664-1673.

188. Gu, J. and Y. Jing, Modeling of wave propagation for medical ultrasound: a review. IEEE transactions on ultrasonics, ferroelectrics, and frequency control, 2015. **62**(11): p. 1979-1992.

Appendices

Appendix A

MATLAB code for acoustic cavitation threshold:

For criteria: $\frac{dR}{dt} = c$

Main:

```
clear all
clc
close all
global Pa0 R0
grad_thres=1540;
Pa0_all = 0.01e6 : 0.02e6 : 10.2e6;       % range of pressure amplitude
R0_all = 0.01e-6 : 0.05e-6 : 10e-6;       % range of initial bubble radii

[~, np] = size(Pa0_all);
[~, nr] = size(R0_all);

Numecs_all = zeros(nr, np);

for ir = 1 : nr
   R0 = R0_all(ir);                    % max dr/dt= c in the medium
   pmax = 0;
   for ip = 1 : np
      Pa0 = Pa0_all(ip);
      [Numecs_all(ir, ip)] = call_case1_bubdual;

      grad_max = Numecs_all(ir, ip);
      if grad_max >= 1540
         pmax = Pa0;
         if ip == 1
           fprintf ('initial Rmax is too large \n')
         end
         break
      end

      if ip == np
         fprintf('pmax is not found \n')
      end

   end
   P_thres(ir) = pmax;
end

 figure(1)
 plot(R0_all,P_thres)
```

Function 1:

```
function [grad_max] = call_case1_bubdual()
global Pa0 R0

tspan=[0*10^-6 40*10^-6];          % set time interval
[t,y] = ode45(@case1_bubdual,tspan,[( R0 ) 0]);

R = y(:, 1);
grad=y(:,2);
Rmax= max(R);
grad_max=max(abs(grad));

end
```

Function 2:

```
%% This file refers to an input of linear combination of 2 pressure waves

function y = case1_bubdual(t,x)
global Pa0 R0

y=zeros(2,1);
% R0=(10^-6);               %Initial bubble radius
Pam1=Pa0;                   %1st Pressure amplitude
Pam2=0;                     %2nd Pressure amplitude
fc1=1.5*(10^6);             %Frequency of pressure
fc2=1.45*(10^6);            %Frequency of pressure
P1=Pam1*sin(2*3.14*fc1*t);    %Pressure wave 1
P2=Pam2*sin(2*3.14*fc2*t);    %Pressure wave 2
Pinf=101*(10^3);            %Fluid pressure
density=1060;               %Density of Fluid
c=1540;                     %Speed of sound in fluid
S=0.056;                    %Surface Tension
k=1.4;                      %Polytropic Index
u=0.005;                    %Viscosity
G=1.5*(10^6);               %Shear Modulus
Pg0=Pinf+(2*S/R0);          %Initial Gas Pressure in bubble

% Seven terms are added to find the double derivative of R, which is solved
% for R, with ode45
RHS1 = (1/ density)*(1 + (x(2))/c)*(Pg0*((R0/x(1))^(3*k)) - Pinf + (P1+P2) - (2*S/x(1))
- (4*u*x(2)/x(1))- (4*G/(3*((x(1))^3)))*((x(1))^3 -(R0^3)));
RHS2 = -1.5*(1 - x(2)/(3*c))*((x(2))^2);
RHS3 = (2*S/(density*c*x(1)))*x(2);
RHS4 = -(4*G*(R0^3)*((x(1))^-3)*x(2))/(density*c);
```

```
RHS5 = (-3*k)*(Pg0/(density*c))*((x(1))^(-3*k))*(R0^(3*k))* x(2);
RHS6 = +(Pam1/(density*c))*2*3.14*fc1*cos(2*3.14*fc1*t)*x(1)+(Pam2/(density*c))*2*3.14*fc2*cos(2*3.14*fc2*t)*x(1);
RHS7 = (((x(2))^2)*4*u/(density*c*x(1)));

%So,
R_doublederivative = (RHS1+RHS2+RHS3+RHS4+RHS5+RHS6+RHS7)/(((4*u/(density*c)) + (1-(x(2))/(density*c))*x(1)));%Double-derivative of R
y(1)=x(2); % get z(1)
y(2)=R_doublederivative; % get z(2)
end
```

For criteria: $R = 2 \times R0$

```
Main:
close all
global Pa0 R0
Pa0_all = 0.01e6 : 0.02e6 : 3.0e6;
R0_all = 0.1e-6 : 0.1e-6 : 5e-6;

[~, np] = size(Pa0_all);
[~, nr] = size(R0_all);

Numecs_all = zeros(nr, np);

% R0  = 10e-6;                    % bubble initial radius in meter
for ir = 1 : nr
   R0 = R0_all(ir);
   R_thres = 2*R0;
   pmax = 0;
   for ip = 1 : np
      Pa0 = Pa0_all(ip);
      [Numecs_all(ir, ip)] = call_case1_bubdual;
%       ip
%       ir
      Rmax = Numecs_all(ir, ip);
      if Rmax >= R_thres
         pmax = Pa0;
         if ip == 1
            fprintf ('initial Rmax is too large \n')
         end
         break
      end
```

```
        if ip == np
            fprintf('pmax is not found \n')
        end

    end
    P_thres(ir) = pmax;
end
figure(1)
plot(Pa0_all,Numecs_all')
figure(2)
 plot(R0_all,P_thres)
```

Function 1:

```
function [Rmax] = call_case1_bubdual()
global Pa0 R0
% Pa0=10^6;
% R0=10^-6;
tspan=[10*10^-6 40*10^-6]; % set time interval
[t,y] = ode45(@case1_bubdual,tspan,[( R0 ) 0]);

R = y(:, 1);

Rmax= max(R);
figure (3)
plot(t,y(:,1));
hold on
xlabel('Time(in microseconds)')
ylabel('Radius(in micrometer)')
end
```

Function 2:

```
%This file refers to an input of linear combination of 2 pressure waves
function y = case1_bubdual(t,x)
global Pa0 R0

y=zeros(2,1);
% R0=(10^-6); %Initial bubble radius
Pam1=Pa0;%1st Pressure amplitude
Pam2=0;%2nd Pressure amplitude
fc1=1*(10^6); %Frequency of pressure
fc2=1.4*(10^6); %Frequency of pressure
P1=Pam1*sin(2*3.14*fc1*t);%Pressure wave 1
P2=Pam2*sin(2*3.14*fc2*t);%Pressure wave 2
Pinf=101*(10^3); %Fluid pressure
```

```
density=1060; %Density of Fluid
c=1540; %Speed of sound in fluid
S=0.056; %Surface Tension
k=1.4; %Polytropic Index
u=0.015; %Viscosity
G=0*10^6; %Shear Modulus
Pg0=Pinf+(2*S/R0);%Initial Gas Pressure in bubble

% Seven terms are added to find the double derivative of R, which is solved
% for R, with ode45
RHS1 = (1/ density)*(1 + (x(2))/c)*(Pg0*((R0/x(1))^(3*k)) - Pinf + (P1+P2) - (2*S/x(1))
- (4*u*x(2)/x(1))- (4*G/(3*((x(1))^3)))*((x(1))^3 -(R0^3)));
RHS2 = -1.5*(1 - x(2)/(3*c))*((x(2))^2);
RHS3 = (2*S/(density*c*x(1)))*x(2);
RHS4 = -(4*G*(R0^3)*((x(1))^-3)*x(2))/(density*c);
RHS5 = (-3*k)*(Pg0/(density*c))*((x(1))^(-3*k))*(R0^(3*k))* x(2);
RHS6                                                                    =
+(Pam1/(density*c))*2*3.14*fc1*cos(2*3.14*fc1*t)*x(1)+(Pam2/(density*c))*2*3.14*f
c2*cos(2*3.14*fc2*t)*x(1);
RHS7 = (((x(2))^2)*4*u/(density*c*x(1)));

%So,
R_doublederivative                                                      =
(RHS1+RHS2+RHS3+RHS4+RHS5+RHS6+RHS7)/(((4*u/(density*c))      +      (1-
(x(2))/(density*c))*x(1)));%Double-derivative of R
y(1)=x(2); % get z(1)
y(2)=R_doublederivative; % get z(2)
end
```

MATLAB code for video/imaging processing:
Main:

```
% 1) Program to extract frames from a movie and save individual frames to separate
image files.
% 2) Program rebuilds a new movie by recalling the saved images from disk.
% 3) Program computes the mean gray value of the color channels (if needed) and detects
the difference between a frame and the previous frame.
% 4) It uses VideoReader and VideoWriter classes.

clc;
close all;        % Close all figures (except imtool figures).
imtool close all;  % Close all imtool figures.
clear;
workspace;  % Make sure the workspace panel is showing.
fontSize = 22;
```

%%%%%%%%%%%%%%%%%%%%%%%%%%%%%%%%%%%% CHECK 1- Open the movie and get the folder %%

folder = fileparts(which('recording.mp4')); % Determine where demo folder is (works with all versions).
movieFullFileName = fullfile(folder, 'recording.mp4');% Pick the two movie.

%%%

```
if ~exist(movieFullFileName, 'file') % Check to see that the video file exists.
   strErrorMessage = sprintf('File not found:\n%s\nYou can choose a new one, or cancel', movieFullFileName);
   response = questdlg(strErrorMessage, 'File not found', 'OK - choose a new movie.', 'Cancel', 'OK - choose a new movie.');
   if strcmpi(response, 'OK - choose a new movie.')
      [baseFileName, folderName, FilterIndex] = uigetfile('*.avi');
      if ~isequal(baseFileName, 0)
         movieFullFileName = fullfile(folderName, baseFileName);
      else
         return;
      end
   else
      return;
   end
end
try
   videoObject = VideoReader(movieFullFileName)
   numberOfFrames = videoObject.NumberOfFrames;                % Determine how many frames there are.
   vidHeight = videoObject.Height;
   vidWidth = videoObject.Width;
   numberOfFramesWritten = 0;                % Prepare a figure to show the images in the upper half of the screen.
   figure;
                                             % screenSize = get(0, 'ScreenSize');
   set(gcf, 'units','normalized','outerposition',[0 0 1 1]);   % Enlarge figure to full screen.

   promptMessage = sprintf('Do you want to save the individual frames out to individual disk files?');  % Ask user if they want to write the individual frames out to disk.
   button = questdlg(promptMessage, 'Save individual frames?', 'Yes', 'No', 'Yes');
   if strcmp(button, 'Yes')
      writeToDisk = true;
      [folder, baseFileName, extentions] = fileparts(movieFullFileName); % Extract out the various parts of the filename.
      folder = pwd;    % Make a new output subfolder for all the separately extracted movie frames to be saved to disk
```

```
    outputFolder = sprintf('%s/Movie Frames from %s', folder, baseFileName);

    if ~exist(outputFolder, 'dir') % Create the folder if it doesn't exist already.
      mkdir(outputFolder);
    end
  else
    writeToDisk = false;
  end

  % Loop through the movie, writing all frames out. Each frame will be in a separate file with unique name.
  meanGrayLevels = zeros(numberOfFrames, 1);
  meanRedLevels = zeros(numberOfFrames, 1);
  meanGreenLevels = zeros(numberOfFrames, 1);
  meanBlueLevels = zeros(numberOfFrames, 1);

  for frame = 1 : numberOfFrames
    thisFrame = read(videoObject, frame); % Extract the frame from the movie structure.

    % Display it
    hImage = subplot(2, 2, 1);
    image(thisFrame);
    caption = sprintf('Frame %4d of %d.', frame, numberOfFrames);
    title(caption, 'FontSize', fontSize);
    drawnow; % Force it to refresh the window.

    % Write the image array to the output file, if requested.
    if writeToDisk
      % Construct an output image file name.
      outputBaseFileName = sprintf('Frame %4.4d.png', frame);
      outputFullFileName = fullfile(outputFolder, outputBaseFileName);

      % Stamp the name and frame number onto the image. At this point it's just going into the overlay, not actually getting written into the pixel values.
      text(5, 15, outputBaseFileName, 'FontSize', 20);

      % Extract the image with the text "burned into" it.
      frameWithText = getframe(gca);
      % frameWithText.cdata is the image with the text actually written into the pixel values. Write it out to disk.
      imwrite(frameWithText.cdata, outputFullFileName, 'png');
    end

    % Calculate the mean gray level.
    grayImage = rgb2gray(thisFrame);
```

```
        meanGrayLevels(frame) = mean(grayImage(:));

        % Calculate the mean R, G, and B levels.
        meanRedLevels(frame) = mean(mean(thisFrame(:, :, 1)));
        meanGreenLevels(frame) = mean(mean(thisFrame(:, :, 2)));
        meanBlueLevels(frame) = mean(mean(thisFrame(:, :, 3)));


      %%%%%%%%%%%%%%%%%%%%%%%%%%%%%%%%%%%%%%%%%%%%    CHECK
2 - Plot the binary image with threshold for clarity of blood clot.  %%

             BW_1=im2bw(grayImage,0.3);

        %%%%%%%%%%%%%%%%%%%%%%%%%%%%
        n_white_with_clot(frame)=sum(BW_1(:));
        n_black_with_clot(frame)=numel(BW_1)-n_white_with_clot(frame);


        %%%%%%%%%%%%%%%%%%%%%%%%%%%%%%%%%%%%%%%%%%%%%%
CHECK 3- Plot binary image of empty tube with threshold for clarity of empty tube.
%%%%%%%%%%%%%%%%%%%%%%%%%%%%%%%%%%%%%%%%%%%%%%

              BW_2=im2bw(grayImage,0.05);

%%%%%%%%%%%%%%%%%%%%%%%%%%%%

        n_white_without_clot(frame)=sum(BW_2(:));
        n_black_without_clot(frame)=numel(BW_2)-n_white_with_clot(frame);

        % Percentage area removed
        percent_area(frame)=((n_white_without_clot(frame)-
n_white_with_clot(frame))/n_white_without_clot(frame))*100;



    end

    % Alert user that we're done.
    if writeToDisk
        finishedMessage = sprintf('Done. Wrote %d frames to folder\n"%s"',
numberOfFramesWritten, outputFolder);
    else
        finishedMessage = sprintf('Done. Processed %d frames of\n"%s"',
numberOfFramesWritten, movieFullFileName);
    end
    disp(finishedMessage); % Write to command window.
```

```
uiwait(msgbox(finishedMessage)); % Also pop up a message box.

% Exit if they didn't write any individual frames out to disk.
if ~writeToDisk
  return;
end

% Ask user if they want to read the individual frames from the disk, that they just wrote out, back into a movie and display it.
promptMessage = sprintf('Do you want to recall the individual frames\nback from disk into a recording?\n(This will take several seconds.)');
button = questdlg(promptMessage, 'Recall Recording?', 'Yes', 'No', 'Yes');
if strcmp(button, 'No')
  return;
end

% Create a VideoWriter object to write the video out to a new, different file.
writerObj = VideoWriter('something.avi');
open(writerObj);

% Read the frames back in from disk, and convert them to a movie. Preallocate recalledMovie, which will be an array of structures. First get a cell array with all the frames.
allTheFrames = cell(numberOfFrames,1);
allTheFrames(:) = (zeros(vidHeight, vidWidth, 3, 'uint8'))F;
% Next get a cell array with all the colormaps.
allTheColorMaps = cell(numberOfFrames,1);
allTheColorMaps(:) = (zeros(256, 3));
% Now combine these to make the array of structures.
recalledMovie = struct('cdata', allTheFrames, 'colormap', allTheColorMaps)
for frame = 1 : numberOfFrames
  % Construct an output image file name.
  outputBaseFileName = sprintf('Frame %4.4d.png', frame);
  outputFullFileName = fullfile(outputFolder, outputBaseFileName);
  % Read the image in from disk.
  thisFrame = imread(outputFullFileName);
  % Convert the image into a "movie frame" structure.
  recalledMovie(frame) = im2frame(thisFrame);
  % Write this frame out to a new video file.
  writeVideo(writerObj, thisFrame);
end
close(writerObj);
% Get rid of old image and plot.
delete(hImage);
delete(hPlot);
% Create new axes for our movie.
```

```
    subplot(1, 3, 2);
    axis off;  % Turn off axes numbers.
    title('Recording recalled from disk', 'FontSize', fontSize);
    % Play the movie in the axes.
    movie(recalledMovie);

    msgbox('Done with this recording');

catch ME
    % Some error happened if you get here.
    strErrorMessage = sprintf('Error extracting frames from:\n\n%s\n\nError: %s\n\n)',
movieFullFileName, ME.message);
    uiwait(msgbox(strErrorMessage));
end
```

Data Analysis

```
% Plot percentage of blood clot left
figure
p = 1 : numberOfFrames;
time=(p/30).';
norm_percent=(100/percent_area(3))*percent_area;
result=(medfilt1(norm_percent,4000)).';
plot(time,result(p));
grid on
xlabel('Time (in seconds)');
ylabel('Percentage of blood clot remaining');
coefficients = polyfit(time, result, 1);
% Now get the slope, which is the first coefficient in the array:
slope = coefficients(1)
```

Appendix B

Calibrated flow rate of the peristaltic pump

setting	time to fill 10 mL (s)	average	rate (mL/s)
2	14.7		
2	14.13	14.43	0.693
2	14.46		
3	12.82		
3	12.36	12.63	0.792
3	12.7		
4	11.05		
4	10.93	11.06	0.904
4	11.2		
5	9.55		
5	9.59	9.63	1.04
5	9.76		
6	8.92		
6	9	9.01	1.109
6	9.12		
7	8.35		
7	8.22	8.21	1.218
7	8.03		
8	7.59		
8	7.4	7.51	1.332
8	7.55		
9	7.02		
9	6.88	6.97	1.435
9	7.01		
10	6.76		
10	6.79	6.72	1.488
10	6.6		

Appendix C

Calculation of pressure measured from hydrophone.

	HNC-0200	HNC-0400	HNC-1000	HNC-1500
Frequency range (±6dB)	1 - 10 MHz			
* EOC Nominal Sensitivity [dB re 1V/uPa]	-271	-259	-245	-239
* EOC Nominal Sensitivity [nV/Pa]	28	112	562	1122
Acceptance angle (-6dB at 5 MHz)	90º	60º	25º	15º
Capacitance [pF]	70	70	90	100
Max. Operating Temperature	50ºC			

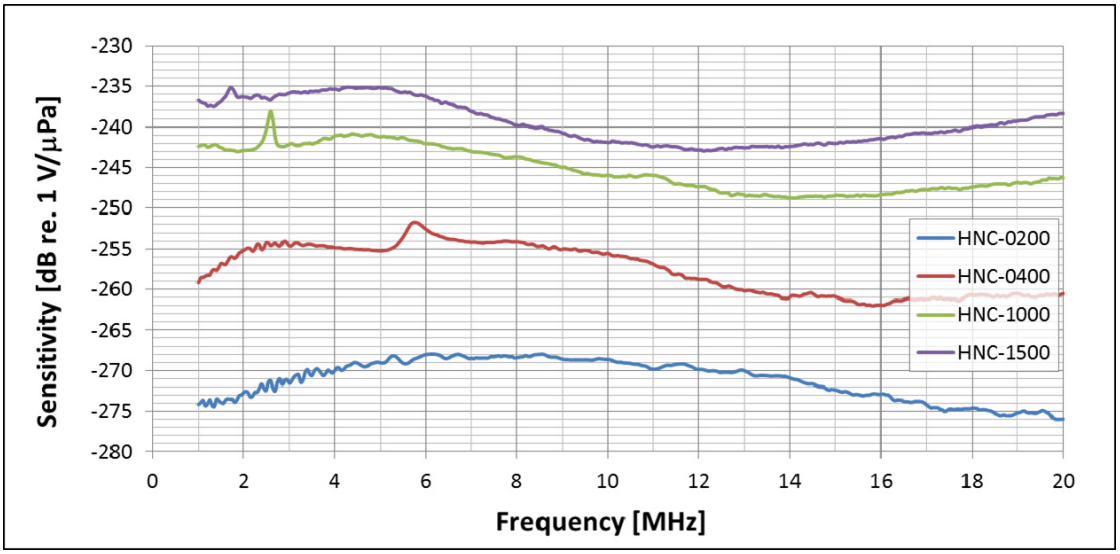

Here are the calculations for sensitivity when taking into account the preamplifier:

$$M_L(f) = G(f) M_c(f) \left(\frac{C_H}{C_H + C_c + C_A} \right)$$

$G(f)$ = Amplifier gain

$M_c(f)$ = Hydrophone End-of-Cable Open Circuit (EOC) sensitivity

C_H = Capacitance of hydrophone

C_A = Capacitance of amplifier

C_c = Capacitance of connector

Hydrophone: HNC 200 → Capacitance = 70 pf ; EOC = -271 dB re $\frac{1V}{\mu Pa}$

Preamplifier: AH 2020 → Capacitance = 8 pf ; Gain = 20 dB

$$Original\ sensitivity\ from\ the\ plots: M_c = 10 \times 10^{-\frac{271}{20}} \times \left(\frac{1}{10^{-6}} \right) = 2.8 \times 10^{-7} \frac{V}{Pa}$$

$$M_L = 10 \times 10^{-\frac{271}{20}} \times \left(\frac{1}{10^{-6}} \right) \times \left(\frac{70 \times 10^{-12}}{70 \times 10^{-12} + 8 \times 10^{-12}} \right) = 2.5281 \times 10^{-7} \frac{V}{Pa}$$

Then the pressure level will be

$$Pressure = Voltage / M_L$$

Appendix D

Clot imaging processing

```
%% credit to Image Analyst and others on MathWorks for ideas

clc;                           % Clear the command window.
close all;                     % Close all figures (except those of
imtool.)
imtool close all;              % Close all imtool figures.
clear;                         % Erase all existing variables..
workspace;                     % Make sure the workspace panel is showing.
format long g;
format compact;
fontSize = 24;
scale = 10/180;
%=========================================================================
=========

%% Initial Clot Condition Image Processing

%% STEP 1.
% Read in the blood clot colour image.

folder = 'E:\robot transducer\dip';
baseFileName = 'single3.5beforetreat.png';

%% STEP2.
% Get the full filename, with path prepended.

fullFileName = fullfile(folder, baseFileName);
if ~exist(fullFileName, 'file')

% Didn't find it there.  Check the search path for it.

fullFileName = baseFileName;             % No path this time.

if ~exist(fullFileName, 'file')

% Still didn't find it.  Alert user.

errorMessage = sprintf('Error: %s does not exist.', fullFileName);
        uiwait(warndlg(errorMessage));
        return;
    end
end
rgbImage = imread(fullFileName);

% Get the dimensions of the image.  numberOfColorBands should be = 3.

[rows, columns, numberOfColorBands] = size(rgbImage);

%% STEP 3.
% Display the original color image of initial clot condition.
```

```
subplot(4,1,1)
imshow(rgbImage);
title('Original Color Image of Initial Clot condition', 'FontSize',
fontSize);

% Enlarge figure to full screen.

set(gcf, 'Units', 'Normalized', 'Outerposition', [0, 0, 1, 1]);

%% STEP 4
% Extract the individual red, green, and blue color channels.

redChannel = rgbImage(:, :, 1);
greenChannel = rgbImage(:, :, 2);
blueChannel = rgbImage(:, :, 3);

%% STEP 5.
% Set the condition to define binary image

binaryImage = redChannel < 100;

% Again display the original color image.

subplot(4,1,2)
imshow(binaryImage);
axis off;
title('Initial Binary Image of Initial Clot condition', 'FontSize',
fontSize);

% Clean it up.

% a. Fill holes.
binaryImage = imfill(binaryImage, 'holes');

% b. Get rid of small blobs.
binaryImage = bwareaopen(binaryImage, 10000);

% c. Smoothen border
binaryImage = imclose(binaryImage, true(5));

% d. Display the cleaned color image.
subplot(4,1,3)
imshow(binaryImage);
axis off;
title('Cleaned Binary Image of Initial Clot condition', 'FontSize',
fontSize);

%% STEP 6.
% Get the boundary and outline it over the original image.

boundaries = bwboundaries(binaryImage);
x_initial = [boundaries(1)(:, 2)]';
y_initial = [boundaries(1)(:, 1)]';
```

```
% First Display the original color image.

subplot(4,1,4)
imshow(rgbImage);
title('Outline over Original Color Image of Initial Clot condition',
'FontSize', fontSize);

% Plot boundaries over it.
hold on;
plot(x_initial, y_initial, 'g-', 'LineWidth', 2);

x_initial=   x_initial*scale;            % scaling to original size
y_initial=   y_initial*scale;            % scaling to original size

%% Final Clot Condition Image Processing

%% STEP.1
% Read in the blood clot color image.

folder = 'E:\robot transducer\dip';
baseFileName = 'single3.5.png';

%% STEP 2.
% Get the full filename, with path prepended.

fullFileName = fullfile(folder, baseFileName);
if ~exist(fullFileName, 'file')

% Didn't find it there.  Check the search path for it.
    fullFileName = baseFileName; % No path this time.
    if ~exist(fullFileName, 'file')

% Still didn't find it.  Alert user.

errorMessage = sprintf('Error: %s does not exist.', fullFileName);
uiwait(warndlg(errorMessage));
        return;
    end
end
rgbImage = imread(fullFileName);
% Get the dimensions of the image.  numberOfColorBands should be = 3.
[rows, columns, numberOfColorBands] = size(rgbImage);

%% Step 3.
% Display the original color image of final clot condition.

figure
subplot(4,1,1)
imshow(rgbImage);
title('Original Color Image of Final Clot Condition', 'FontSize',
fontSize);

% Enlarge figure to full screen.
```

```
set(gcf, 'Units', 'Normalized', 'Outerposition', [0, 0, 1, 1]);

%% Step 4.
% Extract the individual red, green, and blue color channels.

redChannel = rgbImage(:, :, 1);
greenChannel = rgbImage(:, :, 2);
blueChannel = rgbImage(:, :, 3);

%% Step 5.
% Set the condition to define binary image
binaryImage = redChannel < 125;

% Display the original color image.
subplot(4,1,2)
imshow(binaryImage);
axis off;
title('Initial Binary Image of Final Clot Condition', 'FontSize',
fontSize);

% Clean it up.
% a. Fill holes.
binaryImage = imfill(binaryImage, 'holes');
% b. Get rid of small blobs.
binaryImage = bwareaopen(binaryImage, 10000);
% c. Smoothen borders
binaryImage = imclose(binaryImage, true(5));
% d. Display the original color image.

subplot(4,1,3)
imshow(binaryImage);
axis off;
title('Cleaned Binary Image of Final Clot Condition', 'FontSize',
fontSize);

%% STEP 6.
% Get the boundary and outline it over the original image.

boundaries = bwboundaries(binaryImage);
x_final = ([boundaries(1)(:, 2)]');
y_final = ([boundaries(1)(:, 1)]');

% Display the original color image.

subplot(4,1,4)
imshow(rgbImage);
title('Outline over Original Color Image of Final Clot Condition',
'FontSize', fontSize);

% Plot boundaries over it.
hold on;
plot(x_final, y_final, 'g-', 'LineWidth', 2);

x_final=   x_final*scale;            % scaling to original size
```

```
y_final=   y_final*scale;            % scaling to original size

%%                    EXTRACTING DATA FROM INITIAL AND FINAL CLOT
OUTLINES

%%   STEP 1.
%    Plot initial and final clots' outlines on the same figure

figure
plot(x_initial,-y_initial);
hold on
plot(x_final,-y_final)
ylim([-20,20])
grid on
legend('Original clot condition','Final clot condition')
title('Original and final clot condition outline')
xlabel('Movement along x-axis(mm)')

%% STEP 2.
% Define x-limits of clot under interest

% a. Again redefine apended x and y vectors

x = [x_initial,x_final];
y = [(-y_initial),(-y_final)];

%% STEP 3.

y_n=1;  % Initially run the program
% Input left and right limits for shortened x and y vectors for removed
clot visualization
while y_n==1
prompt_input_left = 'Enter left limit of particular segment of clot (in
mm): '; % asks for left limit for shortened clot
input_left = input(prompt_input_left);

prompt_input_right = 'Enter right limit of particular segment of clot
(in mm): '; % asks for left limit for shortened clot
input_right = input(prompt_input_right);




%% STEP 4.
% Finding initial shortened clot area

x_short_limit_initial=x_initial;
y_short_limit_initial=y_initial;
index_left_initial = find(x_short_limit_initial <
input_left);              % y-values for x less than this index (x-
distance) will be deleted

x_short_limit_initial(index_left_initial)=[];
```

```
y_short_limit_initial(index_left_initial)=[];

index_right_initial = find(x_short_limit_initial > input_right);  % y-
values for x more than this index (x-distance) will be deleted

x_short_limit_initial(index_right_initial)=[];
y_short_limit_initial(index_right_initial)=[];

A_short_clot_initial=polyarea(x_short_limit_initial,y_short_limit_initi
al);

%% STEP 5.
% Finding area of final shortened clot

x_short_limit_final=x_final;
y_short_limit_final=y_final;
index_left_final = find(x_short_limit_final <
input_left);               % y-values for x less than this index (x-
distance) will be deleted

x_short_limit_final(index_left_final)=[];
y_short_limit_final(index_left_final)=[];

index_right_final = find(x_short_limit_final > input_right);  % y-
values for x more than this index (x-distance) will be deleted

x_short_limit_final(index_right_final)=[];
y_short_limit_final(index_right_final)=[];

A_short_clot_final=polyarea(x_short_limit_final,y_short_limit_final);


%% STEP 6.
% Calculation of initial, final and removed areas of initial, final and
shortened final clot

Area_of_total_initial_clot= polyarea(x_initial,y_initial)
Area_of_total_final_clot= polyarea(x_final,y_final)
Area_of_total_clot_removed=Area_of_total_initial_clot-
Area_of_total_final_clot
Area_of_removed_clot_in_short_segment=A_short_clot_initial-
A_short_clot_final

%% STEP 7.
% Plot initial and final total clots and area removed from the
shortened clot under investigation

figure
subplot(4,1,1)
fill(x_initial,-y_initial,'r')
title('Initial clot condition')
grid on
hold on
```

```
subplot(4,1,2)
fill(x_final,-y_final,'r')
grid on
hold on
title('Final clot condition')

subplot(4,1,3)
fill(x,y,[1 0.5 0.3])
grid on
title('Total clot removed')
% General visualization of shortened x_final and y_final vectors for
better processing

x_short_limit=x;
y_short_limit=y;
index_1 = find(x < input_left);               % y-values for x less
than this index (x-distance) will be deleted

x_short_limit(index_1)=[];
y_short_limit(index_1)=[];

index_2 = find(x_short_limit > input_right);  % y-values for x more
than this index (x-distance) will be deleted

x_short_limit(index_2)=[];
y_short_limit(index_2)=[];

% Fill area enclosed by area removed in shortened clot

subplot (4,1,4)
area_fill=fill(x_short_limit,y_short_limit,[1 0.5 0.3]);
grid on
xlim([min(x_initial),max(x_initial)])
ylim([-20,0])
title('Clot removed from the queried subsection')

prompt_y_n = 'Continue? (1/0):  '; % asks for left limit for shortened
clot
y_n = input(prompt_y_n);
end

disp ('Image Processing of clot finished.')
```